Mimicking the Human Olfactory System: A Portable e-Mucosa

by
Fauzan Khairi Che Harun
School of Engineering
University of Warwick

A thesis submitted to the University of Warwick
for the degree of Doctor of Philosophy
September 2009

Contents

Heading	Page

Appendix A : Sample XML e-Nose File

Appendix B : Firmware Flow Chart

Appendix C : Portable e-Mucosa Schematics

List of Figures

List of Tables

Heading	Page

Summary

The study of electronic noses has been an active area of research for over 25 years. Commercial instruments have been successfully deployed within niche application areas, for example, the food, beverage and pharmaceutical industries. However, these instruments are still inferior to their human counterparts and have not achieved mainstream success. Humans can distinguish and identify many thousands of different aromas, even at very low concentration levels, with relative ease. The human olfactory system is extremely sophisticated, which allows it to out-perform artificial instruments. Though limited, artificial instruments can provide a lower cost option to specific problems and can be an alternative to the use of organoleptic panels.

Most existing commercial electronic nose (e-nose) instruments are expensive, bulky, desktop units, requiring a PC to operate. In addition, these instruments usually require a trained operator to gather and analyse the data. Motivated to improve the performance, size and cost of e-nose instruments, this research aims to extract biological principles from the mammalian olfactory system to aid the implementation of a portable e-nose instrument.

This study has focused on several features of the biological system that may provide the key to its superior performance. Specifically, the large number of different olfactory receptors and the diversity of these receptors; the nasal chromatograph effect; stereo olfaction; sniff rate and odour conditioning. Based on these features, a novel, portable, cost effective instrument, called the Portable e-Mucosa (PeM), has been designed, implemented and tested. The main components of the PeM are three sensor arrays each containing 200 carbon black composite chemoresistive sensors (totalling 600 sensors with 24 different tunings) mimicking the large number of olfactory receptors and two gas chromatographic columns (coated with non-polar and polar compounds to maximise the discrimination) emulating the "nasal chromatograph" effect of the human mucus. A preconcentrator based on thermal desorption is also included as an odour collection system to further improve the instrument. The PeM provides USB and Multimedia Memory Card support for easy communication with a PC. The instrument weighs 700g and, with dimensions of 110 x 210 x 110 mm, is slightly larger than the commercial Cyranose 320 (produced by Smiths Detection).

This novel instrument generates 'spatio-temporal' data and when coupled with an appropriate pattern recognition algorithm, has shown an enhanced ability to discriminate between odours. The instrument successfully discriminates between simple odours (ethanol, ethyl acetate and acetone) and more complex odours (lavender, ylang ylang, cinnamon and lemon grass essential oils). This system can perhaps be seen as a foundation for a new generation of e-noses.

Acknowledgements

Firstly, I thank Allah (S.W.T) for making all this possible. I would also like to express my upmost gratitude to my academic supervisor, Dr James Covington and Prof. Julian Gardner for giving me the opportunity of studying in this field, and for their constant guidance and support during my PhD. I would also like to acknowledge Universiti Teknologi Malaysia for their financial support during the three years of study. Also to all UTM staff, including Kak Ani and Kak Surati who have helped me a lot during my study.

For practical work associated with my PhD, I would particularly like to thank the members of the Sensors Research Laboratory, School of Engineering, University of Warwick*,* including, Mr F. T. Courtney for his assistance in all mechanical matters and to Mr I. Griffiths for his helped is circuit layout and design. This works would not have been possible without both of you.

I am also thankful to all of my friends and colleagues, including T. Iwaki, J. Khawaja, P.H. King, J. Taylor, M.Talib, Mohd Azhar Abd Razak, Raja Kamaruzaman and S. Pathak for their constant support and encouragement during the course of this study.

I would also like to acknowledge my wife, Siti Rohana Abd Rahman and kids for their constant support during my PhD.

Last but not least, I would like to acknowledge everyone who has helped me in one way or another, without which this would not have been possible.

Declaration

The work described in this thesis is entirely original and my own, except where otherwise indicated.

Parts of this work have been presented at international conferences and published in the scientific literature listed below:

Journal Paper

1. F.K.Che Harun, J.E.Taylor, J.A.Covington, J.W.Gardner, ",An electronic nose employing dual-channel odour separation columns with large chemosensor arrays for advanced odour discrimination", Sensor and Actuator B: Chemical, 2009, Volume 141, Issue 1, 134-140.

Conference papers

1. F.K.Che Harun, P.H. King, J.A. Covington, J.W. Gardner, "Novel Gas Chromatographic Microsystem With Very Large Sensor Arrays For Advanced Odour Discrimination", IEEE Sensors 2007. Presented on October 28 - 31, 2007 in Atlanta, USA.
2. F.K.Che Harun, J.Taylor, J.A. Covington, J.W. Gardner,"Dual-Channel odour separation columns with large chemosensor arrays for advanced odour discrimination", IMCS 12, 2007. Presented on July 13-16 2008 in Ohio, USA.
3. James Taylor, F.K Che Harun, J.A. Covington, J.W. Gardner, "Applying Convolution-Based Processing Methods to a Dual-Channel, Large Array Artifical Olfactory Mucosa", ISOEN 13, 2009. Presented on 15-17 April 2009 at Brescia, Italy.
4. F.K.Che Harun, J.A. Covington, J.W. Gardner, "Portable e-Mucosa System: Mimicking the biological olfactory system", Eurosensor XXIII, 2009.

Selected Abbreviations and Acronyms

TERM	DEFINITION
ADC	Analogue to Digital Conversion
aVLSI	Analogue Very Large Scale Integration
CAD	Computer Aided Design
CMOS	Complementary Metal Oxide Semiconductor
Carbowax 20M	Poly(ethylene glycol)
DAC	Digital to Analogue Conversion
DMD	Digital Micromirror Device
e-mucosa	Electronic Mucosa
E-nose	Electronic Nose
FET	Field Effect Transistor
FID	Flame Ionisation Detector
GC	Gas Chromatography
I/O	Input/Output
LCD	Liquid Crystal Display
LIGA	Lithography Galvonoforming Abforming
LSER	Linear Solvation Energy Relationship
MEMS	Micro-Electro-Mechanical-System
MOS	Metal Oxide Semiconductor
MS	Mass Spectrometry
MSL	Microstereolithography
OB	Olfactory Bulb
OS	Operating System
OR	Olfactory Receptor
PBA	Poly (bisphenol A carbonate)
PCA	Principal Component Analysis
PCB	Printed Circuit Board
PCL	Poly (caprolactone)
PCX	Poly (chloro P xylylene)
PDE	Partial Differential Equation
PDMS	Poly (dimethylsiloxane)
PEG	Poly (ethylene glycol)
PEVA	Poly (ethylene-co-vinyl acetate)
PMMA	Poly (methyl methacrylate)
PSB	Poly (stylene-co-butadiene)
PSF	Poly (sulfane)
PVC	Poly (9-vinylcarbazole)
PVPD	Poly (vinyl pyrrolidone)
PVPH	Poly (4-vinyl phenol)
QCM	Quartz Crystal Microbalance
SAW	Surface Acoustic Wave
Si	Silicon
SiO_2	Silicon Dioxide
SL	Stereolithography
STL	Stereolithography
SPI	Serial Peripheral Interface
UV	Ultra-Violet
VI	Virtual Instrument
VLSI	Very Large Scale Integration
SE-30	Poly (dimethylsiloxane)
OV-1	Poly (dimethylmethylphenyl-siloxane)

CHAPTER 1

1.1 Introduction

This chapter introduces the human olfactory system and compares it to current electronic nose instruments, discussing both the strengths and weaknesses of both. Next, current technology, devices and applications are discussed. The aims and objectives of the research undertaken are then described. Lastly, an outline of the thesis is presented.

1.2 Mammalian olfactory system

The sense of smell is always seen as a minor sense among the five major human senses (sight, touch, taste, hearing and smell). Evolution created the sense of smell as warning mechanism, for finding food, avoiding predators or choosing a mate [1, 2]. However, as humans have evolved, the human olfactory system has degraded in function, due to the its reduced importance for survival.

In order to discuss various components of the biological olfactory system, an anatomy of the human olfactory system is shown in Figure 1.1 [2]. In the human olfactory system, odours are delivered through the nasal passages to the olfactory epithelium where various olfactory receptors are located. The inhaled odorant molecules have to pass through a thin mucous layer (10-100 µm) along the nasal

cavity to reach the olfactory receptor cells, which occupy a small area in the nasal epithelium[3].

Nasal cavity or 'Nasal fossa' is the air filled area located behind the nose in front of the face. The function of the nasal cavity is to precondition the sniffed air by warming and humidifying the air in such a way that it prepares the odour before being sensed and processed [4, 5]. This is a crucial task that assists the olfactory system to perform better. Furthermore, the vibrissae (short, thick hairs located in the nasal cavity), clean the sniffed odour by removing dust and other particulate matter in the sniffed air. The nasal cavity shape allows the odour molecules to accumulate, concentrating the odour to interact better with olfactory receptors.
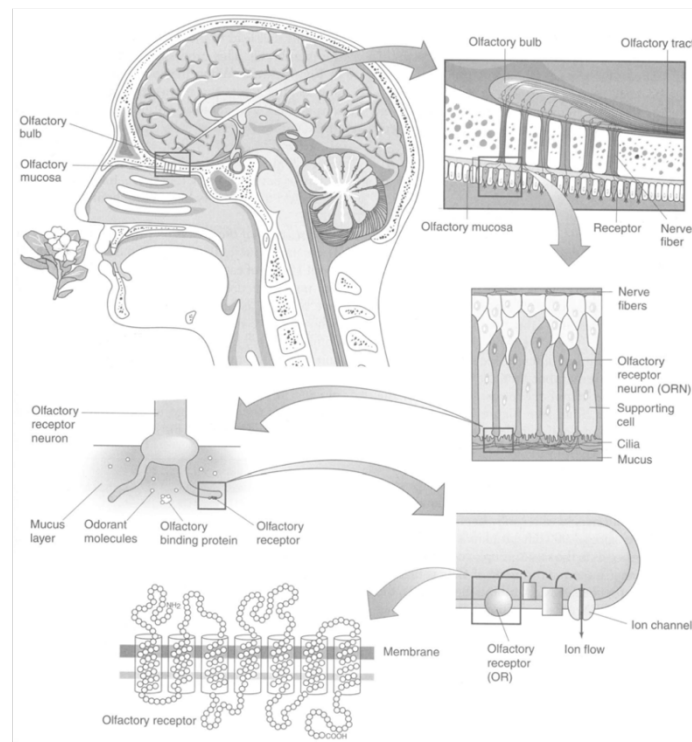
Figure 1.1: Anatomy of a Human Olfactory System

The olfactory receptors, located on the surface of the cilia of the olfactory epithelium in the nasal cavity will detect and carry out thin nerve processes directly to distinct

micro domains, called glomerulus [6, 7] in the olfactory bulb, the primary olfactory area of the brain. Receptors have overlapping sensitivity to different odorants, that is, each of the odorant molecules correspond to an exclusive group of responses from the receptors. Through the olfactory bulb the information of the vapour will reach the olfactory cortex and the brain where the information from several receptors is processed, forming a pattern that can be recognized.

Comparing the olfactory system of humans with other animals, rats are 8 to 50 times more sensitive to odours than humans, whilst dogs are 300 to 10,000 times more sensitive, depending upon the odorant [8]. The sensitivity of dogs' olfactory system is known to be much higher than that of humans[9]. Several factors such as the size of the olfactory epithelium, the density of neuronal cells and the number of olfactory receptor as well as the size of the olfactory bulb, contribute to the sensitivity of mammalian olfactory[10]. The human nose has about 12 million olfactory receptor cells[11] and 1000 different receptor protein types while dogs have 1 billion receptor cells. Furthermore, in dogs, 5% of the dogs genome is given over to smell compared to 1-2% in human genome. Thus it is clear that the number of olfactory receptor cells contributes to the sensitivity of the olfactory system. The reason why a number of sensors are so important is that it increases the diversity of detection, meaning we can get more information from the array, thus detecting more different odours.

1.1 Electronic noses

The research into an artificial bio-mimetic mammalian olfactory system has been an active research area over 20 years, since the idea first came to light in 1980[12]. Later in 1982 at the University of Warwick in UK, Persaud and Dodd made the first

conceptualization of the electronic nose[13]. The term electronic-nose first appears in 1988 [14]; it was later defined formally by Gardner et al. [1] where he defines it as:

'Electronic Nose as an instrument, which comprises an array of electronic chemical sensors with partial specificity and an appropriate pattern-recognition system, capable of recognising simple or complex odours'.
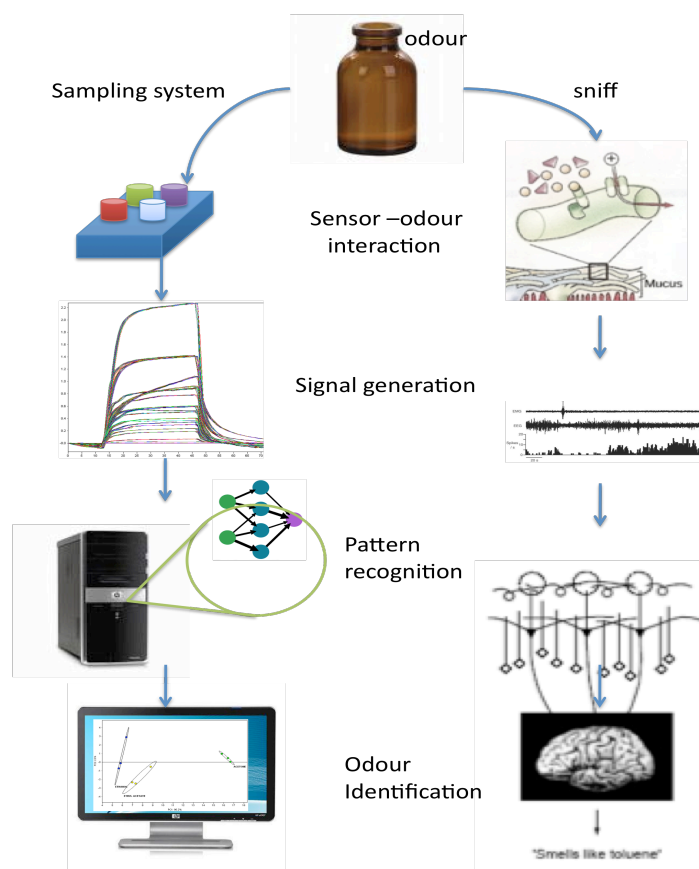
Figure 1.2: (a) Electronic Nose versus (b) Human Olfactory System

Figure 1.2 shows the comparison of a human olfactory system and an electronic nose pathway [15]. In a human olfactory system, when a human sniffs an odour, the olfactory receptor neurons generate a signal and send it to the brain to be identified. Similar to this, an array of chemo-sensors are used to replace the receptors for an

electronic nose. The signal from these chemo-sensors will be fed to a pattern recognition system where it will be recognized and identified. Here we can see that we are able to simulate human olfactory system with two main parts, the sensing part which is mimicked by an array of chemical sensors and the second is the pattern recognition system emulating the olfactory bulb to process the data.

Throughout the years, researchers have come up with different techniques of discriminating and recognizing odours, all with their own advantages and disadvantages. Some researchers have focussed on the chemical sensor array itself while others try to improve the electronic nose (e-nose) by improving the processing technique. Both of these areas are equally important in creating a better electronic nose system. Some research has focussed on developing new e-nose instruments by adding an 'enhancement' to their system, such as SPME, preconcentrator or gas chromatograph [16]. Here we will discuss two approaches of improving electronic nose instruments focussing on sensor-based gas detectors and instrument based gas detectors that employ different detection mechanisms.

1.2.1 Sensor-based gas detectors

A sensor is a device that measures a physical quantity and converts it into a signal, which is readable by an observer or instrument. Hence, a chemical sensor changes some physical or electrical property of itself through chemical reaction when exposed to a reactive gas or vapour.

Sensor-based electronic noses basically consist of some type of sensor with a fluidic system of pumps and valves. The sensors (usually in an array) are interfaced to a signal conditioning and data acquisition circuit to collect data from the sensor. This data will then be processed using a pattern recognition technique (usually software

based) for classification or discrimination. The sensor array, which is the central of the e-nose instrument, utilizes different methods of detecting gas using various principles.

An ideal gas sensor would respond to odour molecules even in low concentrations and also change linearly with the concentration until it reaches saturation. In addition, it should respond and recover quickly to the original value once the odour source is removed. Other desired characteristics also include great reproducibility, wide working range and steady baseline.

In comparison, real sensors suffer from baseline drift, sensor poisoning and sensitivity changes depending on the ambient condition, such as humidity, temperature and flow rate. These are the factors that need to be improved in order to get a better response from the gas sensor.

A nose sensing capability can be realized using various technologies including conductometric chemo-sensors (metal oxide semiconductors[17], carbon black composite and conducting organic polymers[18]), chemo-capacitors, potentiometric chemo-sensors (e.g. MOSFET), gravimetric chemo-sensors (QCM[19], SAW), optical chemo-sensors (SPR, fluorescent sensors, NIR), calorimetric sensors, and amperometric sensors [3]. Electrochemical sensor is a popular types of method used by many researchers. Gardner et al describe the application of conducting polymers for electronic nose [20] and Persaud et al use the conducting polymer sensor arrays to identify a few types of chemicals in their research [21]. Many researches now focus on using different types of gas sensitive material to improve sensitivity and selectivity of the gas sensor. Figure 1.3 shows various commercially available chemosensor in the market.
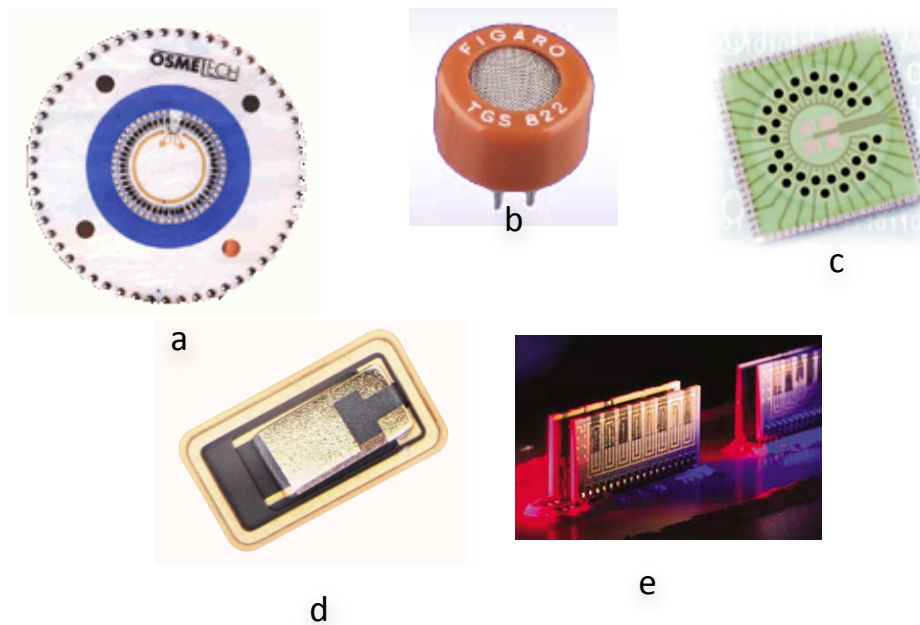
Figure 1.3: Sensor Technology. a) Osmetech 48 Conducting Polymer sensors b) Figaro TGS 822 Tin Oxide sensors c) Smiths Detection (previously known as Cyrano Sciences) 32-sensor integrated array d) Polymer based chemoresistive sensor from Osmetech e) NASA 32 integrated sensor array

The various chemo sensors can also be categorized by the sensing material used alongside the sensing technique, for which the following exists: metal oxide (MOS), conducting polymers (CP), Carbon Nanotubes (CNT), Carbon Black Composite (CB), and Organic Conducting Polymer(COP). A more recent discovery on nanomaterials brings a whole new possibility for electronic nose instruments. Various researches have shown the ability of nanomaterials as gas sensors [22-25]. Table 1.1 shows the different techniques with the advantages/disadvantages of each method.

Table 1.1: Various Sensor Types with advantages and disadvantages

Sensing Technique	Sensor Type	Advantages	Disadvantages	References
Conductometric	Carbon Black Composite	Room Temperature, diverse range of coating	Sensitive to humidity / small response	[26, 27]
	Conducting Polymer	Cheap, good response time, sensitive to polar analytes	Suffer from baseline drift, sensitive to humidity	[28]
	Metal Oxide	Fast response and recovery time, cheap	Operates at high temperature	[28]
Mechanical	SAW	High sensitivity, good response time	Poor reproducibility	[29]
	QCM	Diverse range of coating, Good reproducibility	Complex circuitry, poor SNR	[19, 28]
Thermal	Pellistor Thermocouple	Low Cost	Slow Response	[30]
Radiation	FIbre Optics	Fast Response, not susceptible to electromagnetic	Expensive	[28, 31]

1.2.2 Instrument-based gas detectors

Conventionally, a different type of approach is used as a method for analyzing the composition of a gas or vapour. One of the most common instruments is the Gas Chromatography (GC). GC uses a different approach in detecting gases compared to, for example, solid-state chemo sensors used in an electronic nose. With GC, the tested gas itself is separated to smaller components, by the column, and detected by

a detector on the outlet. An electronic nose on the other hand, detects the gas as a whole and the pattern recognition method will classify or discriminate the odour. Various sensors can be use along side a GC to detect the separated gases, such as discharge ionization detector (DID), electron capture detector (ECD), flame photometric detector (FPD), flame ionization detector (FID), Hall electrolytic conductivity detector (ECD), helium ionization detector (HID), Nitrogen Phosphorus Detector (NPD), mass selective detector (MSD), photo-ionization detector (PID), pulsed discharge ionization detector (PDD) or thermal energy(conductivity) analyzer/detector (TEA/TCD) . There are also some studies suggesting employing gas sensors used in electronic noses, for such detection purposes [32, 33].

Figure 4 : a) HP 6890 Series Gas Chromatography b) zNose 4500[34]

The main problem with conventional GC techniques is the slow analysis time. An example is the HP 6890 series GC (Figure 4(a)) which takes 20-120 minutes per analysis cycle. It is also very bulky, laboratory based, and too costly to be used on-site. Hence, the need for faster chromatogram arises. The first realization of a fast chromatogram was in 1958, when Golay demonstrated separation of air, acetone,

carbon disulfide, methanol, and methylene chloride in less than 10 seconds [35]. A bigger breakthrough than the fast separation was the fact that Golay used a 32 ft long, 254 μm diameter thin film capillary column instead of a packed column commonly used at the time. The fast GC has developed tremendously since then. Now research shows a column less than a meter long with the size 2.4 cm x 4 cm, is able to separate complex odour within a few seconds [36]. Sandia Labs have demonstrated a 2d multidimensional GC just a meter long, smaller than a dime, separating 5 different vapours in less than a minute [37]. The zNose from Electronic Sensor Technology shown in Figure 4(b) is able to detect vapour at part per billion(ppb) level in just 10 seconds (though this does not include the 5 minutes for the pre-concentration stage) [34].

Mass spectrometry is another common analytical method for detecting odorant compounds. This technique separates molecules by ionisation and then separating the ions in the mass spectrometer (MS) according to the mass-to-charge ratio of the ion [1]. Smart Nose is a commercial example of an e-nose utilizing MS methods. The combination of Gas Chromatography with Mass Spectrometry (GC-MS) is a very popular technique for identifying volatile compounds. Many research have utilized GC-MS combination to analyze vapour[38-42].

Another method for identification is called Ion Mobility Spectrometry(IMS) where it is based on the ionization of gas or vapor molecules under atmospheric pressure followed by the drift of the resulting ions in an accelerating electric field. The velocity of the ions depends on mobility coefficients, which in turn are determined by ion masses and other properties. Different ions reach the detector at the end of the drift tube at different time.

1.3   Commercial Electronic Nose

The first commercial version of electronic nose came out in the mid-1990s [43] with the Fox 2000 from Alpha MOS. The main application areas were in the food industries. The advancement in industries calls for a commercial intelligence vapour analyzing device. Some commercial instruments have been given in the following table (Table 1.2).

Table 1.2: Commercial E-Noses

Device	Manufacturer	Sensor Type	Sensors Number	Size
Fox 2000,3000,40000	Alpha MOS	MOS/SAW	6,12,18	Desktop
z-Nose 4500	EST	GC/SAW	2	Laptop
BloodHound ST214	University of Leeds Innovation Ltd	CP	14	Laptop
Heracles	Alpha MOS	GC-MS	-	Desktop
SMart Nose	SMart Nose Inc.	MS	-	Desktop
Cyranose 320	Smith Detection	Carbon Black	32	Portable
PEN-2 WMA	AIRSENSE ANALYTICS	MOS	10	Portable
HAZMATCAD, CW Sentry 3G	Microsensors System	SAW	-	Portable
SensorFreshQ	FQSI	-	-	Portable
LibraNose	TECHNOBIOCHIP	QCM	8	Portable
e-Nose 5000	Marconi Applied	CP	12	-

More than 10 companies have developed their own version of e-Nose ranging from handheld to desktop size instruments. Various methods of detection are used with their own advantages/disadvantages. When discrete sensor arrays are used in e-noses, then the number sensing elements range from 2 to 32 sensors. The e-nose has even gone into the consumer market with the development of SensorFreshQ from FQSI, which can determine the freshness of meat or poultry in less than a minute.

First commercial handheld electronic nose by Cyrano Science (USA) employed a 32 carbon-black polymer composite sensor array, which was designed for on-site applications. Cyranose 320 has proven to be a popular e-nose used in many researches[44-46], probably due to its low unit cost and small size making it easier to be used on-site use.

1.4 Applications of electronic noses

Although current electronic nose technology still lags far behind the human olfactory system in term of selectivity and sensitivity, it is still being used in a wide range of applications, in several industries such as environmental, the food industry and in the medical field. The main reason for this is the ability of an electronic nose to solve specific problems at a lower cost within a shorter period of time. Using humans to evaluate the smell of products such as perfumes, foods and beverages is a costly process, because trained panels of experts are required and they can only work for relatively short periods of time. This topic will discuss several industrial applications that use an electronic nose.

One of the first markets for electronic noses was in the food industry [47]. Electronic noses are used for the inspection of food quality, control of food cooking processes [48] and quality assessment of food production [47]. Even consumer level e-noses have been developed for the food industry such as the SensorFreshQ. It detects the freshness of meat by identifying the odour released by bacteria growing on the meat. The bigger the colony of bacteria, the stronger the smell will be. In the area of environmental monitoring, the application of electronic noses includes analysis of fuel mixtures [49] and detection of oil leaks [50]. Significant research has been undertaken in the area of Biomedical Engineering. Recent development in biomedical engineering using electronic noses includes the detection of Mycobacterium tuberculosis (TB) [51], screening of aroma-producing lactic acid bacteria [52] and monitoring of Haemodialysis [53]. The electronic nose is also used in the brand identification of cigarette [54] and paper quality [55]. As we can see, the electronic nose has been applied to a wide area of applications. Despite this growing number of applications, there is still much work required to realise its full potential. There are currently many limitations to current commercial instruments including high cost (Fox 2000 cost around £40,000), large size and weight, humidity and temperature dependence, poor reproducibility and repeatability, high power consumption, and long analysis time [15]. At present, odour-sensing applications demand high levels of system sensitivity and stability. Traditional engineering approaches have not yet obtained this kind of sensitivity and stability.

1.5 Research objectives

The mammalian olfactory system is far superior compared to any sensing technique available today in indentifying and discriminating odours. However, as discussed in this chapter, presently available instrument are good enough to solve problems in various areas. More research is being done to improve the performance of an electronic nose to bring it close to the mammalian nose. This research focuses on extracting engineering design principles in the mammalian nose and mimicking that design in an artificial nose. As discussed in previous topics, the mammalian nose is many times more sensitive and has the ability to discriminate more different odours, over traditional electronic noses. This is due to the huge number of receptors cells in the mammalian olfactory system. The research undertaken here will try to more closely mimic the mammalian system by developing electronic nose instruments that have significantly higher sensor numbers, compared to present commercial instruments. In addition, we will use many different sensor tuning (equivalent to different binding proteins in the mammalian system). Ultimately, a larger sensor count with a wider range of tunings provides more data for processing, thus increasing the selectivity of an electronic nose.

Another principle from the mammalian olfactory system that will be deployed in this research project is a replication of the nasal mucosa function. As mentioned before, the nasal mucosa acts as a separator to separate complex odours to make it easier for the olfactory system to process the information. It is not proposed to create a full 'gas chromatograph' system, as the mammalian system does not perform this role, but its purpose is to aid in the identification process.

Finally, with large sensor arrays mimicking the large olfactory receptor, and the retentive channel to mimic the nasal cavity, a portable e-nose instrument based on the mammalian nose principles is produced. This portable e-nose instrument is then tested to detect some complex odour to prove its functionality.

1.6 Outline of thesis

The thesis describes the design, development and characterisation of a novel instrument that mimics more closely the mammalian olfactory system towards developing a new generation of portable electronic noses.

Chapter 1 reviews the biological olfactory system and electronic nose instruments comparing their differences and similarities. It also discusses the main application areas of the electronic nose instruments. The aims and objectives of the thesis are then presented.

Chapter 2 describes the project evolution; understanding the olfactory principles to be applied in an artificial nose.

Chapter 3 and 4 cover the design and development of two of the Important components, the sensors array and the microchannel packages.

Chapter 5 discusses the fusion of sensor array and microchannel packages to produce an Electronic Mucosa System. Polymer deposition and stationary phase deposition are also covered here.

Chapter 6 describes development of the portable electronic system which combines control and data acquisition on a microcontroller based platform.

Chapter 7 reports the characterisation results of the fabricated microsystems to evaluate their performance. The central focus here has been geared towards getting spatiotemporal signals from these systems and the benefit of these signals to aid discrimination.

Chapter 8 concludes the research and the latest developments are presented to highlight possible future enhancements.

1.7   References

1.   J. W. Gardner , P.N.Barlett., *Electronic Noses : Principles and Applications*. First ed. 1999: Oxford University Press.
2.   E.B Goldstein , *Sensation and perception*. Sixth ed. 2002: Wadsworth Inc Fulfilment.
3.   T.C. Pearce, H. T.Nagle, J.W. Gardner, *Handbook of Machine Olfaction*. 2003: Wiley.
4.   J.T. Kelly,A.K. Prasad, and A.S. Wexler, *Detailed flow patterns in the nasal cavity.* J Appl Physiol, 2000. **89**(1): p. 323-337.
5.   G.M Shepherd, *The Human Sense of Smell: Are We Better Than We Think?* PLoS Biology, 2004. **2**(5): p. e146.
6.   K.J.Ressler, S.L.S., L.B. Buck, *Information coding in the olfactory system: Evidence for a stereotyped and hihly orgnized epitope map in the olfactory bulb.* Cell, 1994. **79**: p. 1245.
7.   L. Buck , R.Axel., *A novel multigene family may encode odorant receptors: A molecular basis for odor recognition.* Cell, 1991. **65**: p. 175-187.
8.   D.G Laing, R.L.D., W. Breipohl, *The human sense of smell*. 1991, New York: Springer.
9.   S.B Rouquier, D. Giorgi , *The olfactory receptor gene repertoire in primates and mouse: evidence for reduction of the functional fraction in primates. .* Proc Natl Acad Sci, 2000. **97**: p. 2874.
10.   P. Quignon,et al., *Comparison of the canine and human olfactory receptor gene repertoires.* Genome Biology, 2003. **4**(12): p. R80.
11.   D.Shier, J. Butler, R. Lewis, *Hole's Human Anatomy & Physiology*. 2004, Boston: McGraw Hill.
12.   H.Zwaardemaker, a.F.H., *On spray-electricity and waterfall-electricity.* Proc. Acad. Sci. Amst., 1920. **22**: p. 429-437.
13.   K Persaud, , *Analysis of discrimination mechanisms in the mammalian olfactory system using a model nose.* Nature, 1982.
14.   J.W.Gardner, *Pattern recognition in the Warwick electronic nose.* 8th International Congress of the European Chemoreception Research Organisation, 1988.
15.   T.A.Dickinson *Current trends in 'artificial-nose' technology.* TIBTECH, 1998. **16**.
16.   rsquo, et al., *A comparison of warmed-over flavour in pork by sensory analysis, GC/MS and the electronic nose.* Meat Science, 2003. **65**(3): p. 1125-1138.
17.   B.K Dable, et al., *Calibration of microhotplate conductometric gas sensors by non-linear multivariate regression methods.* Sensors and Actuators B: Chemical, 2004. **101**(3): p. 284-294.
18.   A.L. Kukla,et al., *Application of sensor arrays based on thin films of conducting polymers for chemical recognition of volatile organic solvents.* Sensors and Actuators B: Chemical, 2009. **135**(2): p. 541-551.
19.   Y.Han Kim, and K. Jae Choi, *Fabrication and application of an activated carbon-coated quartz crystal sensor.* Sensors and Actuators B: Chemical, 2002. **87**(1): p. 196-200.
20.   J.W.Gardner, *Application of conducting polymer technology in Microsystems.* Sensors and Actuators A, 1995. **51**.
21.   K.C.Persaud, *Sensor array techniques for mimicking the mammalian olfactory system.* Sensors and Actuators B: Chemical, 1996. **35**.

22.   Ashis Modi, E.L., *Miniaturized gas ionization sensors using carbon nanotube.* Nature, 2003. **424**.
23.   N.R.F.Jing Kong, , *Nanotube Molecular Wire as Chemical Sensors.* Science, 2000. **287**.
24.   J.K Abraham, *A compact wireless gas sensor using a carbon nanotube/PMMA thin film chemisresistor.* Smart Sensors and Structures, 2004.
25.   Kay Hyeok, *Enhanced Sensitivity of a Gas sensor Incorporating Single Walled Carbon Nanotube – Polypyrrole Nanocomposites.* Advance Materials, 2004.
26.   B.C.Munoz, , G. Steinthal, and S. Sunshine, *Conductive polymer-carbon black composites-based sensor arrays for use in an electronic nose.* Sensor Review, 1999. **19**: p. 30-30.
27.   D.C.Dyer, and J.W. Gardner, *High-precision intelligent interface for a hybrid electronic nose.* Sensors and Actuators A: Physical, 1997. **62**(1-3): p. 724-728.
28.   H.T. Nagle, G.O., Schiffman S.S, *The How and Why of Electronic Noses.* IEEE Spectrum, 1998.
29.   K.J.Albert, et al., *Cross-Reactive Chemical Sensor Arrays.* Chemical Reviews, 2000. **100**(7): p. 2595-2626.
30.   Zhuang Cao, Joseph R. Stetter,, *The properties and applications of amperometric gas sensors.* Electroanalysis, 1992. **4**(3): p. 253-266.
31.   Z.Jin, , Y. Su, and Y. Duan, *Development of a polyaniline-based optical ammonia sensor.* Sensors and Actuators B: Chemical, 2001. **72**(1): p. 75-79.
32.   C.J Lu, et al., *Portable Gas Chromatograph with Tunable Retention and Sensor Array Detection for Determination of Complex Vapor Mixtures.* Analytical Chemistry, 2003. **75**(6): p. 1400-1409.
33.   P.W. Ash, N.W.B., L. Ebdon, S.J. Rowley, *Configuration and optimisation of semiconductor gas sensors as gas chromatographic detectors.* Analytica Chimica Acta, 1989. **216**: p. 147-161.
34.   Technology, E.S., *Mobile Ultra-Fast GC Analyzer Model 4500*, Electronic Sensor Technology.
35.   M.J.E.Golay, , *Gas Chromatography.* Academic Press, 1958(1).
36.   A.Bhushan, , et al., *Fabrication of micro-gas chromatograph columns for fast chromatography.* Microsystem Technologies, 2007. **13**(3): p. 361-368.
37.   A.Stephen, Casalnuovo, Richard J. Kottenstette, Edwin J. Heller, Carolyn M. Matzke, Patrick R. Lewis, Ronald P. Manginell, Albert G. Baca, Vincent M. Hietala, and Joel R. Wendt, *Gas Phase Chemical Detection with and Integrated Chemical Analysis System.* Sandia National Laboratories, 2000.
38.   F.Fenaille, , et al., *Comparison of Mass Spectrometry-Based Electronic Nose and Solid Phase MicroExtraction Gas Chromatography Mass Spectrometry Technique to Assess Infant Formula Oxidation.* Journal of Agricultural and Food Chemistry, 2003. **51**(9): p. 2790-2796.
39.   A.K.M. Shafiqul Islam, Z.I., A.R. Othman, M.N. Ahmad and A.Y. Md. Shakaff, *Correlation study between the electronic nose response and headspace volatiles of Eurycoma longifolia extracts*, in *1st International Conference on Sensing Technology*. 2005: New Zealand.
40.   Stefanie Montag, , Heiko Ulmer, Dorothee Wernet, Wolfgang Göpel, and Hans-Georg Rammensee, *"Electronic nose" detects major histocompatibility complex-dependent prerenal and postrenal odor components.* Proc Natl Acad Sci 2001. **98**(16): p. 9249–9254.
41.   J.P.Santos, et al., *A comparative study of sensor array and GC-MS: application to Madrid wines characterization.* Sensors and Actuators B: Chemical, 2004. **102**(2): p. 299-307.
42.   S.Van den Velde, , et al., *GC-MS analysis of breath odor compounds in liver patients.* Journal of Chromatography B, 2008. **875**(2): p. 344-348.
43.   J. W. Gardner, and O.O. Awadelkarim, *Microsensors, MEMS, and Smart Devices*. 2001, Chichester: John Wiley & Sons, Ltd.
44.   J.W.T.Yates, , et al., *Data reduction in headspace analysis of blood and urine samples for robust bacterial identification.* Computer Methods and Programs in Biomedicine, 2005. **79**(3): p. 259-271.
45.   R.Dutta, et al., *Identification of Staphylococcus aureus infections in hospital environment: electronic nose based approach.* Sensors and Actuators B: Chemical, 2005. **109**(2): p. 355-362.
46.   R.Dutta, et al., *Stochastic resonance-based electronic nose: A novel way to classify bacteria.* Sensors and Actuators B: Chemical, 2006, 115, p. 17-27.
47.   A.M.Pisanelli, , *Applications of Multi Array Polymer Sensors to Food Industries.* Life Chemistry Reports, 1994. **11**: p. 303-308.
48.   A.Almeida, , *Neural network in oven prevents overcooking.* The Institute, 1994: p. 3.

49.   R.J. Lauf, , *Analysis of Liquid Fuels Using a Gas Sensor Array.* Fuel, 1991. **70**(935-940).

50.   H.V.Shurmur, , *The fifth sense: on the scent of the electronic nose.* IEE Review, 1990: p. 95-58.

51.   A.K.Pavlou, , *Detection of Mycobacterium tuberculosis(TB) in vitro and in situ using an electronic nose in combination with a neural network system.* Biosensors and Bioelectronics, , 2004. **20**(538-544).

52.   L.Marilley, , *Screening of aroma-producing lactic acid bacteria with and electronic nose.* International Dairy Journal, 2004. **14**: p. 849-856.

53.   R.Fend , *Monitoring haemodialysis using electronic nose and chemometrics.* Biosensors & Bioelectronics, 2004. **19**: p. 1581-1590.

54.   D.Luo, *Application of ANN with extracted parameters from an electronic nose in cigarette brand identification.* Sensors and Actuators, 2004. **99**(B): p. 253-257.

55.   M.Holmberg, *Identification of paper quality using hybrid electronic nose.* Sensors and Actuators, 1995. **26-27**(B): p. 246-249.

CHAPTER 2

Project Evolution and Instrument Description

2.1 Introduction

The Electronic Nose has seen significant improvements since the first instruments were conceived in the 1990s. From then on, there have been substantial improvements in sensor materials, signal processing, sample preparation and identification algorithms. However, even with these enhancements in performance, the electronic nose still lags behind the ability of the mammalian olfactory system to detect and identify aromas. In an attempt to reduce this gap, we propose to develop a new generation of e-noses that more closely mimic the discoveries observed in the biological olfactory system [1]. As discussed in the previous chapter, several factors, such as the size of the olfactory epithelium (increased number of receptor), the density of neuronal cells, the number of different types olfactory receptors and the size of the olfactory bulb, contribute to the sensitivity of mammals[2]. Having more receptor with various olfactory binding proteins clearly contribute to the sensitivity and selectivity of biological olfactory. In the e-nose, research has proven that classification performance in general either increases or did not decrease significantly as the number of chemically different detectors increases [3].

Furthermore, the Lewis group (Caltech, USA) suggests that a larger number of sensors are required to detect lower concentration odours.

Some researchers also suggest that the temporal information produced by the olfactory mucosa may offer significant performance enhancement for the mammalian olfactory system [4-6]. These researches have lead to new, more inventive versions of gas sensing device such as the zNose and Heracles where they include a high speed chromatographic column in their device. Although these devices are not actually e-noses, and they separate the complex gas composition to individual component (not using the temporal information for processing), these are good indication that GC technologies have the ability to produce temporal information in e-noses.

In this chapter, we will discuss the project evolution including biological olfactory emulation, the selection of sensor technology, sensing material selection and the technique of spatio-temporal signal generation. This chapter also introduces various sub-systems developed throughout the project. This should allow readers to have a better understanding of the proposed final system before the components are examined in detail in later chapters.

2.2 Mimicking the biological olfactory system

Our understandings of the sense of smell are the least among the five major senses (though the human body is believed to have 21 senses in total). One of the greatest breakthrough in the field of olfactory was made by Richard Axel and Linda Buck when they were awarded with a Nobel Prize in 2004 for their discovery of a gene pool that contains the blueprint for receptors or sensors within the nose that identify

odours[7]. This has lead to many other researches to understand more about the

biological olfactory system of animals including fish [8-10], dogs [11, 12], mice[13]

and insects[14-17].

The idea of mimicking the biological system to improve current technology is

not new; many researches are trying to emulate the way nature works. Often known

as biomimetics, this area of research focuses on mimicking concepts, mechanisms,

functions, and design features that are seen in nature. One of the earliest attempts

of bio-inspired engineering is probably the airplane when humans tried to mimic the

way birds fly. With the advancement in engineering materials and techniques,

currently many researches are geared towards bio-inspired approaches to improve

the current state of engineering. Table 2.1 shows some examples of bio-inspired

techniques compared to their biological counterpart.

Table 2.1: Bio-Inspired Engineering with Nature Counterpart

Nature System	Bio-Inspired Engineering	Reference
Bird's Wing	Airplane Wing	
Biological Immune System	Computer Virus Auto Immune	[18]
Human learning process	Cognitive radios	[19]
Phylogenesis (evolution), Ontogenesis (development) Epigenesis (learning)	Self Repair Electronic Circuit	[20]
Human Control Architecture	Artificial Limb for Humanoid Robot	[21]
Insect Vision and Flight Behaviour	Complex autonomous navigation	[22]
Human Eyes Coordination	Tracking Camera System	[23]
Human Data Processing	Neural Network	[24]

In striving to improve e-nose instruments, we will extract some of the

features in the biological nose that we believe will improve odour discrimination in

our electronic noses. As mentioned in chapter one, nasal cavity functions as a

temperature conditioning and filtering area. It preconcentrates the odour to prepare it for sensing. To mimic this, we will implement an air filter and preconcentrator to collect the tested odour before the test begins. The function of the preconcentrator will be based on thermal desorption technique that will be described later in this chapter. This will prepare the odour for testing by collecting it for a period of time and then pulsing it through the sensor for a short period of time. This will give the sensor a fast initial response to the odour.

Another important feature is the temporal data produced from the mucus odour retention effect. Several researches have proved this idea [4-6] and several researches have also incorporated gas chromatography column within their system in order to take advantage of this information [25-27]. However, all these researches use chromatography to completely separate the data before detection. We suggest a different approach to this, using dual gas chromatograph column coated with a different stationary phase to partially separate the data enough to give different temporal information between two differently coated columns. The advantages of this technique are that a shorter column can be used, heated elements of chromatograph can be eliminated and smaller systems can be developed. Since we are aiming to implement this biomimetic system as a portable/handheld system, these criteria are important in achieving our target.

The third factor that can be emulated to get better odour discrimination is the diversity of the olfactory receptors. With over 1000 different olfactory proteins, humans are able to detect 10000 different smells [28, 29]. As we know, a dog's sense of smell is far more sensitive than the human olfactory system, partly because of the huge number of olfactory receptors even compared to humans (in the dog genome

5% is given over to olfactory receptors, in humans its only 1%). As discussed before, several researches have suggested that higher number of sensors do contribute to higher sensitivity. Due to this, we propose a large sensor array with a diverse range of polymer to mimic the diversity of human olfactory epithelium.

Overall, we are trying to mimic the human nose by mimicking the feature as in the table below. This research will focus on mimicking the nasal cavity, mucosa, epithelium, and receptor. Another research being run parallel to this is going to investigate olfactory bulb and olfactory cortex by finding novel ways of processing spatio-temporal data gathered from this project.

Table 2.2 : Function similarity between Human Nose and E-Nose component.

Human Nose	Electronic Nose
Nasal Cavity	Pre-Concentrator
Nasal Mucous	Retentive Column
Olfactory Epithelium	Large Sensor Array
Olfactory Receptor	Chemo Resistive Sensor
Olfactory Bulb	Signal Processing
Olfactory Cortex/Brain	Pattern Analyzer

2.3 System Module

In short, our effort on mimicking the biological olfactory system will focus on three areas, namely preconcentration, spatio-temporal information from the nasal chromatograph effect and increasing the number of sensor to increase data

diversity. Here, we will review current technology in all these areas and propose reasons for selecting specific types of each method.

2.3.1 Micro gas sensor array

As discussed in Chapter 1, there are various configurations used in chemical detection in an electronic nose, but perhaps the simplest type is the chemical resistor (also called a chemoresistor) in which a change in the electrical conductivity of a chemical-sensitive layer is measured when exposed to a odour.
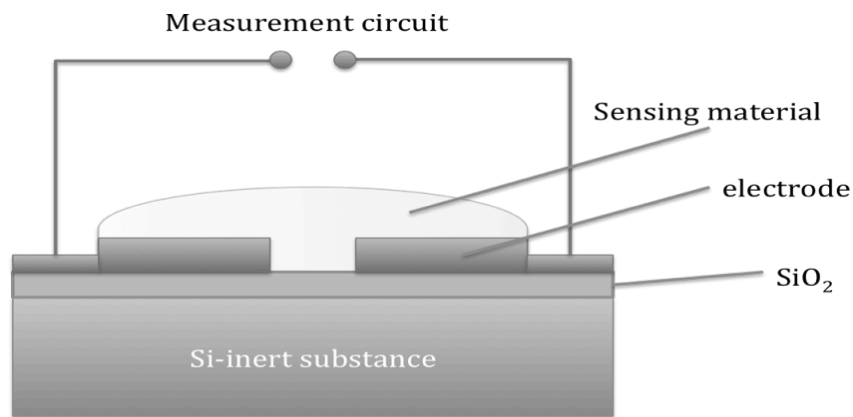
Figure 2.1: General structure of a chemical resistive gas sensor

Figure 2.1 shows a schematic chemical resistive sensor structure, a simple structure with two metal electrodes covered with chemically reactive sensing material. Various sensing materials are available for use as the gas reactive material such as metal oxide, carbon nanotubes [30, 31], carbon black composites [32, 33] and conducting polymers [34].

Metal oxide was one of the common materials used as gas sensor. Metal oxide sensors operation is based on a change in conductance of the oxide during interaction with a gas. There are basically two types of MOS sensor, n-type and p-type. The n-type sensor principles is that when oxygen (O_2) reacts with the surface of

the sensor and traps any free electrons on the surface, a large resistance in these areas is produced due to the lack of carriers. However, if the sensor is introduced to a reducing gas like H_2, CH_4, CO the resistance drops because the gas reacts with the oxygen and releases an electron. This lowers the potential barrier and allows the electrons to flow, thereby increasing the conductivity. P-type sensors respond to oxidising gases like O_2, NO_2, and Cl_2 as these gases remove electrons and produce holes.

Although metal oxides, such as tin dioxide, generally have a fast response and recovery time as demonstrated by Lewis and Doleman[33], it requires high operating temperatures of 250°C to 500°C to have good sensitivity and reasonable response time. The disadvantage of MOS is its poor selectivity and being able to operate only at high temperatures means that it consumes more power.

2.3.2 Carbon Black Polymer Sensor Review

Carbon-black composite polymer materials differ from conducting polymers in a number of ways. The intrinsic material properties of conducting polymers allow electricity to pass through them. In comparison the polymer component of composite polymers is actually an insulator. It is the addition of carbon black, which form electrical bridges through the material, that creates a semiconducting material whose properties change with exposure to vapours. This semiconducting behaviour is believed to be a result of swelling of the polymer. When the composite is exposed to a vapour, it is absorbed into the polymer (based on interaction with chemical components in the vapour) resulting in the polymer swelling. This swelling reduces the number of conducting bridges through the material and the resistance of the composite increases.

The use of carbon black in gas sensing was first described in 1986 by B. Lundberg and B. Sundqvist while they were examining effects of hydrostatic pressures on these composite materials. They have predicted that the material studied has a wide range of potential applications for pressure measurements and as a transducer for gas or liquid concentration [35]. Further research showed polymers loaded with conductive filler near the percolation threshold, (which is the volume fraction mark from where the resistance drops sharply with a small increase in filler volume fraction), swell reversibly in the presence of liquid and gaseous solvents, disrupting the conductive pathways and proportionally increasing the resistance[36]. The magnitude of the swelling, which is related to the magnitude of resistance change, depends on the solubility of a given solvent in the polymer. The recovery time was usually longer than the response time, and could be greatly enhanced by heating the sensor to release the odour.

The response time of the sensor is determined primarily by the thickness of the sensing material, sample volatility and fusion behaviour of the solvent. In the experiment performed in 1996 by Lewis, fabrication of the sensor was performed by dipping it into a solution of dissolved polymer and suspended carbon black[37]. The proportion of the polymer, carbon black and the solvent should be quantitative according to the properties of the analyzed objects. This allows accurate control over the electrical properties of the sensing element by controlling the conductor/insulator ratio in an individual chemo resistor.

Lewis et al. have found that as the carbon black contents of the films were lowered towards their respective percolation thresholds, the baseline conductance of the composites decreased. So the magnitude of the maximum relative differential

resistance response, $\Delta R_{MAX}/R$ (where R is the baseline resistance of the film prior to exposure to the solvent and ΔR_{MAX} is the maximum differential resistance signal) depends upon the constant partial pressure of analyte, which increased as the conductor/insulator ratio decreased [37]. The resistivity of the carbon black polymer composite could be predicted by percolation theory [38]. The advantage of using sensing element whose conductivity is controlled by percolation is that their conducting properties could be readily controlled through changing the composition of the composites. Also by working near the percolation threshold, a very good sensitivity could be achieved in response to tiny changes in vapour pressure, though this is highly non-linear.

Further research by Lewis in 1998 investigated the diversity in a series of carbon-black composite polymer sensors array, each of which blends two compatible organic polymers, with different ratio, as the organic polymer film [33]. Poly(vinyl acetate) and poly(methyl methacrylate) were mixed at various ratios with carbon black. The electrical resistance was found to have a non-linear relationship with respect to the mole fraction of poly (vinyl acetate) in the blend which means the additional discrimination information can be obtained by the blended polymers compared to the reference detector with identical polymer phases. The utilization of a combined polymer phase with two, three, or more polymers blended together is likely to increase the diversity of the composite detector array and therefore, increases its classification performance. Doleman et al. proposed the idea that exploitation of the extensive diversity of a polymer-based vapour-sensing array would be a crucial approach to achieving mimicking human olfactory sense system.

This is one of the primary reasons of choosing carbon black polymer composite as our sensing material.

Further research by Doleman et al. compared carbon black composite sensors, with bulk organic conducting polymer (CP) and tin oxide sensors [33]. Fourteen carbon black sensors, twelve bulk organic CP, and eight tin oxide sensors were tested by resolving 19 solvent specimens. Results indicated that the resolving power of carbon black composite sensor arrays was significantly better than the tin oxide and bulk conducting polymer sensing arrays.

Continued research on carbon black sensor arrays investigated the relationship between its vapour classification performances vs. the number and type of detectors in an array [39]. Excellent classification characteristic of small size sensing array could be achieved under concentrations to produce high enough signal/noise ratios for pure analyte vapours. In the more complicated environment, such as low concentration, high noise, more detectors would be needed. It is shown that generally the classification performance would be enhanced, at least not reduced, as the number of chemically different detectors increased. Reduction in dimensionality was advantageous just when the task was identified in advance, because multiple copies of detectors had performed this given task before. The system had yielded the best training set classification performance compared to the same total number of compositionally different detectors. Furthermore, the excellent analyte discrimination power of an array of semi-selective chemical resistive vapour sensors was observed at least in certain tasks even if no single sensing unit could provide the necessary chemical resolution to differentiate the analytes.

In this research, we have particularly selected carbon black as our sensing material for several reasons but the main reason for choosing carbon black composite is the convenience of using the same polymer with different proportions to create a different set of chemical sensor. With this ability, we are able to generate a diverse set of sensor with only several polymers. Furthermore, carbon black composites works at room temperature with is important factor in designing a portable instrument that has to have low power consumption.

2.3.3 Gas Chromatography Overview

Gas chromatography (GC), is a common type of chromatography used for separating and analyzing compounds that can be vaporized without decomposition. Martin suggested gas chromatography possibility in a paper on liquid chromatography published in 1941[40]. Later in 1952, he published the first gas chromatographic separation, separating a series of fatty acids using titration procedure in conjunction with a micro burette, as the detector [41]. Now, GC has evolved into a more complex instrument mostly controlled with a computer. Some factors that have been investigated extensively to improve the GC system include temperature programming, stationary phase selection, length and dimension of column, and pre-concentration method.

An important component in gas chromatography is the stationary phase around the wall of the column. The most important factor determining the separability of two analytes lies in their difference in partition coefficient with the stationary phase coating. Partition coefficient is the equilibrium distribution of an analyte between the stationary phase and the odour gas phase and is determined by the constant ratio of the solute's concentration in the stationary phase to its

concentration in the mobile gas phase. This is an important factor because the retention power of the column depends on the reaction of the stationary phase and the odour flowing through the column. There are many materials available for use with gas chromatograph as the stationary phase in various groups such as polar, non-polar and ionic. Abraham has developed an extensive list of stationary phase materials along with the partition coefficient of each material [42, 43]. Stationary phase selection and coating technique will be described further in Chapter 4.

One of the challenges of early GC instruments is the length of column, which at around 10-30m produced long analysis times. Trying to improve the speed of analysis, Golay presented the idea of fast chromatography or High Speed Gas Chromatography (HPGC) in 1958. Since Golay first discovered fast chromatograph, many researches have been done to improve the performance of gas chromatography (GC) while decreasing its size. Research on fabrication of microchannel for GC has been very active since 'micromachining' technology was introduced. In 1979, Terry introduced an all in one gas analyzer with a GC column built onto a silicon wafer, then sealed with anodic bonding. One of the most common methods of creating a micro-GC column is by etching the silicon wafer or glass and subsequently sealing/bonding them together. High-quality micro channels with high-aspect ratio have been developed by bulk silicon micromachining followed by fusion bonding [44, 45], and in another research, using anodic bonding [46]. Some other method of creating micro channels has also been studied including polydimethylsiloxane (PDMS) based channels [47], photo patterned epoxy(SU-8) technique [48] and parylenemicromolded channels [49]. These methods have the advantages of being photo-patternable, low fabrication temperature and ease of

processing over traditional silicon etching. Another method that has been shown to produce high aspect ratio structures of very good quality and surface roughness and has the ability to use materials other than silicon is Lithography Galvonoforming Abforming (LIGA). Bushan have demonstrated a micro GC column created with LIGA technology that was able to separate four compounds in just 2 seconds[25].

The reason gas chromatography is discussed here is that the retentive column designed for this system is based on gas chromatography principles. The only difference is that we are not trying to achieve perfect separation of gas, but simply to gain additional information which could be used to aid the identification of a vapour sample.

2.3.4 Microfabrication Overview

Another area that has seen considerable advancements in the last 30 years is the rapid prototyping industries. Rapid prototyping is the automatic construction of physical objects using solid freeform fabrication. As the name suggest, rapid prototyping is used to rapidly produce a prototype by automatically constructing the object using special material. Rapid prototyping has been studied extensively with various prototyping technique available such as Selective laser sintering (SLS), Fused deposition modeling (FDM), Stereolithography (SLA), Laminated object manufacturing (LOM), Electron beam melting (EBM) and 3D printing (3DP). Here, we are going to focus on stereolitography which is one of the more common methods of RP.

Stereolithography is a common rapid prototyping technology for producing parts rapidly with high accuracy and good surface finish. Streolithography is an

additive process whereby a UV curable photopolymer or resin is cured by a UV laser to build parts a layer at a time.

Conventional stereolithography rapid prototyping machine have low resolution (typically > 250 μm). Recently, these systems have been improved to create high-resolution processes employing fine lasers to fabricate components with micrometer resolution. In this research, this technology has been employed to fabricate many of the micro components in this system including the micro retentive gas chromatographic channel package. A more detailed description of this technique called 'Micro Stereo Lithography' will be described in Chapter 4 with all the micro components created with this technique.

2.4 Spatio-Temporal Information

The proposed system is based on spatio temporal information obtained by adding a retentive column along the sensor array to produce the 'nasal chromatograph' effects. Figure 2.2 shows the concept of a system with one retentive column in between the sensor arrays to produce the spatio-temporal signal.

The concept of generating spatio-temporal signal for use in the e-nose has been previously studied. Briglin from Caltech build a system with individual sensors arrange along a micro channel [50] as a way to generate spatio temporal response. The sensor response of each sensor will be slightly delayed between each sensors as the odour pass through the columns reaching the sensors in sequence. Furthermore, the molecule of odour will be absorbed by the sensors along the way making the response magnitude decrease as the odour reach the end of the column.

Similar experiments have also been done by Tan at the University of Warwick. However, in Tans' experiment, the column is coated with stationary phase similar to the one used in gas chromatography. This stationary phase added an extra retention to the odour on top of the delay created by the absorbed odour molecule by the sensors sensing film. These two experiment proof the concept of generating spatio temporal response in e-nose to improve the odour discrimination power[51].
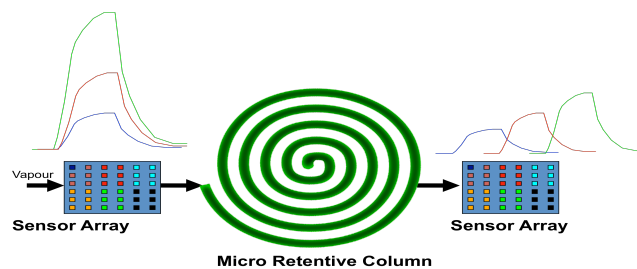
Figure 2.2: Concept of Spatio-Temporal Signal Generation

The term 'Spatio-temporal' response as used here, means that the response contains both space (magnitude of the response) and time (response delay) information. In the concept diagram in Figure 2.2, the initial array containing a large number of sensors will produce a high spatial response to the odour introduced. These large sensors arrays are coated with different gas sensitive materials to obtain a diverse set of responses. Some of the odour passing through the first arrays will be absorbed by the sensitive film on the sensors.

Subsequently, the odour will travel through the coated micro retentive columns into chemo sensor arrays. The second/end sensor arrays are coated with the same gas sensing materials in the same manner to show the differences between responses before and after the gas micro retentive column. The end array, after the column, will produce another set of spatial responses but with lower response magnitudes due to the sample flowing over the sensors at any one time having a

lower concentration (though the total number of sample molecules remaining constant). This is due to the micro retentive column having a band broadening effect creating a wider response with lower magnitude.

The temporal signal is generated by the micro retentive columns in between the sensor arrays. To further improve the system, the column is coated with stationary phase that will react with tested odour. As mentioned before, in a GC column, various stationary phases can be used such as polar, non-polar and ionic. Generally, polar coatings will react with polar compound delaying the compound travelling through the column. Similarly, the non-polar coated column will delay non-polar compounds more than a polar compound. The use of different polarity material as the stationary phase will produce different delays if a similar complex odour is introduced thus generating a different set of spatio-temporal response on the sensor array connected to it.

A wide diversity of information can be gathered from a system as in Figure 2.2. Spatial information with various tunings is acquired from the two sensor array while temporal information is collected from the response of the second sensors array. Furthermore, changing the properties of the retentive column can also provide more information regarding the temporal response. Similar to GC column, properties such as column length, column dimensions, stationary phase coating material, and column temperature contribute to the performance of the retentive column.

2.5 Conclusion

Here we reviewed the technology mainly used in this research, namely carbon black polymer composite sensors, gas chromatographic columns and MSL technology. A

more detailed description of these technologies and how they are used to obtain our goal is discussed in the next few chapters. It is clear that carbon black polymer composites have very good potential in the chemosensor field due to its flexibility to use different polymers and the sensitivity of the composite itself. Furthermore, the ability to be used at room temperature is really important in order to build a portable instrument that has low power consumption.

However, the disadvantages of this material are the slow response time unless submicron layers are used. The main focus of this study is to acquire temporal information as well as spatial information to further improve e-nose instruments. To generate spatio-temporal signals, a retentive column, similar to the GC column is proposed. This column will delay the odour going through it, generating temporal information that is captured by the two sensor array as in Figure 2.4.

There is huge advancement in the area of MSL technique and now more commercial machines are available for research such as the Envisiontec Perfactory Mini allowing research to progress faster.

The next few chapters will discuss the design and fabrication of individual components in the instrument, focussing on the large sensors array and micro retentive column.

2.6 References

1.   T.C. Pearce, H. T. Nagle, J.W. Gardner, *Handbook of Machine Olfaction*. 2003: Wiley.
2.   Quignon, P., et al., *Comparison of the canine and human olfactory receptor gene repertoires.* Genome Biology, 2003. **4**(12): p. R80.
3.   M.C. Burl, T. P. Vaid, N. S. Lewis, *Classification performance of carbon black-polymer composite vapor detector arrays as a function of array size and detector composition.* Sensors and Actuators B: Chemical, 2002. **87**: p. 130-149.

4. M.M. Mozell, and M. Jagodowicz, *Chromatographic Separation of Odorants by the Nose: Retention Times Measured across in vivo Olfactory Mucosa.* Science, 1973. **181**(4106): p. 1247-1249.

5. M.M.Mozell, , *Evidence for a Chromatographic Model of Olfaction.* J. Gen. Physiol., 1970. **56**(1): p. 46-63.

6. M.M.Mozell, , Sheehe, P.R., Hornung, D.E., Kent, P.F., Youngentob, and a.M.S.J. S.L., *"Imposed" and "inherent" mucosal activity pattern. Their composite representation of olfactory stimuli.* Journal of Gen Physiol, 1987. **90**(5): p. 625-650.

7. L. Buck, and R. Axel, *A novel multigene family may encode odorant receptors: A molecular basis for odor recognition.* Cell, 1991. **65**(1): p. 175-187.

8. T.Shoji, et al., *Olfactory responses of a euryhaline fish, the rainbow trout: adaptation of olfactory receptors to sea water and salt-dependence of their responses to amino acids.* J Exp Biol, 1996. **199**(2): p. 303-310.

9. F Laberge, *Neurobiology of fish olfaction: a review.* Brain Res Brain Res Rev., 2001. **36**: p. 46-59.

10. D.A.Wilson, *Fish Smell. Focus on "Odorant Specificity of Single Olfactory Bulb Neurons to Amino Acids in the Channel Catfish".* J Neurophysiol, 2004. **92**(1): p. 38-39.

11. L.Tite, *How does your dog smell? Olfactory detection of human bladder cancer.* STUDENTBMJ, 2004. **12**.

12. W.A.See, , *Olfactory detection of human bladder cancer by dogs: proof of principle study: Willis CM, Church SM, Guest CM, Cook WA, McCarthy N, Bransbury AJ, Church MR, Church JC, Department of Dermatology, Amersham Hospital, Amersham, United Kingdom.* Urologic Oncology: Seminars and Original Investigations, 2005. **23**(3): p. 217-217.

13. L. B. Buck, *Olfactory Receptors and Odor Coding in Mammals.* Nutrition Reviews, 2004. **62**(s3): p. S184-S188.

14. B.S.Hansson, , *A bug's smell - research into insect olfaction.* Trends in Neuroscience. , 2002. **25**: p. 270-274.

15. L.B.Vosshall, , *Olfaction in Drosophila.* Current Opinions in Neurobiology, 2000. **10**: p. 498-503.

16. L.B. Vosshall, A.K., *Decoding olfaction in Drosophila.* Current Opinions in Neurobiology 2003. **13**: p. 103-110.

17. K.Sato, et al., *Insect olfactory receptors are heteromeric ligand-gated ion channels.* Nature, 2008. **452**(7190): p. 1002-1006.

18. J.Kephart, *A biologically inspired immune system for computers*. 1994: MIT Press.

19. C.Rieser, *Biologically inspired cognitive radio engine model utilizing distributed genetic algorithms for secure and robust wireless communications and networking*. 2004.

20. Y.Thoma, et al., *POEtic: an electronic tissue for bio-inspired cellular applications.* BioSystems, 2004. **76**(1-3): p. 191-200.

21. S.Northrup, N. Sarkar, and K. Kawamura. *Biologically-inspired control architecture for a humanoid robot*. 2001.

22. G.Barrows, J. Chahl, and M. Srinivasan, *Biologically inspired visual sensing and flight control.* Aeronautical Journal, 2003. **107**(1069): p. 159-168.

23. Y.Yamaguchi, et al., *A bio-inspired tracking camera system.* Artificial Life and Robotics, 2007. **11**(1): p. 128-134.

24. L.Long, and A. Gupta. *Biologically-Inspired Spiking Neural Networks with Hebbian Learning for Vision Processing*, Aerospace Sciences Meeting, 2008.

25. A.Bhushan, et al., *Fabrication of micro-gas chromatograph columns for fast chromatography.* Microsystem Technologies, 2007. **13**(3): p. 361-368.

26. J.A.Ragazzo-Sanchez, P. Chalier, and C. Ghommidh, *Coupling gas chromatography and electronic nose for dehydration and desalcoholization of alcoholized beverages: Application to off-flavour detection in wine.* Sensors and Actuators B: Chemical, 2005. **106**(1): p. 253-257.

27. C.J.Lu, et al., *Portable Gas Chromatograph with Tunable Retention and Sensor Array Detection for Determination of Complex Vapor Mixtures.* Analytical Chemistry, 2003. **75**(6): p. 1400-1409.

28. B.Malnic, et al., *Combinatorial receptor codes for odors.* CELL-CAMBRIDGE MA-, 1999. **96**: p. 713-724.

29. L. Buck , R.Axel, *A novel multigene family may encode odorant receptors: A molecular basis for odor recognition.* Cell, 1991. **65**: p. 175-187.
30. S.Y.J.Kay Hyeok, , *Enhanced Sensitivity of a Gas sensor Incorporating Single Walled Carbon Nanotube – Polypyrrole Nanocomposites.* Advance Materials, 2004.
31. E.L. Ashis Modi, , *Miniaturized gas ionization sensors using carbon nanotube.* Nature, 2003. **424**.
32. B. J. Doleman, E. J. Severin, T. P. Vaid, and Nathan S. Lewis, *Quantitative Study of the Resolving Power of Arrays of Carbon Black-Polymer Composites in Various Vapor-Sensing Tasks.* Analytic Chemistry, 1998. **70**: p. 4177-4190.
33. B.J.Doleman, et al., *Use of Compatible Polymer Blends To Fabricate Arrays of Carbon Black-Polymer Composite Vapor Detectors.* Anal. Chem., 1998. **70**(13): p. 2560-2564.
34. J.W.Gardner, *Application of conducting polymer technology in Microsystems.* Sensors and Actuators A, 1995. **51**.
35. B.Lundberg, and B. Sundqvist, *Resistivity of a composite conducting polymer as a function of temperature, pressure, and environment: Applications as a pressure and gas concentration transducer.* Journal of Applied Physics, 1986. **60**(3): p. 1074-1079.
36. G. R. Ruschau, J. Runt, and B. E. Smith, *O-3 Ceramic/Polymer Composite Chemical Sensors.* Sensors and Actuators, 1989. **20**: p. 269-275.
37. M.C.Lonergan, , et al., *Array-Based Vapor Sensing Using Chemically Sensitive, Carbon Black Polymer Resistors.* Chemistry of Materials, 1996. **8**(9): p. 2298-2312.
38. H-K Honga, D. H. Yuna, S.R Kima, C. H. Kwona, K. Leea, and and T. Moriizumib, Sensors and Actuators B: Chemical, 1996. **36**: p. 338-341.
39. M.C.Burl, , et al., *Classification performance of carbon black-polymer composite vapor detector arrays as a function of array size and detector composition.* Sensors and Actuators B: Chemical, 2002. **87**(1): p. 130-149.
40. A. Martin, and R. Synge, *A new form of chromatogram employing two liquid phases: A theory of chromatography. 2. Application to the micro-determination of the higher monoamino-acids in proteins.* Biochemical Journal, 1941. **35**(12): p. 1358.
41. A. T. JAMES , A.J.P.M., *Gas-liquid partition chromatography: the separationmicroestimation of volatile fatty acids from formic to dodecanoic acid.* J. Biochem, 1952. **50**: p. 679.
42. J.W.Grate, and M.H. Abraham, *Solubility interactions and the design of chemically selective sorbent coatings for chemical sensors and arrays.* Sensors and Actuators B: Chemical, 1991. **3**(2): p. 85-111.
43. M.H.Abraham, C.F. Poole, and S.K. Poole, *Classification of stationary phases and other materials by gas chromatography.* Journal of Chromatography A, 1999. **842**(1-2): p. 79-114.
44. A. Sayah, et al., *Development of novel low temperature bonding technologies for microchip chemical analysis applications.* Sensors and Actuators A: Physical, 2000. **84**(1-2): p. 103-108.
45. R.W.Tjerkstra , et al., *Etching technology for chromatography microchannels.* Electrochimica Acta, 1997. **42**(20-22): p. 3399-3406.
46. S.Terry , J. Jerman, and J. Angell, *A gas chromatographic air analyzer fabricated on a silicon wafer.* IEEE Transactions on Electron Devices, 1979. **26**(12): p. 1880-1886.
47. G.Subrebost, , et al. *In Situ Fabricated Microchannels Using Porous Polymer and Xenon Difluoride Etchant*. 2002.
48. R.Jackman, et al., *Microfluidic systems with on-line UV detection fabricated in photodefinable epoxy.* Journal of Micromechanics and Microengineering, 2001. **11**(3): p. 263-269.
49. H.Noh, Y. Huang, and P. Hesketh, *Parylene micromolding, a rapid and low-cost fabrication method for parylene microchannel.* Sensors & Actuators: B. Chemical, 2004. **102**(1): p. 78-85.
50. S.M.Briglin, et al., *Exploitation of spatiotemporal information and geometric optimization of signal/noise performance using arrays of carbon black-polymer composite vapor detectors.* Sensors and Actuators B: Chemical, 2002. **82**(1): p. 54-74.
51. S.L.Tan, *PhD Thesis*. 2005, University of Warwick. p. 260.

CHAPTER 3

The design and fabrication of large chemoresistive sensor arrays

3.1 Introduction

In Chapter 2, we explained the inherent advantages given by employing a large sensor array, predominantly the significantly richer information available compared to a lesser array. Previously, many researchers have studied and produced high density sensor arrays[1-4]. Furthermore, it has been shown that a set of identical sensors coated with the same material can create redundancy that is useful during data processing. For example, sensor selection can be made to eliminate sensors with poor responses (due to poisoning or aging), or signal averaging on the set of sensors to improve the dataset. Here we discuss the design and fabrication of large chemo sensor arrays that consists of up to 300 sensors, coated with 24 different conducting polymers.

3.2 Sensor Array Design

The development of the sensor arrays can be divided into two distinct steps; the fabrication of the sensor substrate and the deposition of sensing material.

Although the basis of the chemoresistive sensor is simple, comprising of two electrodes with a sensing material deposited on top, developing a large sensor array

brings along its own difficulties of encapsulation, fabrication and cross talk, as discussed below.

3.2.1   Design of chemoresistive sensor substrate

The structure of an individual chemoresistive sensor was presented in Figure 2.1, where a sensor consists of two metal electrodes with a small gap (typically between 10 µm to 100 µm) in between them. On to the electrodes a gas sensitive film is deposited; in our case, a carbon black polymer composite. As stated previously, in the case of carbon black composites, when the sensing film is exposed to a test vapour, the film swells depending on the polymer/vapour interaction and the concentration of the vapour. These swelling increases the resistance of the film, through a reduction in conducting bridges, formed by the carbon, through the sensing film. The sensitivity and selectivity can be modified by changing the polymer, as the vapour/polymer interactions are polymer specific. Carbon black polymer composites are now widely used in gas sensors [1-3]. A standard response of a carbon black composite chemoresistive sensor is shown in Figure 3.1.
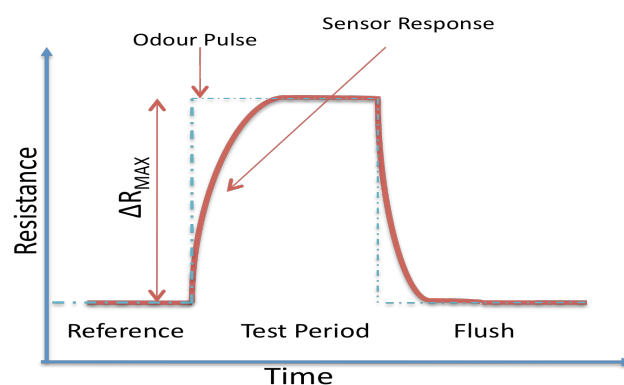
Figure 3.1: Basic response of a chemo resistive sensor

Initially, the sensor is exposed to a reference gas (usually air or a carrier gas, such as N_2 or Ar), followed by a pulse of test gas (shown by blue dotted line). Once the

vapour reacts with the sensing film, the sensor starts to swell and will increase in resistance until the vapour within the polymer is in balance with those in the air. The sensor response is the difference between the resistance in the reference gas and the maximum resistance, when exposed to a test vapour, shown as R_{max}. Finally, the gas sensor is flushed with air again to remove all the test vapour on the sensor. The recovery time is the time it takes for the sensor to reach its reference resistance from its maximum resistance (though in data processing we would normally take the time to fall to 10% of the initial resistance – or t90).

Since carbon black composite materials work at room temperature, a temperature sensor is built onto the design to monitor the temperature of the chip during tests.

The resistive sensor structure is the simplest of all the sensor structures, and is compatible with silicon processing. A multi layer metal structure, as in Figure 3.2, has been employed in the sensor design to make rooting easier. Another important element is pad sharing, where some of the sensors share the same pad electrode. This will reduce the number of pads required, making data acquisition for the large sensor array easier. The gap distance between the electrodes and the size of electrodes are also taken into consideration in the design. By having a high aspect ratio (width of channel / length of channel), the resistance of the material would be reduced, and it is easier to measure small changes in resistance when the initial value is low (1kΩ-100 kΩ) [4].
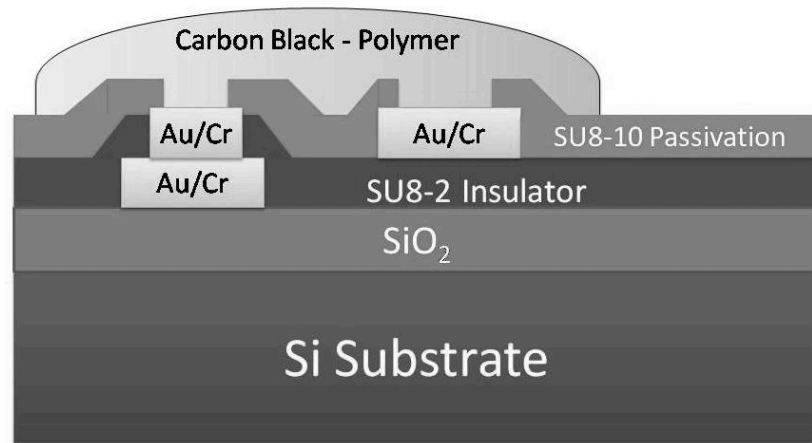
Figure 3.2: Basic Structure of single gas sensor

Some design considerations are taken into account while determining the dimension of the electrode and the gap between electrodes. Firstly, the minimum resolution is 5 μm in the silicon fabrication laboratory here at the University of Warwick. Hence, adhering to the width rule, overlap rule, and space rule in CMOS layout design, the resolution in this design is 20 μm and spacing distance of two electrodes is 30 μm in order to guarantee the gap between two metals [5].

To further avoid sensing material cross-contamination, there is a space of 200μm in the horizontal direction and 250 μm in the vertical direction between two sensors, as shown in Figure 3.3.
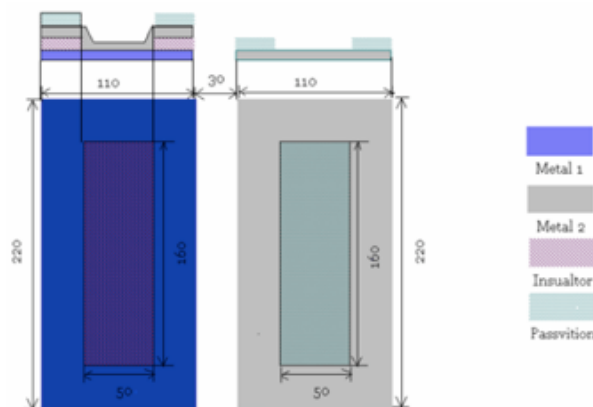
Figure 3.3: Dimension of individual sensor

Another design consideration is crosstalk between electrode/sensors, where electromagnetic noise is transmitted between leads or circuits in close proximity to each other. Gas micro sensor arrays often have closely-spaced elements, in our case just 20-250 micron gaps. Cross-talk between elements operated within a gaseous environment is possible because sensing materials held at elevated temperatures have an increased probability for disrupting gas flows and activating gas-film interactions that can consume analytes or evolve reaction products [6]. To reduce the cross talk, several strategies have been employed, including maximizing the trace space between lines to reduce the possibility of cross talk when controlling the temperature. Pad size was chosen at 220 μm and the spacing between pads was 30 μm. The final dimensions chosen for a single individual sensor pad is as follows.

Table 3.1: Pad Dimensions (unit : μm)

Layer	Pad 1	Pad 2	Pad Temp Sensor
Metal 1	220 x 220	n/a	500 x 500
Metal 2	220 x 220	220 x 220	500 x 500
Insulator Opening	160 x 160	n/a	420 x 420
Passivation Opening	140 x 140	140 x 140	380 x 380

Using these dimensions as a guideline for a single sensor, we have designed several sensor arrays with different sizes so that different sensor arrays could be used for different applications (though only the 300 sensors were used here). Alignment marks, as in Figure 3.4, allow the precise alignment of the mask with the pattern on the wafer. Layers are not necessarily aligned sequentially to a preceding layer, but to some important previous layer. In this design, the target layer for all further layers is Metal1, thus the precision control is realized by covering the hole of alignment mark

on target layer with the shape on alignment of matching layer, and vice versa. The

two alignment keys are distributed symmetrically on the two sides of the wafer, the

longer the distance departed from each other, the higher rotational resolution.
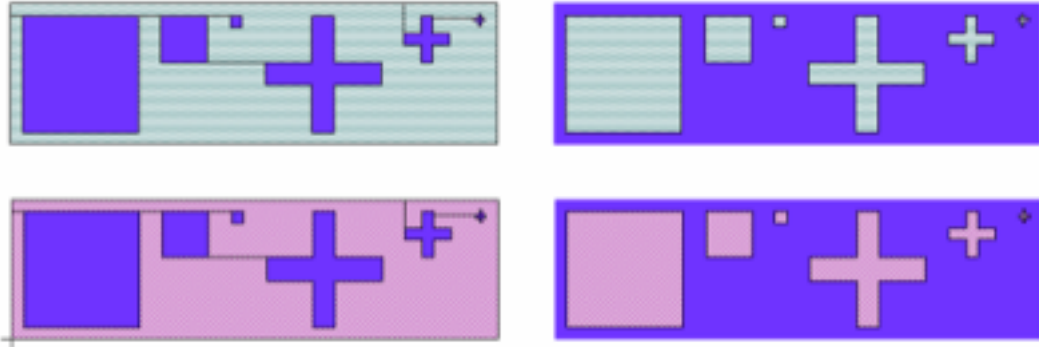
Figure 3.4: Alignment mask for large sensor array

The final wafer design, as shown in Figure 3.5, contains thirteen 300 sensor

arrays (in array of 25 rows by 12 columns), eleven 150 sensor arrays (25 rows by 6

columns), and eleven 75 sensor arrays (25 rows by 3 columns), with die dimensions

13mm × 8.5mm, 13mm × 5.5mm, and 13mm × 4mm respectively. All these sensor

arrays have integrated temperature sensors based on a gold resistor. The dimensions

for the temperature sensor pads are shown in Table 3.1. This design was done in

Tanner EDA L-Edit v11 and was used to generate photo masks for fabrication

purposes.
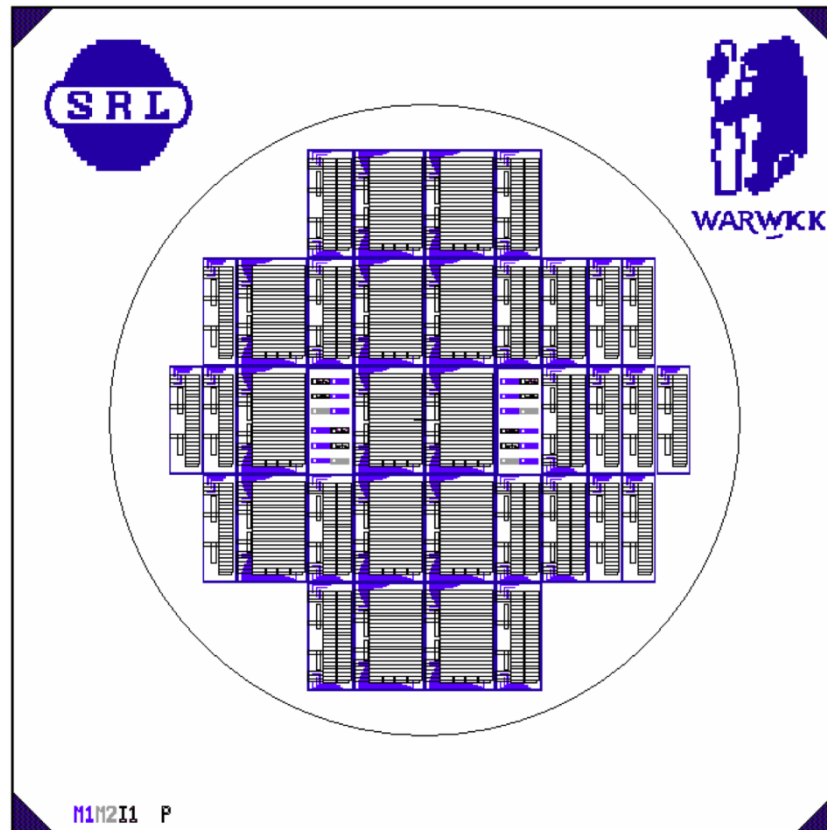
Figure 3.5: Final wafer design with several sensor array sizes

3.2.2 Multiplexed Array Pad Design.

The sensor array design is laid out in a matrix configuration (12 columns and 25 rows) to reduce the pad count. If a single sensor used 2 electrode pads each, this will come to a total of 602 pads including the temperature sensor. This would make packaging and data acquisition very difficult. Hence, a multiplexed system has been implemented to obtain 300 sensors with only 37 multiplexed pads plus 2 pads for the temperature sensor. In this configuration, the unilateral electrodes in one sensor share the pads with the sensor electrodes in the same row or column. The resistance signal of each sensor in the array is then measured by scanning the array in a sequential order. This is the main reason multi metal layer configuration is used, where it separates traces for electrode one and two with an insulation layer.
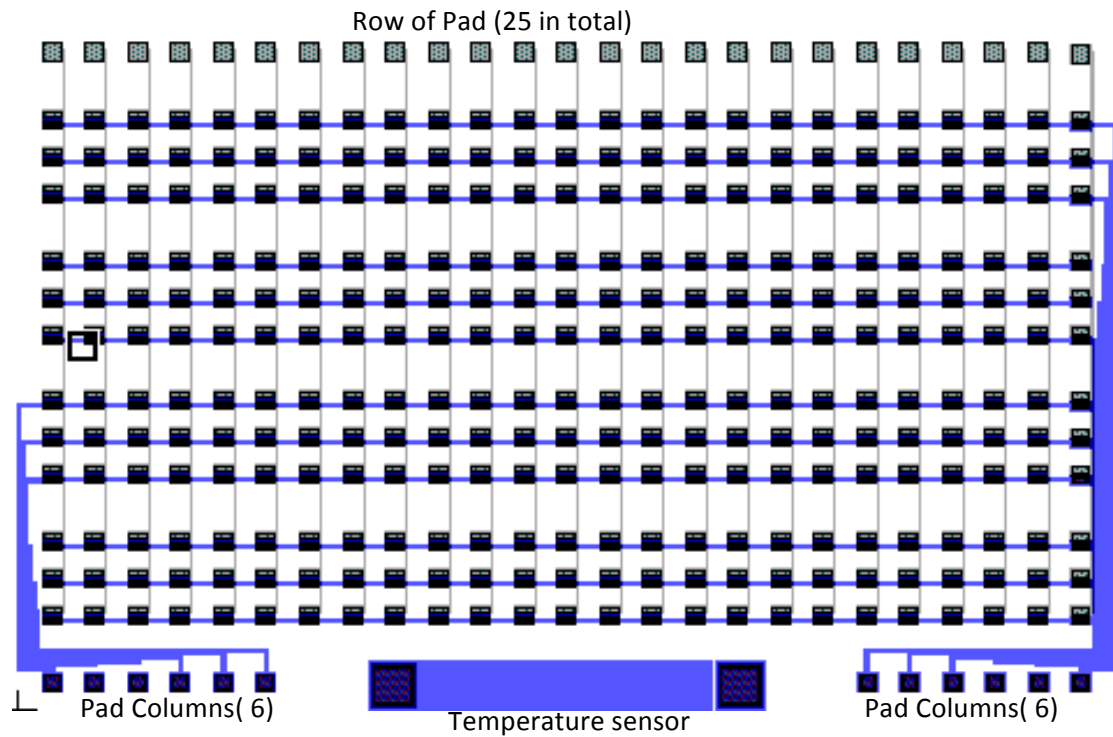
Figure 3.6: Array of 300 sensors in 25 x 12 configuration

Every sensing element was assigned an address, comprised by a row index and a column index. Figure 3.6 displays all 300 sensors with a 25 × 12 configuration. This combination of row and column addressing will be utilized when designing data acquisition circuit for this array. A low number of pads would also mean less switching for any sensing circuitry, which will improve the overall speed of the system.

However, one potential problem with this structure is the long distance transmission effect. The transmission trace has its own resistance, so there would be a baseline difference between the sensors nearest to and furthest from the pad. To resolve this, the transmission line trace width was increased to 70 μm in order to decrease the transmission line resistance.

3.3 On Board Temperature Sensor

A temperature sensor was integrated onto the sensor array chip to monitor the temperature during testing. A sensor heater is implemented on the PCB package instead of on board the chip. One of the main reasons is that carbon black composite sensor have the highest sensitivity at room temperature (or lower). However, we are still implementing the PCB heater to improve sensor flushing in order to decrease recovery time and to ensure that the sensors are at a constant temperature (to improve repeatability). Another reason is the fact that integrating a heater underneath the sensor would make the fabrication process more complex as an additional metal layer is required.

3.3.1 Gold Resistive temperature sensor

As mentioned before, the on board temperature sensor is based on the thermal resistivity of gold. Above 220°C, the relationship between temperature and resistivity, r, is nearly proportional and is determined by electron-phonon scattering, whereas, at a very low temperature (around < -200°C), r is independent of temperature due to electron-impurity scattering [7]. The linear condition covers a wide range of -220°C to +1000°C. Hence, a gold metal resistor can be employed since we are only running the sensor near room temperature. Temperature based on resistive material, gold in this case, can be calculated with the following formula[8],

$$R = R_0 \left[1 + \alpha(T - T_0)\right] \qquad \dots (eq\ 3.1)$$

where

R = Resistance at temperature, T
R_0 = Initial Resistance
α = Temperature coefficient of Gold
T = Temperature in degree Celsius
T_0 = Initial Temperature in degree Celsius

The linear relationship between the resistivity of gold and temperature is shown in Figure 3.7 where the gold resistivity is displayed over the temperature range of 0 through 900K[9].
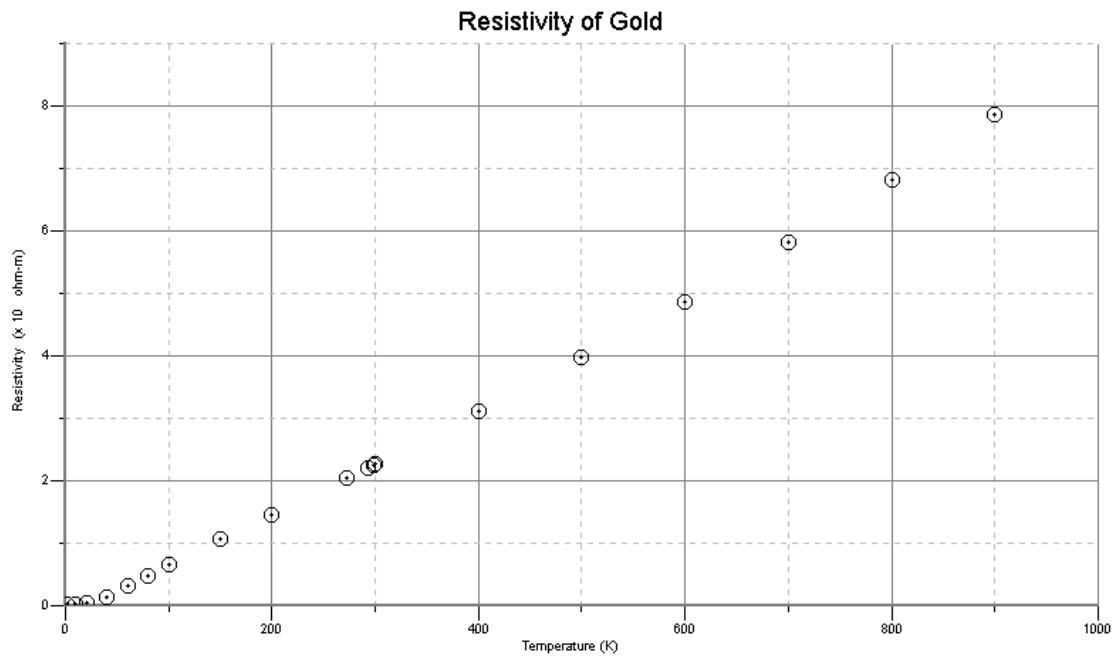
Figure 3.7: Gold resistivity vs Temperature [9].

The temperature sensor is designed in folded design as in Figure 3.8 with a total length of 39040 µm and width 20 µm.
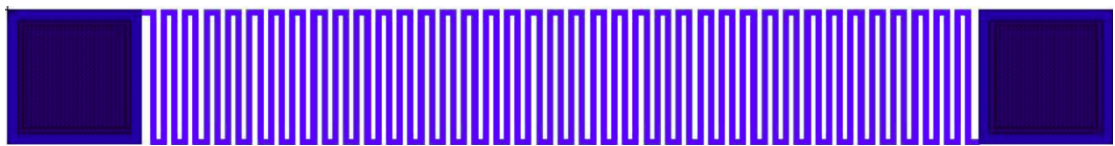
Figure 3.8: Gold temperature sensor design layout

The resistance of a rectangular region is given by[10],

$$R = \rho_n (\frac{L}{Wt})$$

…(eq 3.2)

Where L = length, W= width, t = thickness and p_n = bulk resistivity (Ω-m). Calculating

the resistance of the temperature sensor at room temperature =20°C (p_n=2.049x10^{-8}

Ω-m), L=39040μm, W= 20μm, t= 200nm we get the resistance as R ≈ 200 Ω. To get

the function of temperature in voltage, we simply use equation 3.1 with gold

temperature coefficient 3.4 x 10^{-3} / °C.

$$V=I\ (200\ [1+3.4\ x\ 10^{-3}\ (T-20)])\qquad …\ (eq\ 3.3)$$

In conclusion, the temperature sensor is designed using the thermal resistivity of

gold with the dimension of 39040μm x 20μm in folded design. The baseline

resistivity of 200 Ω at room temperature (assumed 20°C) is calculated and used to

get an equation where changes in temperature could be transduced to voltage.

3.4 Sensor Fabrication

The sensor was fabricated with a series of standard silicon processing techniques.

Using the layout design discussed in the previous section, photomasks have been

sent out for fabrication to a printing company (JDPhoto Ltd, UK) to print these masks

in high resolution on an acetate sheet. The acetate sheets are then attached to a

glass plate so to fit into the mask aligner.

The sensor arrays were fabricated using four photomask process: namely

metal1, insulator, metal2, and passivation layer. Figure 3.9- Figure 3.15 illustrate the

silicon processing techniques used to fabricate this device.
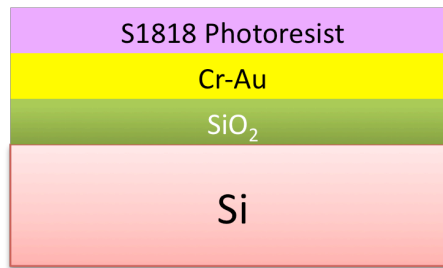
Figure 3.9: Silicon Oxide coated with Au and Cr layer with photoresist

The process is started by oxidizing 3 inch silicon wafer with 1 micron thermal silicon dioxide layer. Then, a 25nm layer of Cr is deposited onto the thermal oxide film followed by a 170 nm gold film. The thin layer of Cr is deposited first to improve adhesion between Au to the silicon wafer[11]. These thin films were deposited using metal evaporation technique with Edwards Auto 306 Thermal Evaporator. A 1.8µm positive photoresist Shipley S1818 is then spin coated on to the metal1 layer. After spin coating, the substrate with metal layers are put into a soft bake oven (90°C for 5 minutes) to clear out the solvent in the photoresist thus transforming the resist from liquid to solid state. The bake process can also improve adhesion to the substrate. After that, the wafer is left to cool before the next process. Figure 3.10 shows the substrate with all the coated layers.
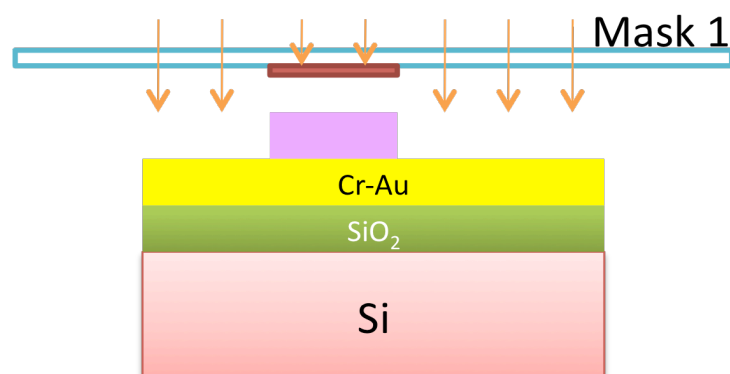
Figure 3.10: UV Light exposed through Mask 1

Using Karl Suss mask-aligner (Zeiss), photomask 1 (metal 1) was aligned to the wafer and exposed to 350nm UV light for 20 second (shown in Figure 3.10). This exposure steps in photolithography process transfers the desired pattern on the mask to the photoresist on the substrate. The appropriate exposure light wavelength of the UV light must be chosen carefully according to the photoresist sensitivity. Normally, the shorter the wavelength, the better the patterning resolution while the thickness of the photoresist material determines the exposure time. The substrate is then placed in an oven for a hard bake (120°C for 1 hour).
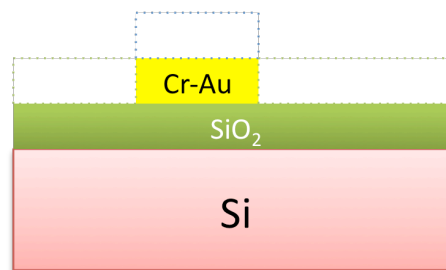
Figure 3.1: Etching process removing Metal1

The next process is wet etching illustrated in Figure 3.11 to remove the exposed metal 1 layer from the previous process. It removes all the metal layers uncovered by the photoresist. Wet etching is done by dipping the substrate in Au etchant for 30 seconds to remove the Au and another two minutes to remove Cr layer (in a Cr etchant). Subsequently, acetone and IPA is used to rinse and dry the substrate to remove photoresist and any residue on the substrate surface [12].
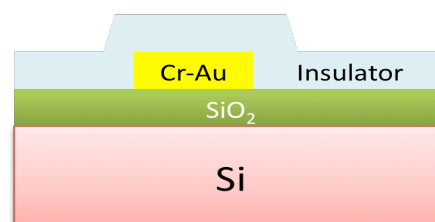
Figure 3.2: Coating substrate with insulator layer

The next step is coating the substrate with an insulator layer, as shown in Figure 3.12. SU8-2 was used as the insulator layer material, which is a non-conductive, negative-tone, epoxy based photoresist. They are exposed under UV and subsequently cross-linked portions of the film are rendered insoluble to liquid developers[13]. SU8-2 was spin-coated, with a typical thickness of 2μm, by spinning it at 4000rpm for 15 seconds. The substrate is then soft baked (90°C for 5 minutes) to evaporate the solvent and solidify the film.
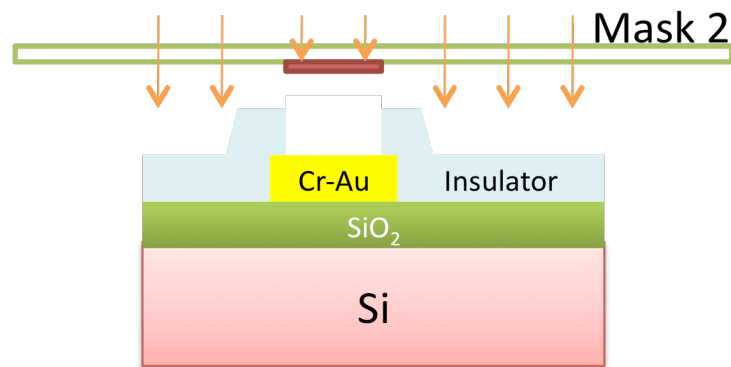
Figure 3.3: UV exposure using Mask 2 for insulator layer

SU8-2 is a negative photoresist, which means UV light exposure causes the resist to polymerized, and become more difficult to dissolve. Therefore, the UV exposed area of the negative resist will remain on the surface, and the developer solution will only remove the unexposed area. Figure 3.13 shows UV exposure of the insulator layer. After being developed, it is hard baked at 120°C for half an hour to further cross-link the material.
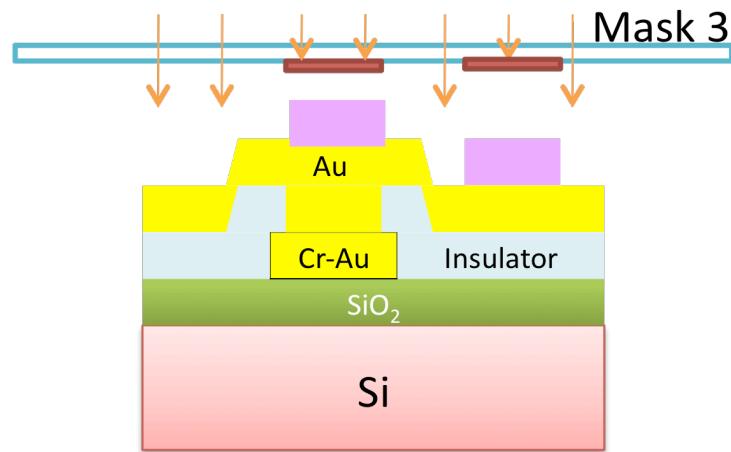
Figure 3.4: Metal2 fabrication with Mask 3

Next, metal 2 (Au) is fabricated by repeating the procedure of metal 1 with a different mask (photomask 3), shown in Figure 3.14. After wet etching of the metal 2 layer, a 10 µm layer of passivation (SU8-10) is coated on the surface using the same procedure as coating the insulator layer. The passivation layer is also negative resist and was patterned by photomask 4 (shown in figure 3.15). SU8-10 is used as a final passivation layer as its thickness provides additional protection. The finished cells are then diced with a 150µm saw blade using a Tempress Model 602 dicing saw.
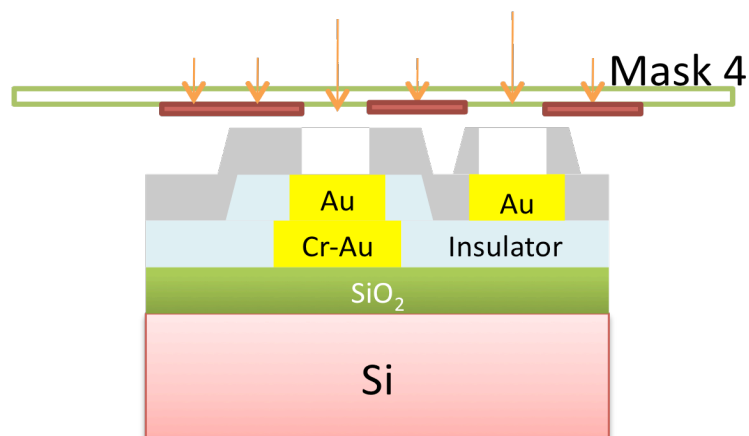
Figure 3.5: Passivation layer UV exposure

Figure 3.16(a) shows the metal 1 layer after the etching and rinsing processes and Figure 3.16(b) shows the final device after finishing all the processes. In order to

interface the sensor chip with the data acquisition system, it needs to be bonded

onto a package. A wire-bonding machine was used to bond gold wire from the chip

to the package (in the form of a PCB). The wire bond is then glued down to ensure it

is intact when covering the sensor with the sensor chamber. Figure 3.9(c) shows the

sensor bonded to the PCB package.
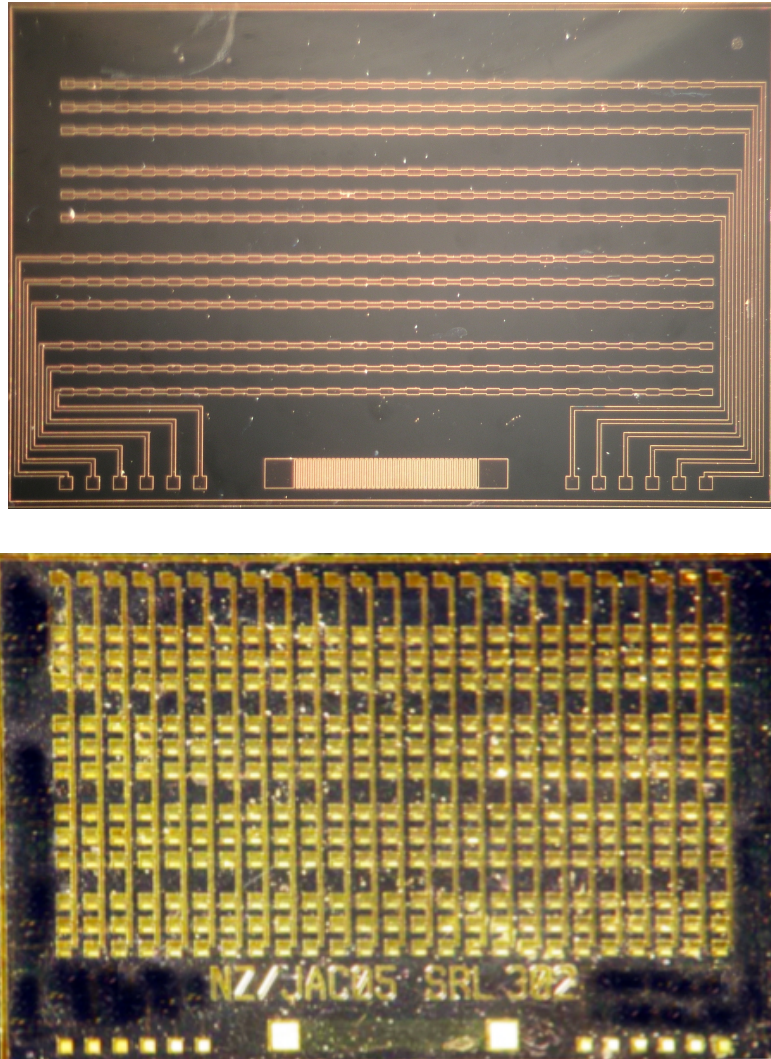
Figure 3.6: a) Wafer with Metal 1 b) Wafer with Metal 1 and 2 layer

The next step in creating a chemo sensor array is to deposit the carbon black

composite as the gas sensitive layer on top of the metal electrode (as shown in

Figure 3.17).
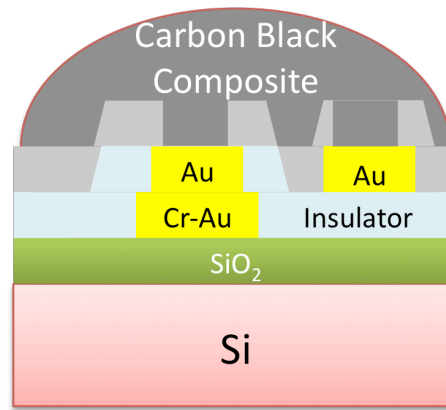
Figure 3.7: Carbon Black Composite deposited onto metal electrode

3.5 Carbon Black- Polymer Deposition

Generally, a chemoresistive sensor consists of 2 electrodes with a polymer-composite sensing material deposited in between them. To complete the chemoresistive sensor, a carbon black composite layer is deposited on top of the electrode as in Figure 3.10. There are various ways available to deposit a thin layer of carbon black composite onto the sensor. Lee et al has demonstrated deposition using syringe into a bulk micromachined 'well' in between the electrodes[14]. They managed to deposit very small amounts of composite solutions (3nl to 30 nl) into the well using an automated syringe (Nanojet II, Drummond Scientific Company). The disadvantage of this drop coating technique is that the resulting film is usually not uniform [15]. Another technique is a microlithography process where the whole sensor array is spin coated with a solution [16]. However, this will limit the diversity of the sensor as the entire 300 sensors will be coated with the same material. This technique is suitable for an array with low sensor numbers. Other techniques include dip coating[17], spin casting[18], and electrochemical deposition[19]. However, these techniques are not suitable for a large sensing array as it is difficult to deposit

individual sensors with different gas sensitive layers. For high density sensor deposition, Dickson has demonstrate spray coating through a physical mask[20]. This technique is suitable for large sensor arrays because it is possible to deposit the sensor individually through the mask without affecting the neighbouring sensors. However, this technique is time consuming for very large sensor arrays. We are utilizing the spray coating method to spray our large sensing arrays with a diverse set of materials. Here we will discuss material, equipment and deposition technique for our large sensor array set.

3.5.1 Material

As mentioned before, we are utilizing carbon black polymer composite as our gas sensitive film. There has been much research using various polymers as composites, [3, 4, 6, 18, 24-27]. However most of these researchers use less than 20 different polymers in their arrays. One of the reasons is the time consuming process of coating the sensors. Doleman has demonstrated using a similar polymer with different proportions to gain additional sensor diversity, providing a non-linear reaction compared to the main polymer[21]. Table 3.2 shows the list of polymer with the composition as our gas sensitive layer with 10 pure phases and 14 polymer blends.

Table 3.1: List of Polymer Composite Composition with Solvent

Code	Polymer	Polymer A(g)	Polymer B(g)	Carbon Black(g)	Solvent (20 ml)
P1	PSB	0.7	0	0.175	Toluene
P2	PEVA	1.2	0	0.3	Toluene
P3	PCL	1.2	0	0.3	Toluene
P4	PVC	0.7	0	0.175	Toluene
P5	PMMA	1.2	0	0.3	Toluene
P6	PEG	1.2	0	0.3	Ethanol
P7	PVPH	1.2	0	0.3	Ethanol
P8	PVPD	0.7	0	0.175	Ethanol
P9	PBA	0.7	0	0.175	Dichloromethane
P10	PSF	0.7	0	0.175	Dichloromethane
P11	PSB 50% + PEVA 50%	0.35	0.35	0.175	Toluene
P12	PSB 50% + PCL 50%	0.35	0.35	0.175	Toluene
P13	PEVA 50% + PCL 50%	0.6	0.6	0.3	Toluene
P14	PEG 50% + PVPH 50%	0.6	0.6	0.3	Ethanol
P15	PSB 50% + PVC 50%	0.35	0.35	0.175	Toluene
P16	PEVA 50% + PVC 50%	0.35	0.35	0.175	Toluene
P17	PCL 50% + PVC 50%	0.35	0.35	0.175	Toluene
P18	PMMA 50%+ PSB 50%	0.35	0.35	0.175	Toluene
P19	PMMA 50% + PEVA 50%	0.6	0.6	0.3	Toluene
P20	PMMA 50% + PCL 50%	0.6	0.6	0.3	Toluene
P21	PMMA 50% + PVC 50%	0.35	0.35	0.175	Toluene
P22	PEG 50% + PVPD 50 %	0.35	0.35	0.175	Ethanol
P23	PVPH 50% + PVPD 50%	0.35	0.35	0.175	Ethanol
P24	PBA 50% + PSF 50%	0.35	0.35	0.175	Dichloromethane

3.5.2 Solution Preparation and Deposition

The polymer composite solution was prepared by dissolving a polymer (or blend) with 20ml of solvent in a vial. The solution was put on a magnetic stirrer overnight at 40°C to make sure the entire polymer dissolved entirely. Then, 20% of carbon black (by weight) was added to the solution, then shaken using a Griffin and George (UK) flask shaker to disperse the carbon black into the solution. The solution is then poured into an air brush to be deposited on the sensor.

The sensors were coated using an Iwata CP-30 Airbrush, by spraying the solution through a MSL machined mask, as shown in Figure 3.18(a). The mask

fabrication will be described in the next chapter. However, before deposition, the

sensor needs to be aligned properly through the mask, as shown in Figure 3.18(b). A

custom-built aligner system, as shown in Figure 3.18(c), was used to align the mask

to the sensor. The deposition process coated 12 sensors in the arrays at once (8

sensors for Portable e-Mucosa as discussed later) so that all 12(or 8) will have similar

properties. These replicate sensors (12 sensors) for the same odorant will improve

the redundancy of the system thus giving more information for signal processing.
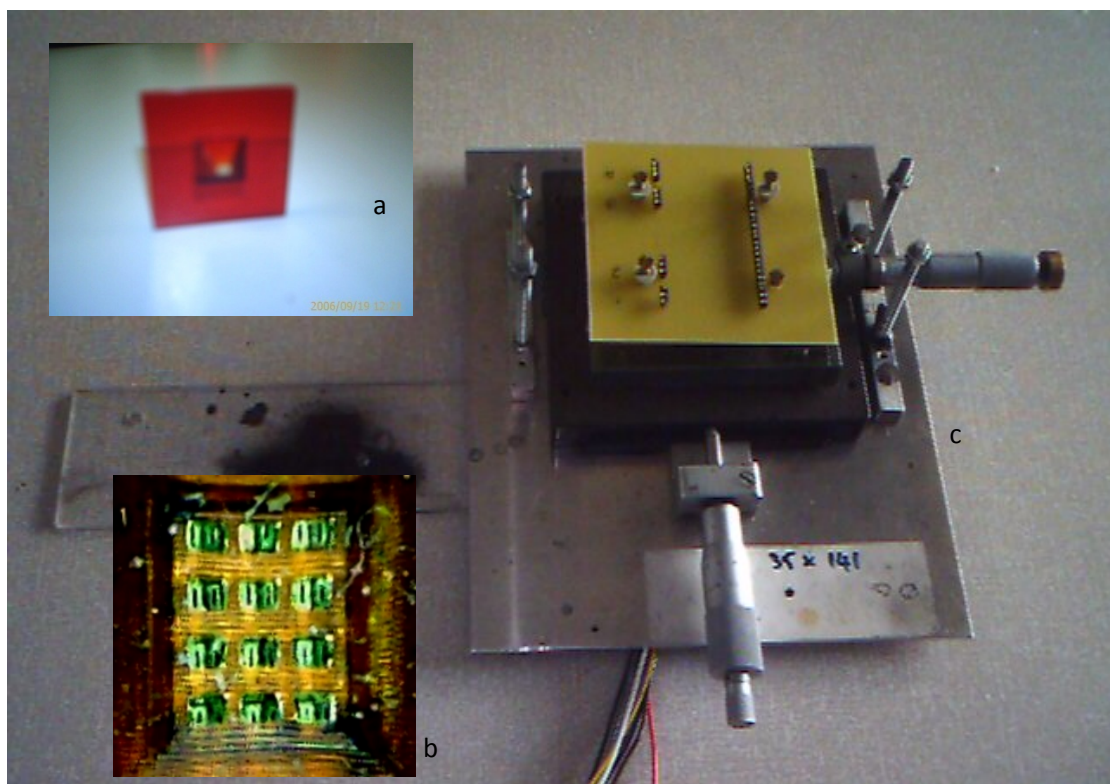
Figure 3.8: a) MSL Mask b) Mask aligned to sensor c) Mask Aligner machine

Since we are depositing 12 sensors at once, it is necessary to monitor the resistance

for all 12 sensors during deposition to ensure they are all within the right range. An

interface to the data acquisition system was built in order to monitor the change in

resistance during deposition. This live monitoring allows us to control the deposition

to be as similar as possible. It is important to maintain the location of deposition and similar baseline resistance between all the sensors to ensure valid data comparison between the arrays. The sensor-based resistance was controlled while depositing to be around 5 – 15kΩ with typical thickness of 15 µm to 25 µm. Figure 3.19 shows the location of deposition of the 24 different polymer composite blends. The sensor numbering, also shown in the same figure, provides an easy way to identify the right sensor response during processing.

R/C	C1	C2	C3	C4	C5	C6	C7	C8	C9	C10	C11	C12
R1	1	2	3	4	5	6	7	8	9	10	11	12
R2	13	14	15	16	17	18	19	20	21	22	23	24
R3	25	26	27	28	29	30	31	32	33	34	35	36
R4	37	38	39	40	41	42	43	44	45	46	47	48
R5	49	50	51	52	53	54	55	56	57	58	59	60
R6	61	62	63	64	65	66	67	68	69	70	71	72
R7	73	74	75	76	77	78	79	80	81	82	83	84
R8	85	86	87	88	89	90	91	92	93	94	95	96
R9	97	98	99	100	101	102	103	104	105	106	107	108
R10	109	110	111	112	113	114	115	116	117	118	119	120
R11	121	122	123	124	125	126	127	128	129	130	131	132
R12	133	134	135	136	137	138	139	140	141	142	143	144
R13	145	146	147	148	149	150	151	152	153	154	155	156
R14	157	158	159	160	161	162	163	164	165	166	167	168
R15	169	170	171	172	173	174	175	176	177	178	179	180
R16	181	182	183	184	185	186	187	188	189	190	191	192
R17	193	194	195	196	197	198	199	200	201	202	203	204
R18	205	206	207	208	209	210	211	212	213	214	215	216
R19	217	218	219	220	221	222	223	224	225	226	227	228
R20	229	230	231	232	233	234	235	236	237	238	239	240
R21	241	242	243	244	245	246	247	248	249	250	251	252
R22	253	254	255	256	257	258	259	260	261	262	263	264
R23	265	266	267	268	269	270	271	272	273	274	275	276
R24	277	278	279	280	281	282	283	284	285	286	287	288
R25	289	290	291	292	293	294	295	296	297	298	299	300

Figure 3.9: Sensor numbering and polymer deposition location

3.6 Deposition Process

The spray coating process starts by aligning the sensor to the spray mask, under a microscope, to ensure a good match. Then the airbrush is filled with the solution previously prepared. Before spraying, the alignment machine is connected to the data acquisition system for sensor monitoring. The deposition is performed inside a fume cupboard for safety reasons. Then, during spraying, the sensor baseline is monitored to ensure similar properties between sensors.

The deposition process is time consuming since much of the equipment requires cleaning between depositions to avoid contamination with other polymer composites. After deposition, the airbrush and mask needs to be cleaned. The airbrush is dismantled and put in a beaker filled with water and cleaning solution (micro 90). It is then placed inside an ultrasonic water bath to remove carbon black/polymer residue inside the airbrush and blown dry with an air gun. Finally, it is assembled back again and is ready for the next polymer composite. The mask is cleaned using the same process.

3.7 Sensor Characterization

The large chemo sensor arrays have been characterised to determine their responses to simple analytes and complex odours. Figure 3.20 shows seven-sensor responses to simple analytes.
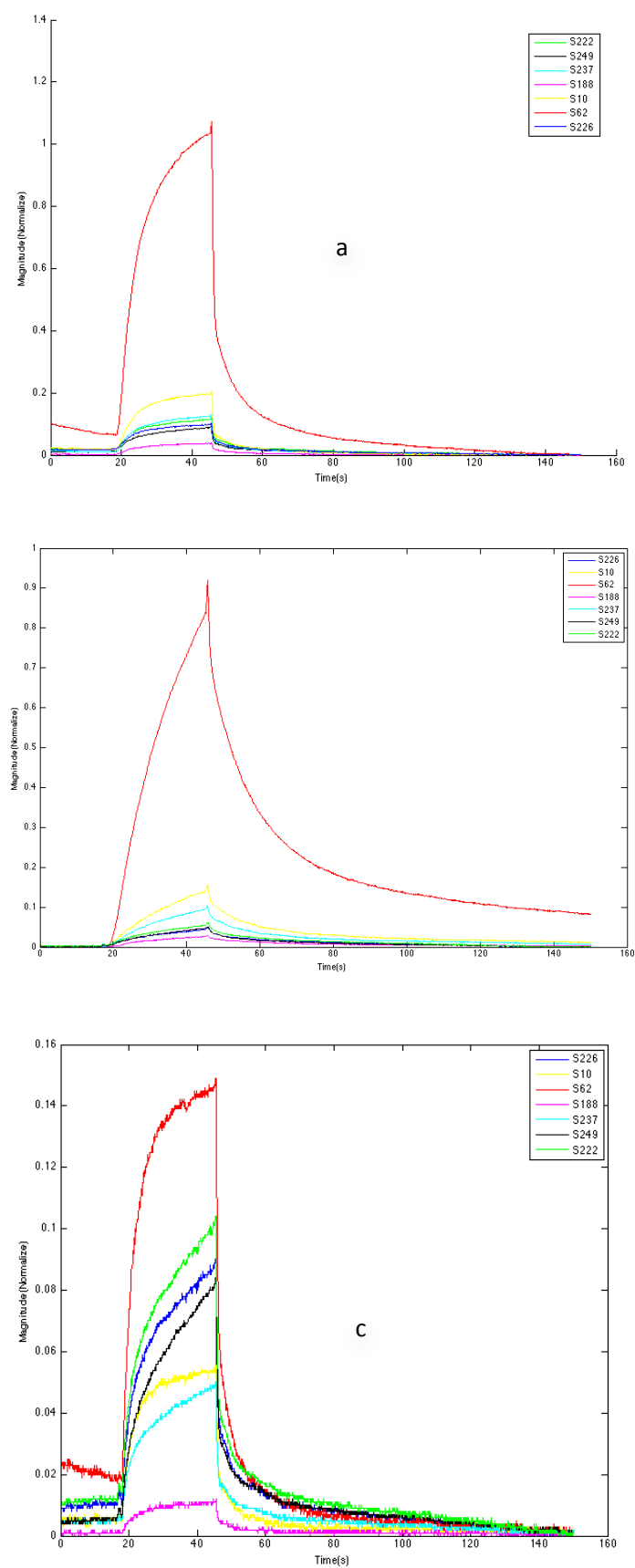
Figure 3.20: Seven sensor responses to simple analyte, a) ethyl acetate b) toluene c) ethanol vapour in air

Sensor response to simple analytes was tested passing through ethanol, toluene and ethyl acetate vapour over the sensor for 30 seconds. A reference baseline is initially defined by passing air through the sensor for 20 seconds. Finally, the sensor is flushed with air for 100 seconds to return it to the baseline. The test was done at 23°C and humidity (10% r.h.).
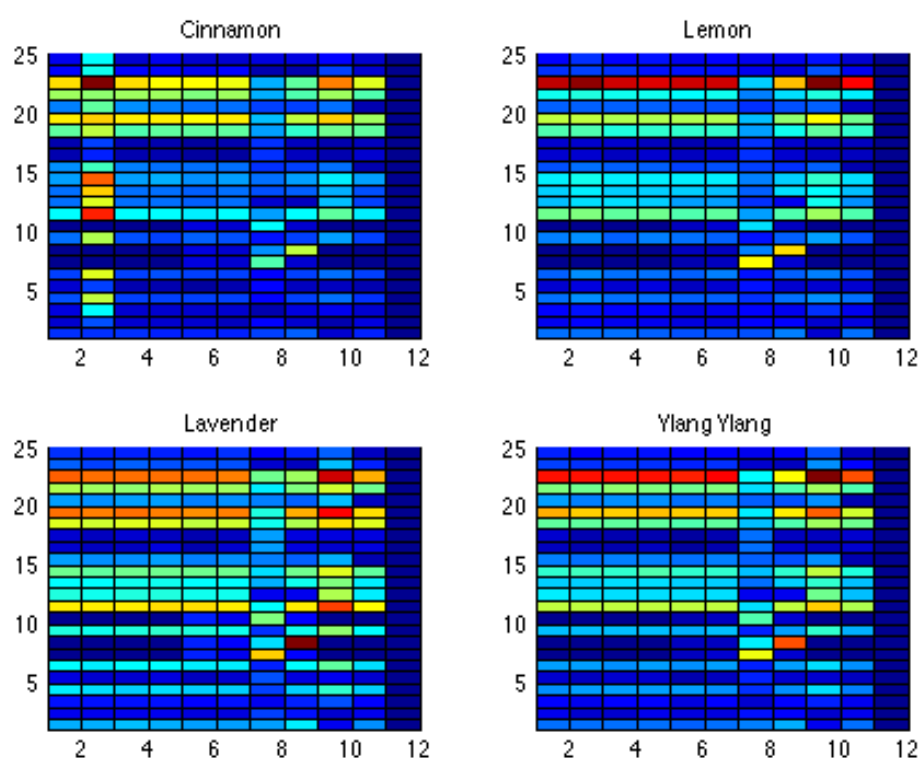
Figure 3.10: Colour map for 300 sensor response to essential oils

Next, shown in Figure 3.21, are the responses to essential oils (lavender, cinnamon, lemon and ylang ylang) were used to demonstrate the sensor response to more complex odours. The sensor was exposed to the analytes for 1 minute; with baseline reference 1 minute and 3 minutes flushing with air. The test condition was at 23 C, humidity at 10% r.h. and flow rate 100 ml/m. The plot of R_{MAX}-R_{MIN} on all 300 sensors (array of 25 x 12) clearly shows the discrimination power of the large sensor arrays.
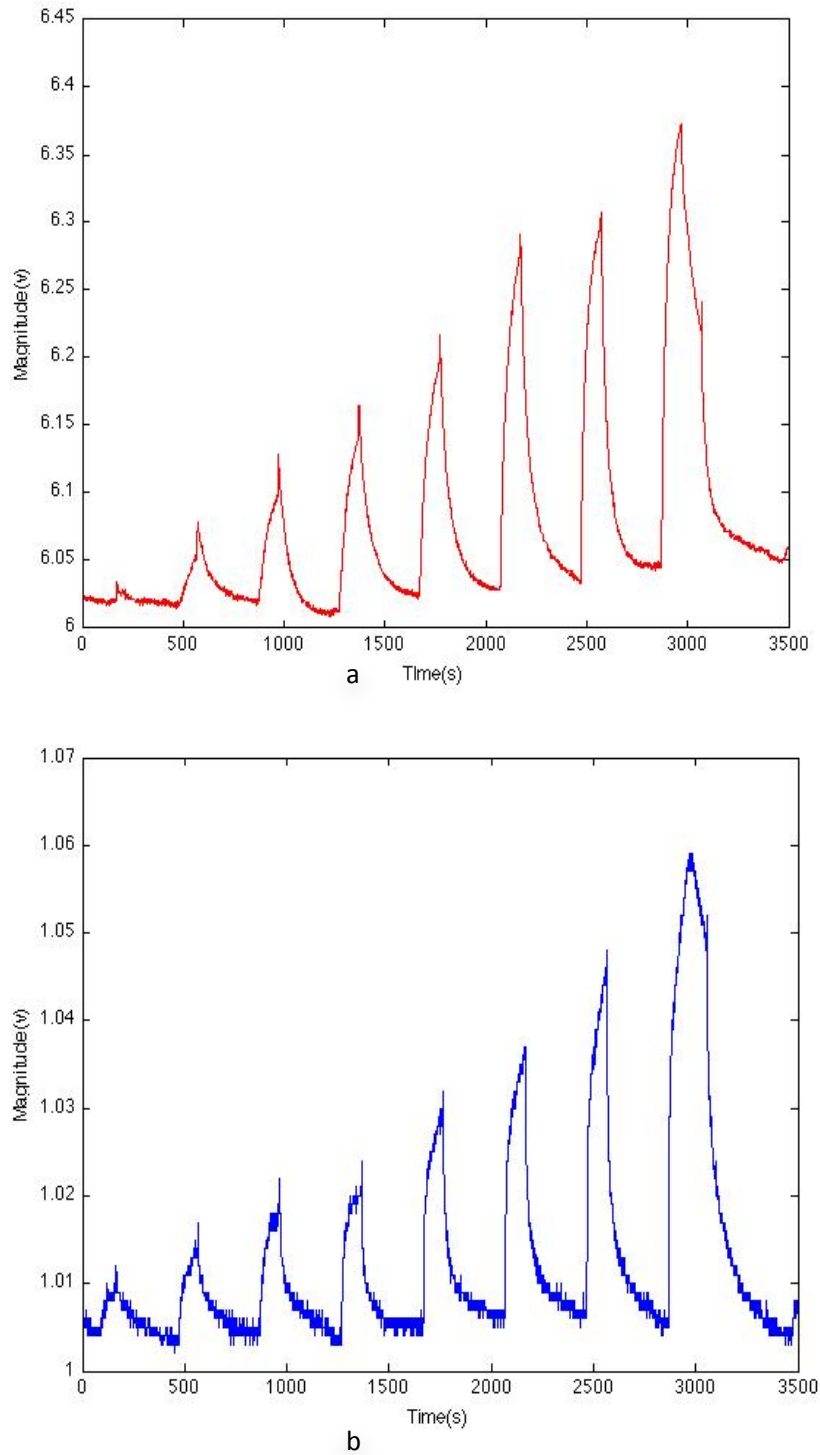
Figure 3.11: Sensor response to different concentrations of a) toluene and b) ethanol vapour in air

To examine the sensor response to different concentrations, ethanol and toluene vapour were passed over the sensors at 8 different concentrations as shown in figure 3.22. The minimum concentration that the sensor can detect is 200ppm for ethanol

vapour and 400 ppm for toluene vapour. Some research has demonstrated ability to detect lower concentration with a thinner layer of gas sensitive material. However, in this research, we are focusing on developing larger sensor arrays with temporal information; hence the reason for choosing a coating technique that produces a slightly thicker gas sensitive film.
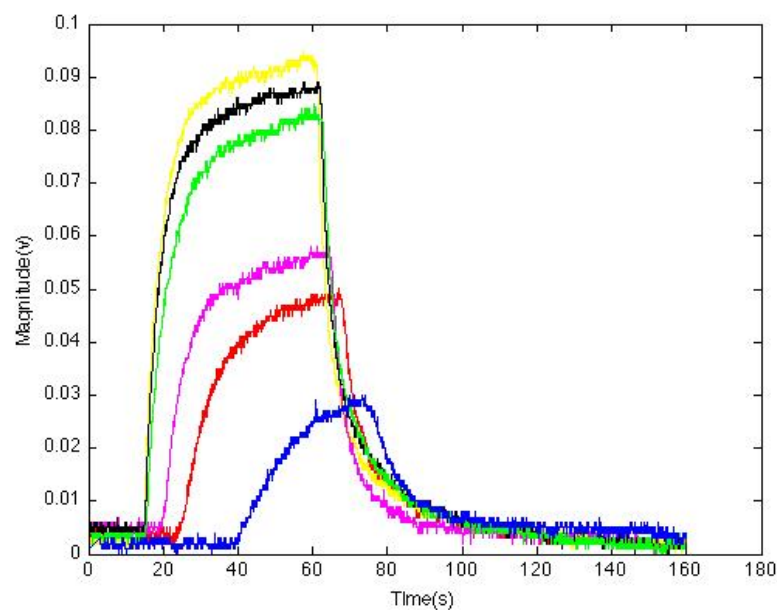
Figure 3.12: Sensor response taken at seven different flow rates

Finally, the sensors were tested for flow velocity effect on sensor response. Figure 3.23 shows the sensor response at different velocity. This information can help determine the velocity range that can be used for the combined system which will be discussed in later chapters. It can be seen from the graph that the sensor response time becomes faster as the flow rate increases while the response magnitude decreases with increasing flow rate. However, there is not a significant difference in response time between flow rate 90, 110 and 130 ml/m. A more detailed characterization of the large sensor array will be described in Chapter 7.

3.8 Portable e-Mucosa design consideration

As mentioned before, the portable e-mucosa is designed based on the complete e-nose system. Here, the same 300 sensors are used in the portable system. However, in order to reduce the size and complexity of the portable system, only 200 sensors (array of 25 x 8) are utilized from the 300 sensors in the array.

In order to use only 200 sensors, some of the components and processes related to the 300 sensor arrays need to be modified. Firstly the sensor package is redesigned with smaller dimensions and different connectors as in Figure 3.24(a). In order to fit the sensor onto the same deposition alignment machine, an interface board was designed and fabricated to fit the alignment machine (Figure 3.24(b)). Secondly, the mask is redesigned to fit eight sensors in a row configuration. Design and modification for portable e-Mucosa will be discussed in further chapters.
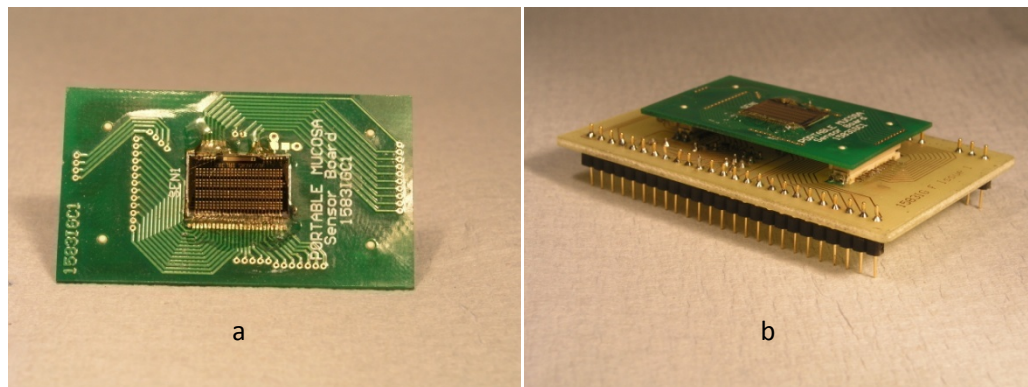
Figure 3.13: a) Sensor array on Portable e-Mucosa sensor package b) Sensor package plugged onto mask aligner adapter

3.9 Conclusions

In this chapter, the large chemosensor array used in this study has been described. This covers the decisions made on the dimensions, layout, fabrication process and

coating. This work resulted in the production of a 300 elements chemoresitive array. We have described how the sensor array is accessed, where by a single sensor would be switched on only when the two corresponding pads are connected. Therefore, the multi-metal layer structure has been employed to reduce the pad number and total size of the sensor arrays. The elements taken into account here are the cross-contamination effect between sensors, cross-talk between tracks, convenience for wire bonding, and long transmission distance influence brought by the shared pads. A resistive based gold temperature sensor was designed on-chip to aid temperature monitoring during testing. The temperature sensor was designed with a baseline resistance of 200Ω at room temperature (assumed $20^{o}C$).

The use of carbon black composites as the gas sensitive layer allows the sensor arrays to operate at room temperature. A number of deposition techniques for these materials have been described and compared. Spray coating has been favoured, compared to dip coating, spin coating and electrochemical coating due to the convenience of coating individual sensors allowing a large diversity of polymer blends to be used as the gas sensitive layer. The deposition process is also described including material combination, equipment (usage and cleaning) and sensor monitoring during coating.

Finally, initial sensor characterization was presented including drift and noise factors, magnitude of response to ethanol and toluene vapour, concentration effect and flow velocity effect.

3.10 References

1.   M.C.Lonergan, et al., *Array-Based Vapor Sensing Using Chemically Sensitive, Carbon Black Polymer Resistors.* Chemistry of Materials, 1996. **8**(9): p. 2298-2312.

2.   J.R.Li, et al., *Carbon black/polystyrene composites as candidates for gas sensing materials.* Carbon, 2003. **41**(12): p. 2353-2360.
3.   Z. Xu, A. Gu, Z. Fang, *Electric conductivity of PS/PA6/carbon black composites.* Journal of Applied Polymer Science, 2007. **103**(2): p. 1042-1047.
4.   J.A.Covington, *PhD Thesis.* University of Warwick, 2001.
5.   D.Clein, , *CMOS IC layout: concepts, methodologies, and tools*. 2000: Newnes.
6.   M.Wheeler, , et al., *Chemical crosstalk between heated gas microsensor elements operating in close proximity.* Sensors & Actuators: B. Chemical, 2001. **77**(1-2): p. 167-176.
7.   J. Gardner, and F. Udrea, *Microsensors: principles and applications*. 1994: Wiley.
8.   C.R.Nave, *Resistance: Temperature Coefficient*. 2006; Available from: http://hyperphysics.phy-astr.gsu.edu/hbase/electric/restmp.html.
9.   J. Baptiste, *Resistivity of Gold*. 2004; Available from: http://hypertextbook.com/facts/2004/JennelleBaptiste.shtml.
10.   R.Howe, and C. Sodini, *Microelectronics: an integrated approach*. 1997.
11.   J. W. Gardner and O.O. Awadelkarim, *Microsensors, MEMS, and Smart Devices*. 2001, Chichester: John Wiley & Sons, Ltd.
12.   S.Franssila, , *Introduction to microfabrication*. 2004: Wiley.
13.   T.NANO, *SU-8 negative tone photoresist formulations 2-25, MicroChem*.
14.   F.Zee, and J.W. Judy, *Micromachined polymer-based chemical gas sensor array.* Sensors and Actuators B: Chemical, 2001. **72**(2): p. 120-128.
15.   H.Bai, and G. Shi, *Gas sensors based on conducting polymers.* Sensors, 2007. **7**(3): p. 267–307.
16.   S.Wang, et al., *Multi-walled carbon nanotube-based gas sensors for NH3 detection.* Diamond & Related Materials, 2004. **13**(4-8): p. 1327-1332.
17.   J.Cho, et al., *Sensing behaviors of polypyrrole sensor under humidity condition.* Sensors & Actuators: B. Chemical, 2005. **108**(1-2): p. 389-392.
18.   G.Prasad, et al., *Ammonia sensing characteristics of thin film based on polyelectrolyte templated polyaniline.* Sensors & Actuators: B. Chemical, 2005. **106**(2): p. 626-631.
19.   G.Lu, , L. Qu, and G. Shi, *Electrochemical fabrication of neuron-type networks based on crystalline oligopyrene nanosheets.* Electrochimica Acta, 2005. **51**(2): p. 340-346.
20.   J.Dickson , et al. *An integrated chemical sensor arrays using carbon black polymers and a standard CMOS process*. 2000.
21.   B.J.Doleman, et al., *Use of Compatible Polymer Blends To Fabricate Arrays of Carbon Black-Polymer Composite Vapor Detectors.* Anal. Chem., 1998. **70**(13): p. 2560-2564.

CHAPTER 4

Design and Fabrication of Microfluidics Component

4.1 Introduction

This chapter describes the design and fabrication of novel microfluidic packages by 3D direct manufacture. Such systems are a direct result of the invention and deployment of Rapid prototyping machines, which have been used for over two decades to decrease product development time[1-3]. Initially, such machines were limited to creating large replicas with minimum feature sizes in the order of a millimeter, but later machines are now approaching the resolution of more traditional silicon micro-machining techniques.

Although various silicon micromachining methods, such as LIGA[4] and DRIE[5], are able to construct high aspect ratio microchannels and microstructures, these techniques, in general, only produce planar structures (sometimes described as extruded 2D) and are not able to construct full 3D components. Furthermore, fabricating structures using silicon machining is time consuming and costly. Here Micro stereo lithography (MSL – a form of micro-direct manufacture) has been favoured over silicon micromachining as it allows full 3D structures to be designed and constructed in a very short period of time and be highly cost effective. MSL has evolved from the stereolithography (SL) technique, based on a light-induced layer-

stacking manufacturing technique. The advantages of MSL are that it allows rapid development of high-resolution three dimensional micro size objects.

Here we will first review various MSL techniques and then discuss the design and fabrication of microfluidic channel and various chamber for sensors/preconcentrators used in this instrument. The stationary phase coating of the column will also be described.

4.2 Microstereolithography Fabrication

Most stereolithography systems (SL and there micro-versions - MSL) predominantly work through an additive layer process, where each layer is cured into a photosensitive resin by a light source (a process called photopolymerization). In photopolymerization, a source of light such as UV laser[6] or Near IR laser[7] is used to trigger a chain reaction in the monomer, which induces the polymerization of liquid monomer into solid polymer. Once the polymer is cross linked, it cannot dissolve again in a monomer [8]. The surface of photosensitive liquid (resin) is exposed to the laser source creating a 2D image on the surface. When the layer is finished, a fresh layer of resin is spread on top of the 2D object and the light induced solidification of the next layer is started. This process is repeated layer-by-layer to construct a full 3D structure.

The first report work on a micro 3D structure, using a stereolithography process, was made by N. Nakajima and T. Takagi in 1993 when they demonstrated an apparatus that could produce a 3D structure at a resolution 0.8 μm[9]. In the same year, K. Ikuta and K. Hirowatari showed their apparatus which was able to achieve up to 0.25 μm in XY direction and 1 μm in the Z direction[10]. The process developed by

Ikuta and Takagi are similar in a way where they both use vector by vector scanning method is used to produce a 2D layer. Later researches are more extensive but use relatively similar concept. The vector by vector scanning technique uses a fixed light source that focuses and cures the resin spot by spot while the XY stage or phothoreactor(object holder) is moved around. Although spot by spot curing is time consuming, it can produce a high-resolution structure, due to the fact that the UV light is focused optimally onto the resin surface.

The next generation of microstereolithography machine known as integral MSL uses a slightly different technique. In integral MSL, the 2D layer is built by focusing a whole image through onto the resin surface. This method is significantly faster because a whole layer is cured in a single process, whereas the vector by vector technique requires every pixel to be cured one by one. However the problem with this method is the difficulty to get high resolution. The first reported use of this technique is by Bertsch, where they developed an integral MSL machine using 260 x 260 pixel LCD as the UV light mask [11].

The next stage in the development of MSL machine is the use of digital micro mirror device (DMD) as pattern generator. Developed by Texas Instrument, the DMD is a microelecromechanical system working as a light switch[12]. In 1999, Bertch introduce a MSL machine utilizing DMD technology as the pattern generator with VGA resolution at 640 x 480 [13].
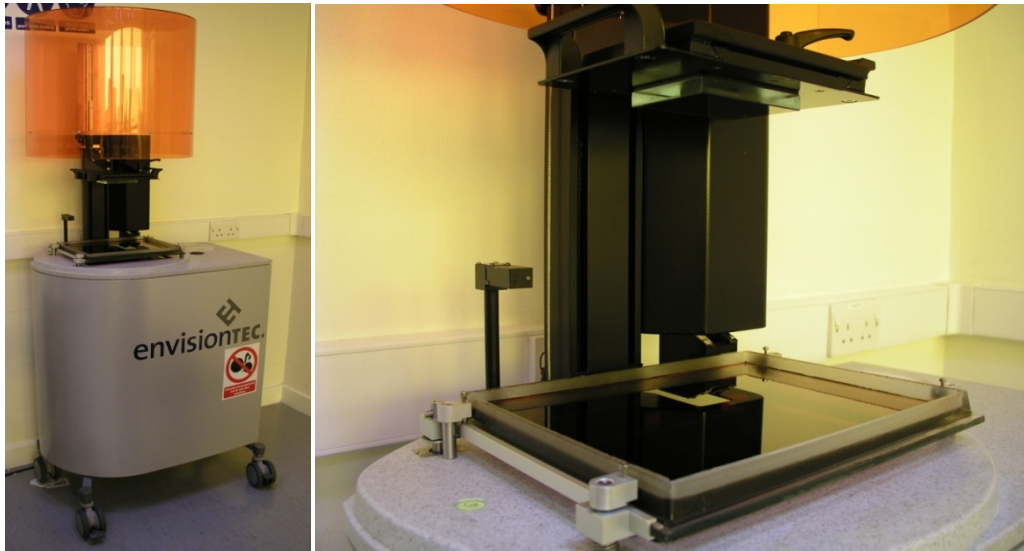
Figure 4.1: Envisiontec Perfactory Mini

In the School of Engineering, at Warwick University, we have access to two MSL machines namely the Envisiontec Perfactory Mini (Figure 4.1) and Envisiontec Perfactory Desktop. In this research, we are using the Perfactory Mini that is able to produce objects with an outer dimension of $41.98 \times 33.59 \times 230$ mm^3 at a resolution of 32.8 μm × 32.8 μm × 25 μm. The hardware consists of a dynamic mask modulator (with a DMD chip), visible light source, focusing optics with shutter, a build platform (photoreactor), a Z-stage for moving the base (build platform) and an embedded PC running Linux. Figure 4.2 show the Perfactory Mini functional diagram. The resin used in this research is R11. It is a liquid, orange, poly-methyl-methyl-acrylate. Unlike other resins, which require UV laser source, this type of resin only requires a high-pressure mercury vapour lamp to stimulate photopolyimerisation[14]. The material offers great chemical resistance and a good balance of properties between rigidity and functionality[15].
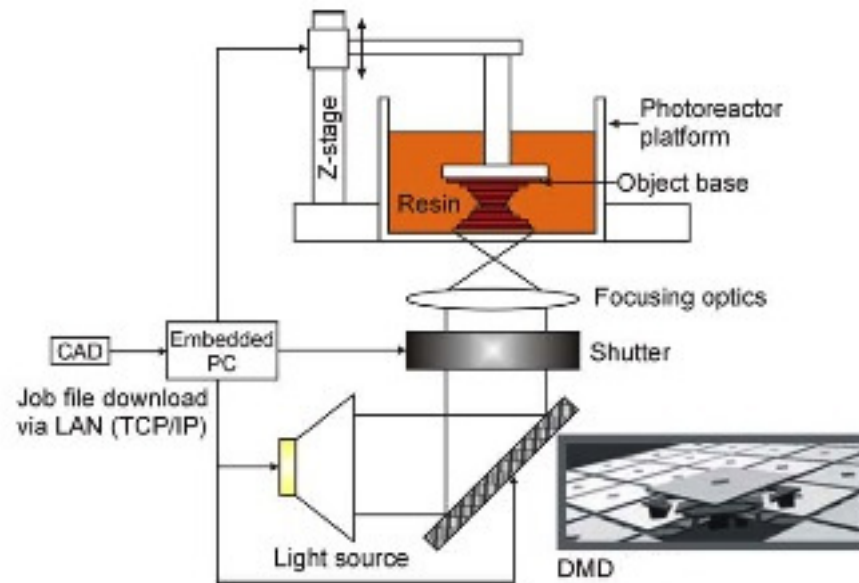
Figure 4.2: Envisiontec Perfactory Mini Functional Diagram[14]

Development of a 3D object starts with a 3D CAD design of the object, using CAD software, in our case Solidworks 2006. The Perfactory Mini system accepts object data files in the form of "STL"(stereolithography) file. This file format is widely used in most rapid prototyping applications, especially among stereolithography systems. The CAD design is saved as "STL" file in Solidworks before the next step. This 3D object is then sliced to 2D layers using the Envisiontec Perfactory Direct application. Some of the build that has irregular unflat surfaces requires support to hold the part together during the build. In cases where support is needed, Magics 11 from Materialise Software is used to generate 3D support for the 3D structure before it is sliced. The slice data is then sent to the machine to start the building process. Each2D slice is projected into the resin surface, layer by layer, to produce the 3D object.

Upon completion, the object is removed and cleaned to remove any uncured resin on its surfaces and within the microchannels. The object is cleaned by placing it

in a beaker filled with isopropanol before being immersed in an ultrasonic bath (Otto model 300, Italy). After ultrasonic cleaning, the object is blown with compressed air to dry and cured using a UV light box (Metalight QX1, Primotec, Germany) for 5 minutes. The steps for MSL fabrication process is summarised in Figure 4.3.

MSL Fabrication   CAD Design

Cleaning

Curing   3D Structure
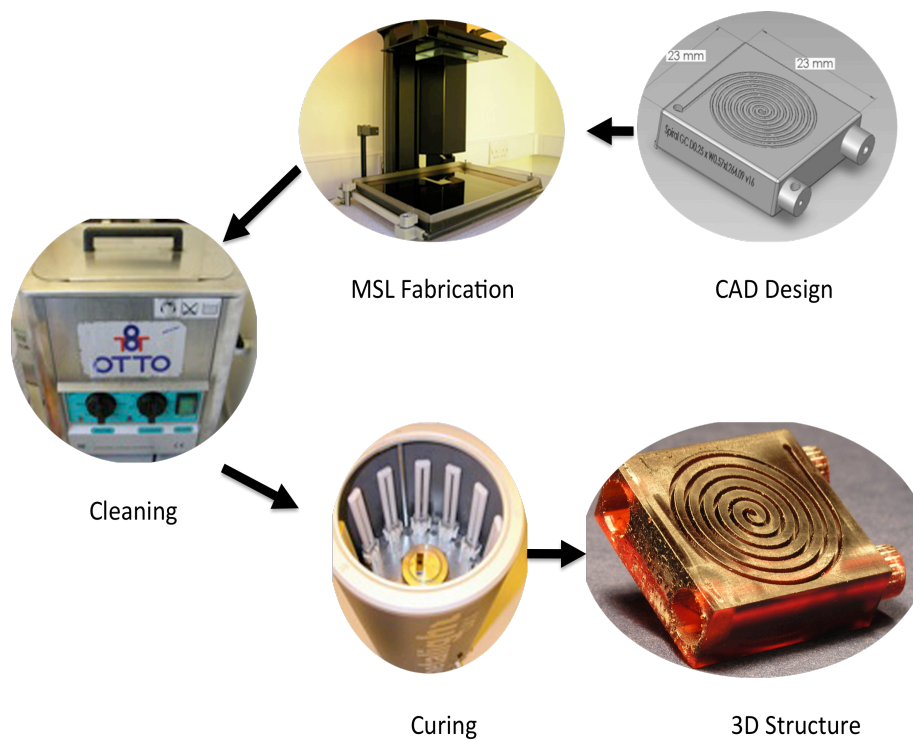
Figure 4.3: Fabrication Process for MSL 3D Structure

4.3 Microfluidics Design Evolution

The micro-column that mimics the olfactory mucosa 'nasal chromatograph' effect was designed to behave similarly to a gas chromatographic column. As discussed earlier, a gas chromatographic column separates a complex mixture of chemicals by delaying each chemical component at a different rate, depending upon the interaction between the chemical component and the retentive layer. The main objective of the micro retentive column, as used here, is to ensure that an odour going through the column is delayed before being detected by a sensor array.

Sample odours will be delayed differently depending on the partition coefficient between the odour and the stationary phase. We are not aiming for complete separation of the odour, as in gas chromatography, only a temporal delay that we believe will improve odour discrimination. In addition, by deploying dual micro retentive columns, coated with two different polarity phases, we are hoping to further increase the diversity of the system.

Many of the microfluidic components have gone through changes throughout the design process in order to improve the system as a whole. Here we are going to discuss the evolution of the components in this system, focusing mainly on the micro retentive column.

4.3.1 Preliminary Design - Box Type
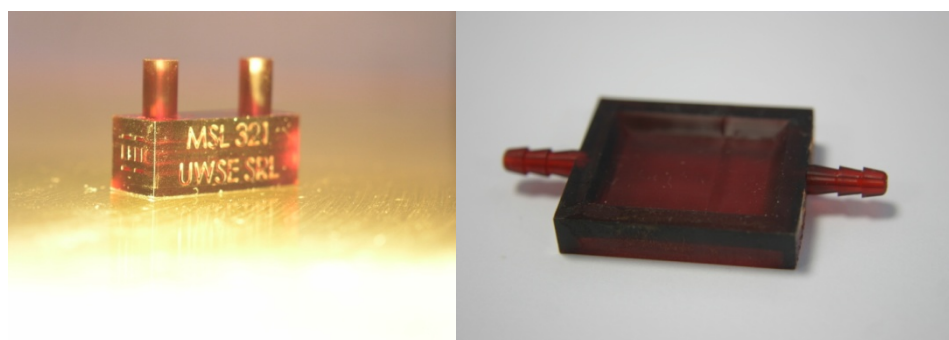
Figure 4.4: a) Boxed Type Micro Retentive Column b) Preliminary Chamber design

Initially, the micro-GC column was designed as in Figure 4.4(a), where the channel is incorporated in a box like component. The column size is 200µm x 200 µm. The column is completed after sealing both end of the component with glass slides (glued onto end). The advantage of this design is that it is easy to increase the length of the column, by adding additional rows. However, in order to increase the length of

each column section, we need to modify the CAD Design. In this design, the column

is separated from the chamber as shown in Figure 4.4(b).
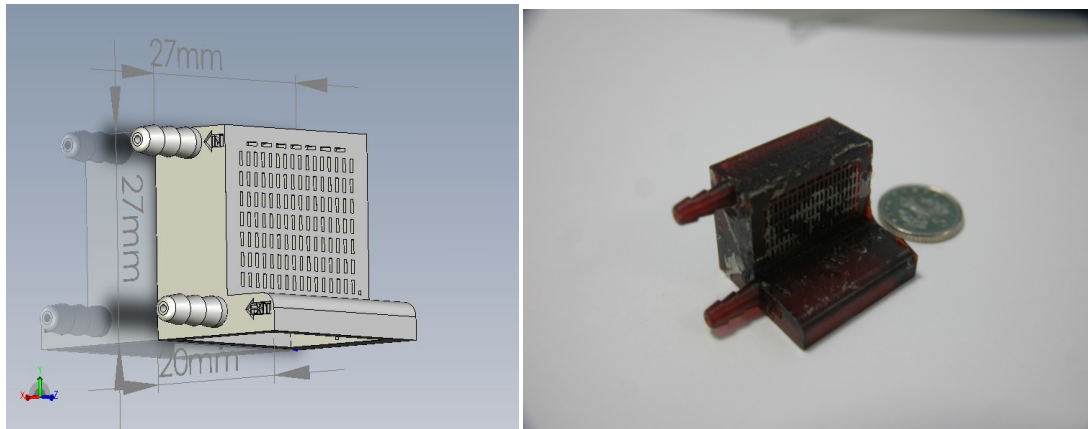
Figure 4.5: a) CAD design of Hybrid Column-Chamber b) Hybrid Column-Chamber (with 5
pence piece for scale)

The next version of the micro column incorporates both the column and the

chamber in one piece. The reason behind this is to reduce dead volume within the

system, giving higher sample concentration over the sensors. Another advantage of

this design is that it eliminates the need of connecting tube that can increase the

possibility of leakage around the connector. However, the problem of having to

redesign the column for different sizes remains. Furthermore, this design creates a

lot of sharp bend that generate higher pressure drops, making it difficult to create

enough flow for longer column. Previously, we have successfully reported a working

column with a square block design[16]. Although the original column produced

reasonable results, the square column reduced laminar flow within the column.
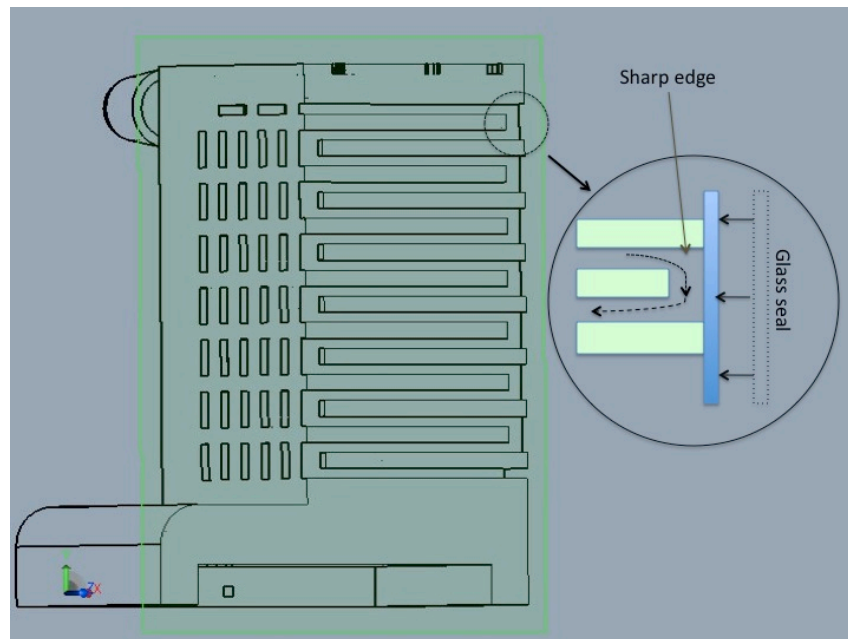
Figure 4.6: Sharp edge created when the column is sealed with glass

Figure 4.6 illustrates the sharp edge that would make cleaning difficult. Cleaning this type of column is difficult due to the fact that there are a lot of channels within the component and the channel are small and long. After the process, the small and long channel and full of resin. The problem that we had is that the middle part of the component cannot be cleaned properly. The longer the column, the more difficult it is to clean, as isopropranol (the solution used in the cleaning process) is unable to penetrate through the thick resin. Thus, we expect the column to have trouble during stationary phase coating, where the process requires flushing the column after filling it with coating solution.

Although there are fewer problems in coating this device using a vapour deposition technique, there will be a problem when coating with a stationary phase using a static or dynamic coating technique. The sharp bends and edges will attract more stationary phase materials, thus creating an uneven coating within the channel.

4.3.2 Spiral Design
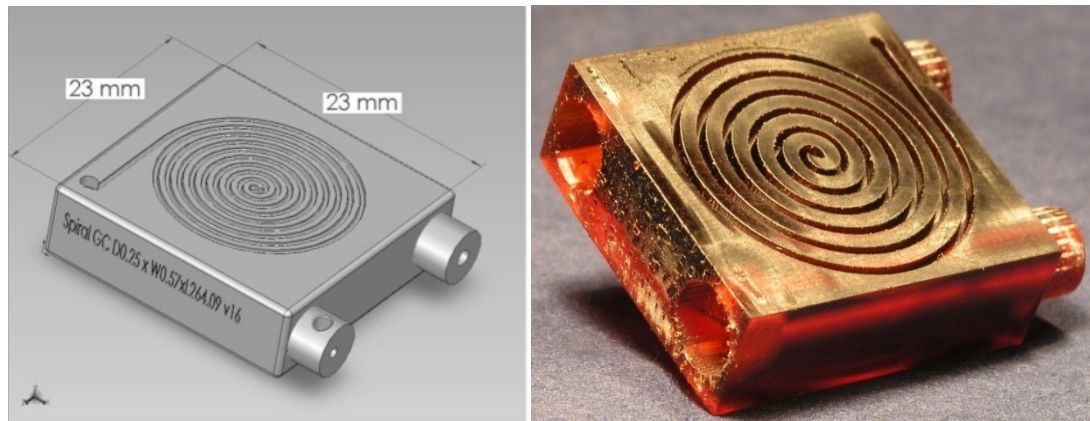
Figure 4.7: Spiral based Micro Retentive Column

In order to overcome this issue, a spiral based column, as in Figure 4.7, was designed. The spiral micro channel has a depth of 250 µm and width of 380 µm, is placed on both sides of the component in order to increase the length of the column in one single component. The odour will flow from one side to the middle of the column then through a hole to the next spiral where the flow starts from the middle of the spiral.

This spiral-based design eliminates most of the sharp corner and edges, thus aiding flow separation. However, the disadvantage of this design is that it is difficult to create a longer channel. However, this was solved by creating a 'lego-like' component so that the column length can be increased by stacking components together. This will allow the performance of different column lengths to be tested, easily, just by adding or reducing the number of stacked components. Figure 4.8 shows how column scan be stacked together. It is built with integrated pipe fittings on the top and bottom of the package, for easy connection to more packages and/or the sensor chamber.

Figure 4.8: Stacked Lego(TM) like structure in chamber and micro retentive column

The figure above demonstrates that multiple columns can be stacked together to create a longer channel. Furthermore, the chamber has also been designed to connect to the columns creating a hybrid chamber-column similar to the preliminary boxed type design. The stacking concept removes the problem of redesigning CAD model for different channel lengths.
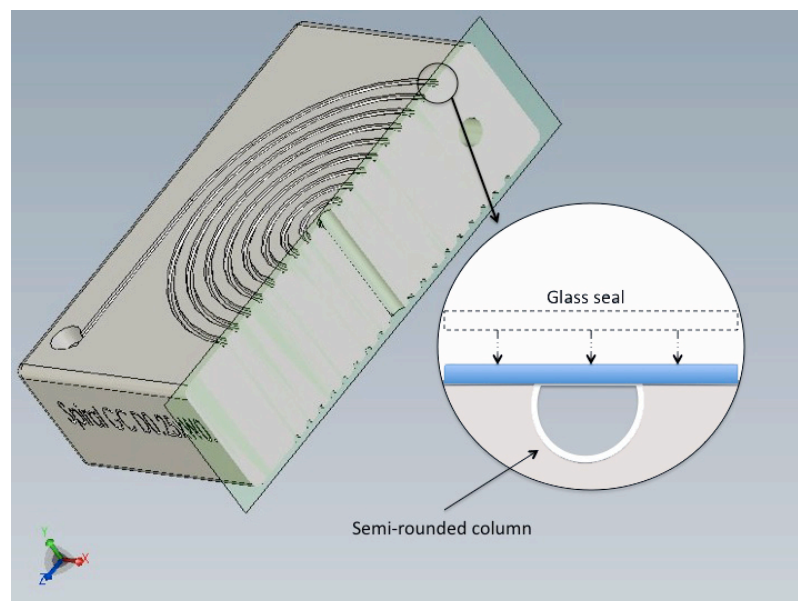
Figure 4.9: Semi rounded column sealed with glass

The column is purposely built unsealed to aid stationary phase coating (discussed later). This unsealed design also helps during cleaning. Figure 4.9 illustrated the sealing of the semi-rounded column using glass. The semi-rounded design also

makes stationary phase coating easier since there are no sharp edges within the column.

Using this design concept, we built columns with different geometries in order to demonstrate the effect of column size on the sensor response/temporal delay. Meanwhile, the length of the column was also be varied by stacking together a number of spiral columns. Table 4.1 shows the size of different column geometries fabricated for the system. As shown in table 4.1, each block contains a spiral column of at least 528 mm per block.

Table 4.1: Dimension of spiral columns

Code	Width(mm)	Depth(mm)	Total Length(mm) (per block)
MSL 501	0.5	0.25	528
MSL 502	0.38	0.25	540
MSL 503	0.25	0.25	548

Thus to obtain a channel length of 1.5 m, three blocks of spiral column are stacked together. It is already known that narrower channel geometries or longer channels produce better separation in gas chromatography. However, in this research we need to balance the dimension of the column with the vacuum pump strength. In gas chromatography, a small or longer channel would require a higher pressure to operate. Since our focus is to build a handheld device, we need to ensure the pump power is enough to pull the odour through both microchannel and sensor array. Hence the reason of selecting channel size of 250 µm and above is to ensure enough flow in going through the system to operate properly.

4.4 Post Fabrication

4.4.1 Sealing

Sealing the column is a very important part of the fabrication process. It is necessary to have the column leak free in order to obtain the maximum flow through the column. Several methods have been investigated to ensure the micro channel is properly sealed. Initially sealing was performed using a glass slide cut to the size of the microchannel block. A thin layer of adhesive (epoxy based) was coated onto the glass slides and it was pressed against the column. Since the adhesive required time to cure, it flowed into the small micro column producing a blockage. To overcome the problem, a cover with protruding spiral was created (using the MSL process instead of glass) so that it can be aligned to the column and produce a close seal, as shown in Figure 4.10.
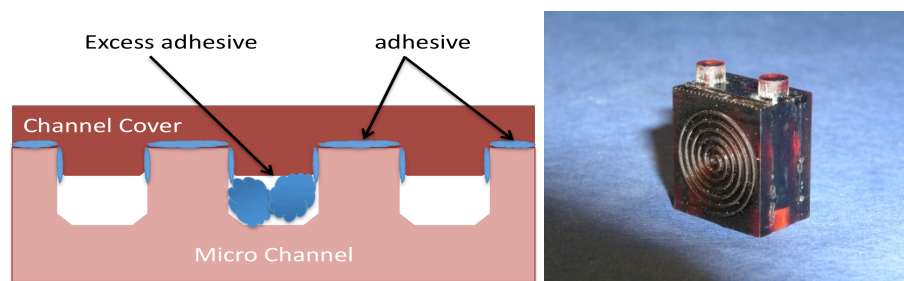
Figure 4.10: Blockage created by excess adhesive

Although this method can create a good seal, and is made of the same material as the channel, problems still occur, as the channel cover is not flat. Furthermore, it is difficult to apply a thin layer of glue onto the channel cover groove. More often than not, excess adhesive will flow into the channel, causing channel blockage. Thus, to

overcome this channel blockage issue we proposed to use a very thin layer of adhesive, which cures rapidly.

To achieve this, we spun coated a clear glass slide with UV adhesive (Loctite Glass Bond) and placed it on top of the micro channel. Then, it is placed in a UV box for 2 minutes to cure the adhesive through the transparent glass slide. To ensure the column was hermetically seal, it is tested by flowing water through it and checking for leakage around the column. Figure 4.11(b) shows the column is filled with water to confirm that it is sealed properly. Although column created with this method is leakage free, there was concern that the small layer of UV adhesive, on the top of the column, is reacting with the odour being tested.
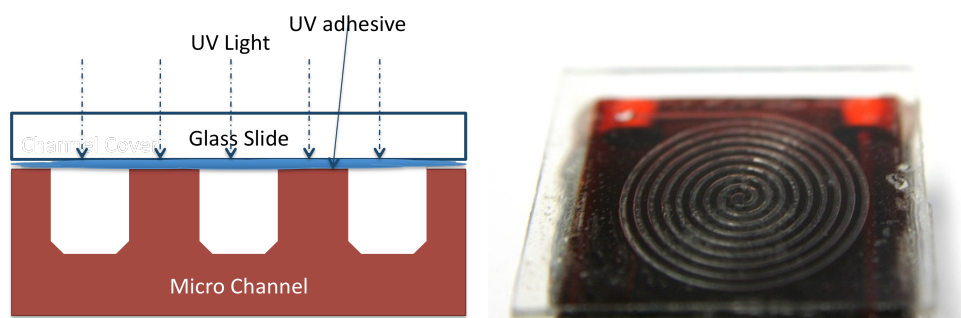
Figure 4.11: a) Microchannel sealed with UV adhesive b) Micro column filled with water

Hence, to improve sealing further, we used the same technique as before, only with a different adhesive. Here the same resin (R11) as used to form the micro channel was utilized instead of the UV glue. This resin will also cure under UV light, creating a stronger seal.

4.4.2 Stationary Phase Coating

In gas chromatography, the stationary phase is the one of the most important components. The greater the interaction, of a chemical compound, with the stationary phase the more it will be retained, thus the slower the compound will advance through the column. There are many types of stationary phases, which are mainly classified based on their interaction with a sample (polar, non-polar, and ionic). The most common method used to evaluate a stationary phase is the McReynolds system[17]. McReynolds constant can be used to determine the selection of stationary phase for a specific compound. McReynolds has analyzed more than 200 stationary phases[18], from which Delley suggested, four phases: OV-101, OV-17, OV-225, and Carbowax 20M, can provide satisfactory GC analysis for over 80% of all applications [19]. The general rule, when choosing a stationary phase, is to use a polar phase for polar compounds and a non-polar phase for non-polar compounds, with further fine tuning according to the McReynolds system. Non-polar phases are more resistant to oxidation and hydrolysis than polar phases. Polysiloxane based phases are the most common stationary phases used in GC because of their high thermal stability and the wide range of polarities[4]. Here, we have chosen OV-1(100% Polydymethilsiloxane) as our non-polar stationary phase because of its wide range of polarities and Carbowax 20M (polyethylglycol) as our polar stationary phase.

Conventional gas chromatography column stationary phase coating techniques are mainly divided into two groups, namely dynamic and static coating [20]. Generally, dynamic coating is performed by driving a plug of stationary phase solution through the column. This causes a thin layer of stationary phase to adhere

to the wall of the column. This process is repeated a few times until the desired stationary phase thickness is achieved. Figure 4.12 illustrates this concept on an open tubular capillary column. The flow velocity at the end of the column usually increases sharply, resulting in a thicker film at the end of the column. The most common method to avoid this problem is to use a buffer column at the end of the GC column.
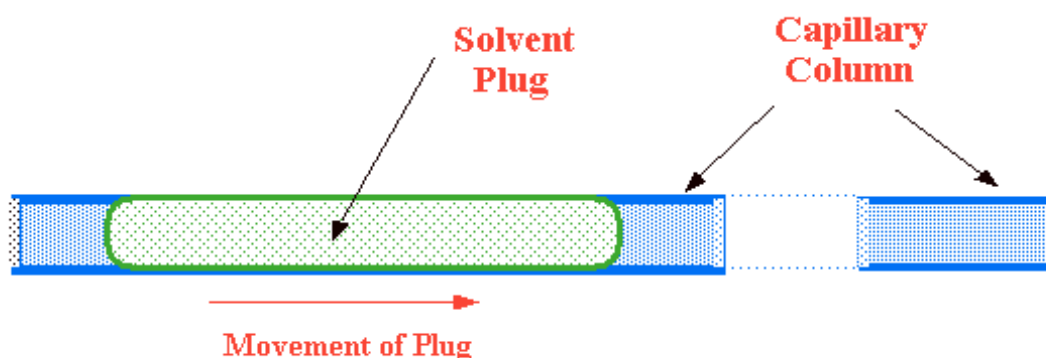
Figure 4.12: Dynamic coating example of open tubular capillary column [21]

Figure 4.13 demonstrates static coating of an open tubular capillary column. Static coating is performed by filling the entire column with a stationary phase solution and one end of the column is sealed. The other end of the column is connected to a vacuum pump, which pulls evaporated solvent from the column. The column is successfully coated when all the solvent has evaporated from the solution leaving a coating on the walls. Static coating usually yields a more uniform coating, however it is more time consuming.
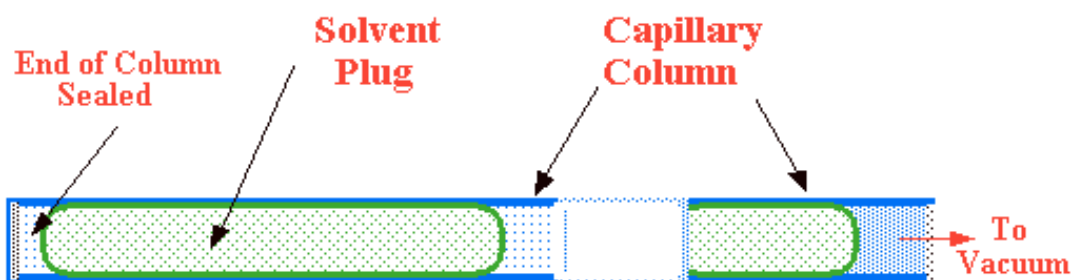
Figure 4.13: tatic coating of open tubular capillary column [21]

Various researchers have demonstrated different techniques for coating their micro fabricated gas chromatographic column. Most use a dynamic coating technique, by driving the stationary phase dissolved in a volatile solvent through the column at a constant velocity[4, 22-24]. Noh and Kolesar have demonstrated vapour deposition of a stationary phase onto a micro column. This deposition technique offers the advantage of uniformity of the stationary phase layer on a micro sized column. Noh coated their microcolumn with parylene using a vapour deposition machine from Specialty Coating System[25]. Kolesar used sublimation technique to evaporate the stationary phase onto an unsealed silicon micro-GC column[23]. Then, the wafer was polished prior to anodically bonding it to a Pyrex lid to seal the column creating a coated micro-GC column.

We tested several methods of coating our micro retentive columns including spray coating, static coating and vapour deposition. The static coating technique was conducted in a similar way as demonstrated by Reidy(where they successfully coated 0.1 – 0.2 μm of stationary phase(OV-1) onto a silicon fabricated micro-GC channel[24]).

The stationary phase solution was prepared by dissolving 0.05g of OV-1(non-polar) or Carbowax 20M(polar) (both acquired from Sigma Aldrich UK), in 10 ml dichloromethane. The mixture was then agitated for 30 min by shaking it in a flash

shaker (George and Griffin, UK) to ensure complete dissolution. Although Reidy suggested adding dicumyl peroxide, a cross-linking agent, to the stationary phase before coating, we have decided not to use the agent due to the fact that the column is not going to be exposed to high temperatures. The function of the cross-linking agent is to stabilise the coating for when the column is heated to high temperatures during operation [4].

The column was then filled with the solution using a syringe. Once filled, one end of the column is sealed and the other end was connected to a vacuum pump. The pump removed all the solvent leaving the stationary phase coating on the surface of the column. When the column appeared empty (after around 15 minutes for a 0.5m column), the column is placed in an oven at 50°C to ensure that all the solvent is completely evaporated. Although this method produces a working column, the solvent seems to dissolve the column if being left for too long.

The next method we studied was the vapour deposition of parylene-C demonstrated by Noh[25]. Although parylene-C has retention like characteristics is has not been extensively studied. Noh suggested it had similar retention characteristics to Poly-Ethylene Glycol (PEG). Parylene-C was coated using a PDS 2010 Labcoater 2, (Specialty Coating Systems, USA) as shown in Figure 4.14.

Figure 4.14: SCS PDS 2010 Parylene-C vapour deposition system

The parylene deposition process starts by loading a fixed amount of parylenedimer (parylene-C) into the machine. The amount of dimer required depends on the desired coating thickness (2 μm per 1g). The machine then vaporizes the solid phase dimmer at 175°C. The parylene dimer is then pyrolized into reactive monomers at 690 °C. The monomers are introduced into the chamber where the vapours become polymerized as soon as they get in contact with any surface inside the sample chamber. Excess dimmer is collected in a chiller thimble to protect the vacuum pump. This method has the advantage that the process is performed under vacuum and at room temperature, thus, is well suited our MSL created packages. Using this machine, we have successfully coated a 250 x 250 μm channel with 5 μm parylene-C as the stationary phase.

For spray coating, we utilized a similar method to that deployed for the deposition of the gas sensitive films, discussed in the previous chapter. The stationary phases were prepared by dissolving 0.05 g of polymer in 10 ml

dichloromethane. This solution was then stirred using a magnetic stirrer at temperature 50°C until the polymer was fully dissolved. An airbrush (Iwata SP-30) was then filled with exactly 1 ml of the dissolved stationary phase solution and sprayed onto the spiral column before sealing it. After coating, the column was sealed using a glass slide that was spin coated with a thin layer of UV adhesive as described in the previous section. As expected, the coating produced via this technique was not very uniform at 5-50µm. However, this method produces a working column faster and with fewer blockages then any other methods we tried, except for the vapour deposition technique.

The final method studied was static coating. This method was carried out differently from the conventional GC static coating technique. In the latter method, a sealed channel is filled with coating solution and the solvent is evaporated. Here, we performed the coating with the channel unsealed. Firstly, the middle and end hole on the spiral column is temporarily sealed with a small amount of pressure-sensitive adhesive. Then, a fixed amount of prepared solution is collected into a micropipette. Then, the unsealed channel is filled with the solution carefully. After it was entirely filled up, it was placed inside an oven at 50°C for 3 hour to completely evaporate the solvent leaving a layer of stationary phase coated on the micro channel. This process is performed twice for each spiral package since it has channel on both sides of the package. This technique requires adequate gap (400µm for easy execution) between the channels to ensure the stationary phase only flow inside the channel. This method was successful and produces a uniform layer of stationary phase of between 10-20 µm.

4.5 Design of Other Components

There are several other micro components that were built using the MSL machine. Similar to the micro retentive column, many of the components went through an evolution process in order to improve their performance. Here we discuss the design, fabrication and evolution of these components.

4.5.1 Sensor Chamber

The preliminary design of the sensor chamber was a simple cubic shape with connectors, as shown before in Figure 4.4b. As discussed before, in order to reduce the dead space within the system, the sensor chamber was built integrated into the column, as in Figure 4.15. Similarly, we retain the integrated chamber design in the spiral column by creating a chamber that is able to connect to the spiral column. Until now, the chamber design was a simple cubic (dimensions 20 mm x 14 mm x 2 mm) covering the sensor area. The initial design of the chamber is shown in Figure 4.15a. One of the problems with this design is that the sensor chamber is sitting on a layer of epoxy adhesive that covers the wire bonds between the sensor chamber and the PCB, as illustrated in Figure 4.15b. Another issue is that the height of the sensor chamber will vary slightly depending on the epoxy layer covering the bonds.
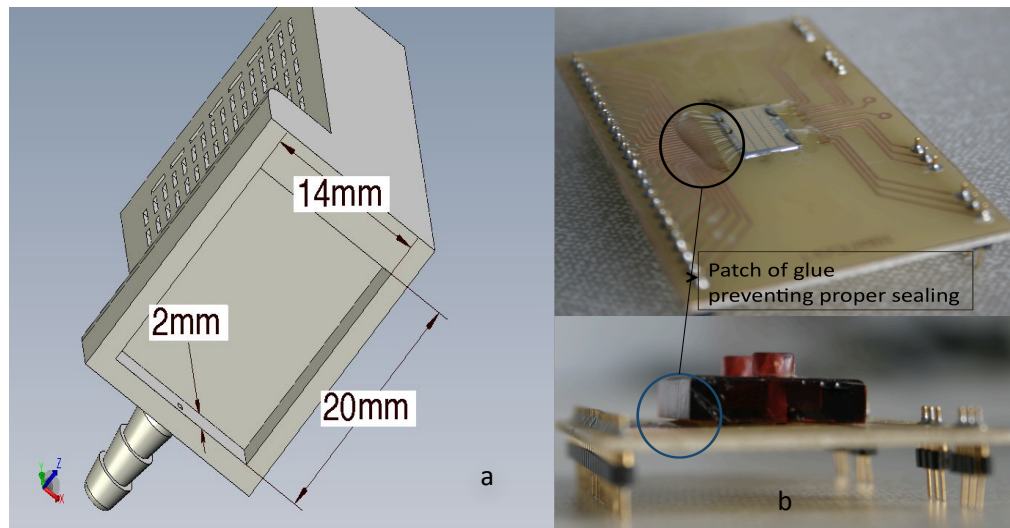
Figure 4.15: a) Initial design of sensor chamber b) Patch of glue blocking chamber sealing properly

To improve the chamber design, we decided to build a smaller chamber that would sit directly on the sensor array. This has two advantages a) in improved sealing of the sensor chamber and b) it increases the flow velocity over the sensors, thus improves the sensor response time. It has previously been demonstrated, by Tan, that higher flow velocities over a sensor reduces the response time[26]. Another advantage of miniaturizing the chamber is that the smaller chamber translates to a lower dead space, hence improving the system further. Based on the design by Tan, we have designed and fabricated a chamber with channel flowing through the sensor as in Figure 4.16. This design allow for smaller headspace on top of the sensor since it is placed exactly on the sensor chip instead of around the outside of the sensor chip (on top of adhesive covering wire bond) as in the previous design.
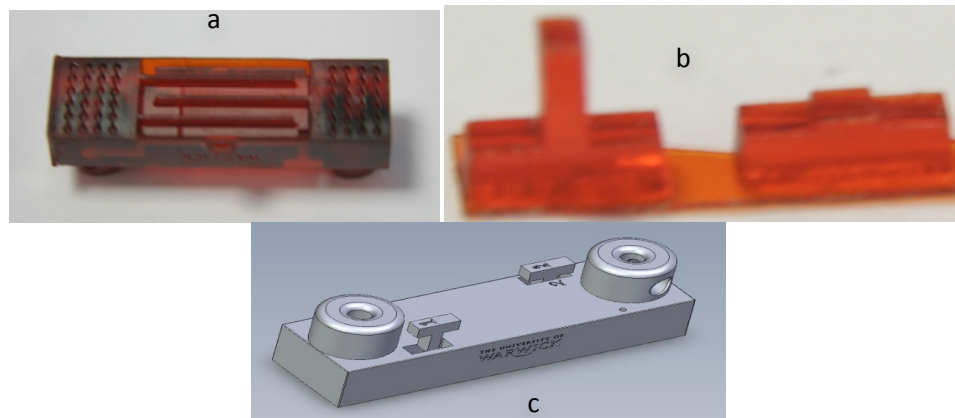
Figure 4.16: a) Miniaturised sensor chamber design b) alignment hole cover c) Exploded view of chamber assembly

Although it is no longer necessary to cover the wire bonds with glue, as the chamber (shown in Figure 4.16a is now sitting on top of the sensor itself, having the chamber sitting exactly on the sensor creates another challenge - alignment. Now, the sensor chamber needs to be aligned onto the sensor so that each channel fits perfectly on top of the designated row of sensors. To overcome this, we have created two alignment holes on the sensor chamber so that we can align it to the sensor (using a microscope) before gluing it to the sensor board. Figure 4.16b shows the alignment hole cover, which has been designed to fit perfectly into the alignment holes, creating a sealed micro channel. It is important to have the alignment holes fit perfectly as the spiral micro channel package is going to be placed on top of the chamber.

4.5.2 Odour Distribution Chamber

As described in Chapter 2, the complete system will have two micro retentive columns and three sensor arrays. The first sensor array does not need a retentive column connected to it. The chamber for the first sensor array will distribute the

incoming odour to the other columns. The odour distribution chamber, for the first

sensor array, needs to have three connectors, one inlet and two outlets to the

column. Figure 4.17 shows the odour distribution chamber.
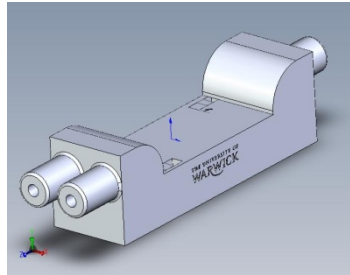
Figure 4.17: Odour distribution chamber

4.5.3 Deposition Mask

The deposition mask was also built with the MSL machine in order to get good

alignment while spraying the sensors with polymer composite films. As discussed in

the previous chapter, the mask was built with 12 holes (in a 4 x 3 format) with

dimensions as shown in Figure 4.18a. The built mask was attached to a Perspex

holder and fitted into an in-house alignment machine before spraying. Figure 4.18b

shows the mask being aligned to the sensor array under a microscope.
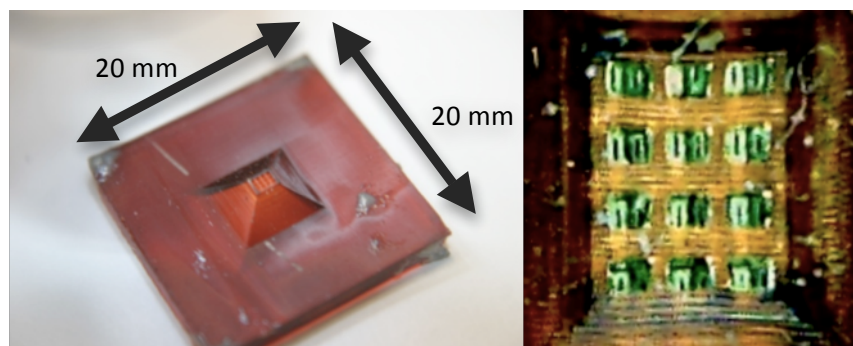
Figure 4.18: a) Deposition mask with dimensions b) Deposition mask aligned under
microscope

4.6 Portable Device Adaptation

Some modifications were required to adapt some of the components for the portable e-mucosa instrument. For the portable instrument, stacking the columns vertically (on top of the sensor chamber) would result in a bigger system. Thus, we decided to separate the chamber and spiral column in order to fit both components in a smaller space. Figure 4.19(a) shows the modification made to the connector of the chamber for the portable instrument. No modifications were needed for the odour distribution chamber. It is also worth noting that the connector was changed from Figure 4.19(b) in the initial design to Figure 4.19(c). The main reason was that the initial connector was easily snapped at the connecting grooves.
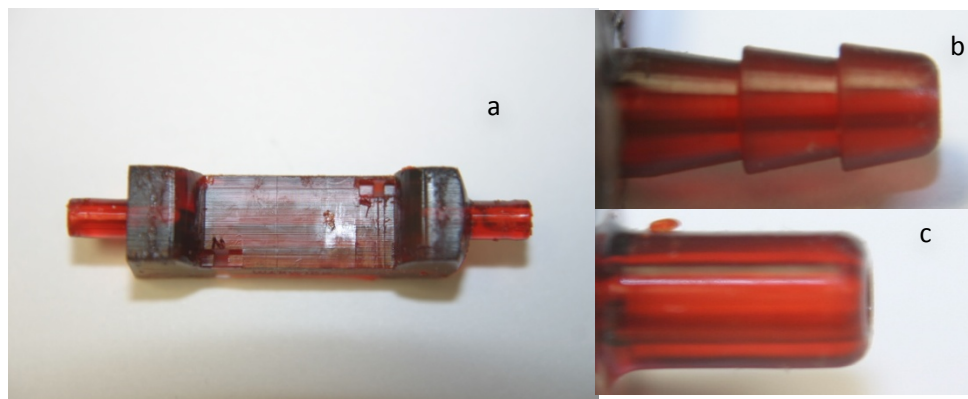
Figure 4.19: a) Modified sensor chamber b) Preliminary sensor connector c) Current sensor connector

For deposition of the polymer composites, as the portable mucosa only utilizes 200 sensors out of the 300, a new mask was designed and fabricated to deposit 8 sensors at a time. With 25 polymer blends available, a total of 200 sensors were fabricated in a series of 8 per block. Figure 4.20 shows the deposition mask with 9 holes (1 x 8 arrangements).
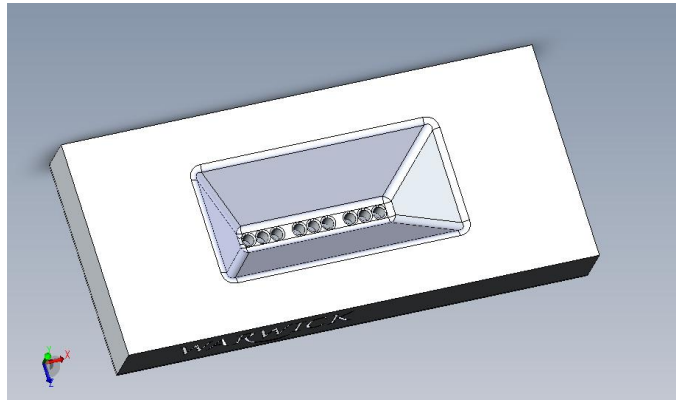
Figure 4.20: Mask for Portable e-Mucosa sensor deposition

Two new chambers were fabricated for the portable mucosa, namely the preconcentrator chamber and the inlet temperature chamber, both shown in Figure 4.21. The preconcentrator chamber is similar to the initial sensor chamber design, with three connectors. The preconcentrator will be described in more detail in Chapter 6. The inlet temperature/humidity chamber houses a Sensirion SHT15 temperature sensor, to monitor the odour temperature at the inlet of the system. Figure 4.21 shows is the connection converter that converts the spiral column connector to a smaller connector type and the column bridge that connects the column back side together.
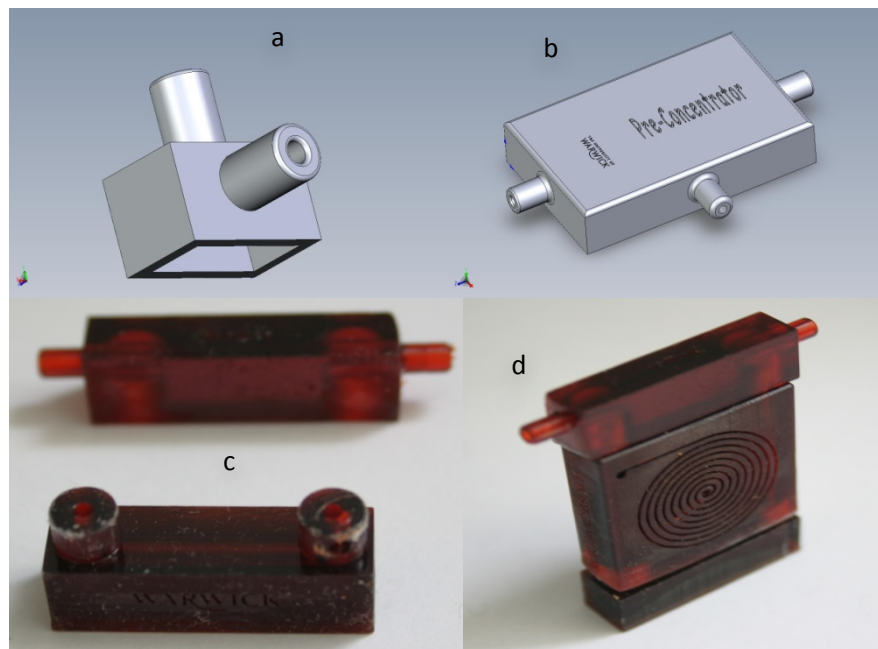
Figure 4.21: a) CAD Design of Temperature/Humidity Sensor chamber b) CAD Design of preconcentrator chamber c) Connection Converter & column bridge d) Assembled Column for Portable e-Mucosa

4.7 Conclusions

This chapter has discussed general concepts of stereolithography and microstereolithography fabrication. Micro retentive column and supporting components CAD Design has been designed using Solidworks and fabricated with an Envisiontec Perfactory Mini MSL machine. Design of the micro retentive column has evolved from a box type to a spiral column. Problems created by the box design, such as cleaning and coating difficulty, were solved by using a spiral column. Furthermore, integrating the sensor chamber into the column design reduced the dead space inside the system. The spiral column has been designed so it can be stacked together, to create a longer channel with the same feature size (MSL501-500µm x250 µm x 528mm, MSL501-380µm x250 µm x 549mm, MSL503 – 250µm x250 µm x 548mm).

Methods for sealing the microchannel were also discussed. Generally, the channel is sealed by placing glass spin coated with UV adhesive (LoctiteUV Glass Bond). A brief introduction and evaluation of gas chromatography stationary phases has been given. From this study OV-1(100 % PDMS) as our non-polar stationary phase and Carbowax 20M(100% PEG) as the polar phase was chosen. Then a review of common methods for stationary phase coating was described. Several methods have been investigated to achieve a thin uniform layer of stationary phase including vapour deposition, stating coating and spray coating.

Towards the end of the chapter, several more components built with the MSL machine were described including the sensor chamber, odour distribution chamber and deposition mask. The sensor chamber has been designed as small as possible to increase flow velocity at the headspace of the sensor in order to improve sensor response time [26]. Finally, the design, fabrication and adaptation of several components to fit into the portable e-mucosa were described. In the next chapter, the combination of the large sensor array with the micro retentive column, to create a complete system, will be described. Characterization of the micro retentive column will be described in detail in Chapter 7.

4.8 References

1. P.Webb, *A review of rapid prototyping (RP) techniques in the medical and biomedical sector.* Journal of Medical Engineering &# 38; Technology, 2000. **24**(4): p. 149-153.
2. W.Yeong, , et al., *Rapid prototyping in tissue engineering: challenges and potential.* TRENDS in Biotechnology, 2004. **22**(12): p. 643-652.
3. A.Stroock, and G. Whitesides, *Components for integrated poly (dimethylsiloxane) microfluidic systems.* Electrophoresis, 2002. **23**: p. 3461-3473.
4. A.Bhushan, et al., *Fabrication of micro-gas chromatograph columns for fast chromatography.* Microsystem Technologies, 2007. **13**(3): p. 361-368.
5. S.Kandlikar, and W. Grande, *Evolution of microchannel flow passages–thermohydraulic performance and fabrication technology.* 2003.

6. H.B.Sun, S. Matsuo, and H. Misawa, *Three-dimensional photonic crystal structures achieved with two-photon-absorption photopolymerization of resin.* Applied Physics Letters, 1999. **74**(6): p. 786-788.

7. S.Maruo, and S. Kawata, *Two-photon-absorbed near-infrared photopolymerization forthree-dimensional microfabrication.* Microelectromechanical Systems, Journal of, 1998. **7**(4): p. 411-415.

8. A.Bertsch, et al., *Microstereolithography: a review*. 2003, SWISS FEDERAL INST OF TECHNOLOGY LAUSANNE (SWITZERLAND).

9. T.Takagi, and N. Nakajima. *Photoforming applied to fine machining*. 1993.

10. K.Ikuta, and K. Hirowatari. *Real three dimensional micro fabrication using stereo lithographyand metal molding*. 1993.

11. A.Bertsch, et al., *Microstereophotolithography using a liquid crystal display as dynamic mask-generator.* Microsystem Technologies, 1997. **3**(2): p. 42-47.

12. L.Hornbeck, *Digital light processing TM for high-brightness, high-resolution applications*. 1997.

13. L. Beluze, A. Bertsch, and P. Renaud. *Microstereolithography: a new process to build complex 3D objects*. 1999.

14. S.L.Tan, , *PhD Thesis*. 2005, University of Warwick. p. 260.

15. Envisiontec. *envisionTEC R 05 / R 11 Technical Data*. Available from: http://www.envisiontec.de/index.php?id=54&L=%23%23%23LANGID%23%23.

16. F.K. Che Harun, P.H.King, J.A. Covington, J.W. Gardner, *Novel gas chromatographic microsystem with very large sensor arrays for advanced odour discrimination.* IEEE SENSORS 2007 Conference, 2007: p. 1361-1363.

17. W.Reynolds, *Gas chromatographic retention data*. 1966.

18. F. Eugene, R.L.G., *Columns for gas chromatography: performance and selection*. 2007: Wiley-Interscience.

19. R.A. Friedrich, Chromatographia, 1977. **10**(10): p. 593.

20. M.Lee , F. Yang, and K. Bartle, *Open tubular column gas chromatography: theory and practice*. 1984: John Wiley & Sons.

21. R.Scott, *Gas Chromatography*. Available from: http://www.chromatography-online.org/GC/GC-Columns/Capillary/Dynamic-Coating/rs29.html.

22. S. Terry, J. Jerman, and J. Angell, *A gas chromatographic air analyzer fabricated on a silicon wafer.* IEEE Transactions on Electron Devices, 1979. **26**(12): p. 1880-1886.

23. R. Reston, and E. Kolesar, *Silicon-micromachined gas chromatography system used to separate and detect ammonia and nitrogen dioxide. I: Design, fabrication, and integration of the gas chromatography system.* Journal of microelectromechanical systems, 1994. **3**(4): p. 134-146.

24. S. Reidy, et al., *High-Performance, Static-Coated Silicon Microfabricated Columns for Gas Chromatography.* Analytical Chemistry, 2006. **78**(8): p. 2623-2630.

25. H. Noh , P. Hesketh, and G. Frye-Mason, *Parylene gas chromatographic column for rapid thermal cycling.* Microelectromechanical Systems, Journal of, 2002. **11**(6): p. 718-725.

26. S.L.Tan, et al. *Ultra-fast/low volume odour delivery package for chemical microsystems*. IEEE Sensors, 2004, 3, p. 1171-1174.

CHAPTER 5

Electronic Mucosa-Nose: Integration

5.1 Introduction

Previously we have discussed the design and fabrication of major components of the e-mucosa instrument, specifically covering the development and deployment of the large sensor array and Micro-GC column packages. This chapter discusses the electronics circuitry used in the instrument, followed by integration of the large sensor arrays and micro retentive column creating an improved miniaturised electronic nose instrument. A brief description about the electronic mucosa nose instrument will be outlined followed by the large sensor array connection and circuitry. Then the micro retentive channel functionality will be described along with the flow system of the electronic mucosa. Finally, software development for the instrument is explained, including a brief introduction to the Nose II Network e-nose file format standard.

5.2 Electronic Mucosa-Nose Instrument

The electronic mucosa instrument has been realised by combining three 300 element chemoresistive-sensor arrays, employing composite polymer materials as

the sensing layer (carbon black, mixed with 24 combinations of different sensing polymers), and two micro retentive polymer columns, coated with polar and non-polar retentive layers. Figure 5.1 illustrates the concept of electronic mucosa system.
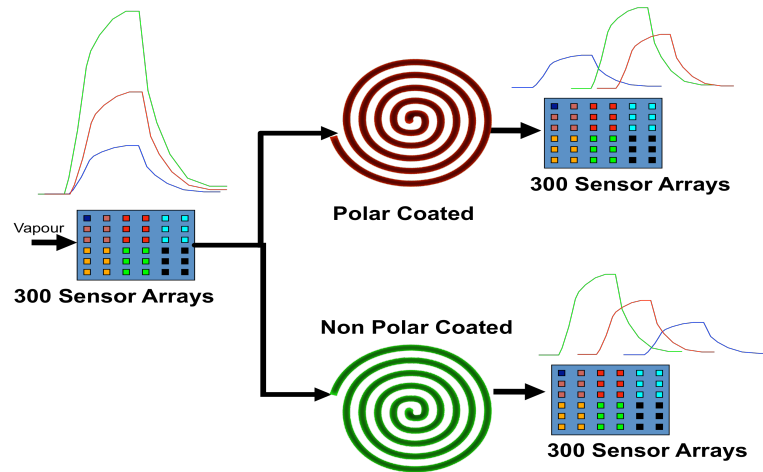
Figure 5.1: Diagram of Electronic Mucosa Dual Dimensional concept

The electronic mucosa instrument consists of three similarly coated (sensing material) chemoresistive sensor arrays and two differently coated (polarity) micro retentive columns [1]. In operation, a tested odour will pass through the first sensor array giving a high magnitude spatial representation of the odour. As mentioned earlier, the sensor arrays are coated with 24 different gas sensitive films in order to obtain a variety of responses to the same odorant. Furthermore, 12 of the 300 sensors were coated with a similar material (coatings deposited at the same time) providing redundancy that is useful during data processing. For example, sensor selection can be used to choose the best sensor among the 12 to be processed. One of the main reasons why redundancy is important, in this particular situation, is the difficulty of spraying sensors with similar properties, due to the inherent variations in the deposition process.

After passing over the first sensor array, a test sample will be distributed equally between two-spiral columns coated with different polarity stationary phases.

The flow to the two columns was maintained at the same rate using two micro valves connected to the end of each column. Depending on the tested odour, the column will delay the sample based on the reaction between the chemical components and the stationary phase coating. Polar molecules will be retained longer in the polar column and on the non-polar column, based on the samples boiling point. Using this method, we are able to acquire two varieties of temporal data with the same tested odorant. This information, combined with spatial data, termed 'spatio-temporal' data is used to classify the odorant. The end two-sensor array will provide the spatio-temporal response of the odorant. The concept of using spatio-temporal data in the biological olfactory system was demonstrated by Mozell in 1974, when he studied the 'nasal chromatograph' effect in humans[2]. In 2006, Scott et.al. studied various areas that contribute to the sensitivity of biological olfactory processing system, including spatio-temporal coding in several species (salamanders, mice and frogs [3]). Several researchers have developed artificial systems that produce spatio-temporal data. In the field of electronic noses, Tan and Briglin have both demonstrated spatio-temporal response by flowing a test odour through a sequential sensor array inside a microchannel[4,5]. Based on Briglin works, the initial sensor will absorb some of the odour leaving less odour molecules to be processed on the next sensor, creating a sequential spatio-temporal response within the system. Both researches only experimented with one-dimensional spatio-temporal response. Here we demonstrate dual micro retentive column creating a more diverse set of information. We believe that the spatio-temporal signal, alongside various other advancements (larger sensor array, sensor redundancy, large

sensor tuning set and dual spatial response) in the instrument will improve odour discrimination for simple and complex odours.

5.3 Large Sensor Array Electronics Circuitry

The electronics for the large sensor arrays has been specially designed and developed for extracting the high number of signals from individual sensing units. The electronic circuitry supports up to 4 × 300 sensors. Each sensor is driven by a tailored constant current to circumvent any issues of varying resistance. The circuitry for driving the sensor arrays is distributed on two separate PCBs, one contains the current sources and the second the signal conditioning for the sensors. The second PCB also contains a multiplexer that switches between four different sensor arrays (thus one batch of measurement circuits can be used on up four different arrays). In addition, this PCB contains the flow control circuitry for the fluidic system.

Here we will describe the design and fabrication of these two boards. Figure 5.2 shows the block diagram of the interfacing between the two boards. In its simplest form, board 2 is just an extension to board 1, multiplexing the 4 sensor arrays, so that only one sensor array is connected to board 1 at any one time. Board 2 also includes control circuitry for the fluidic system, performing the role of odour selection and delivery achieved by controlling the valves and pump.
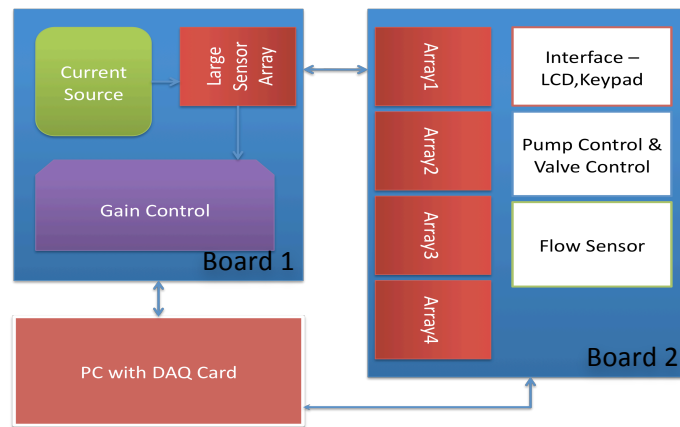
Figure 5.2: Block diagram of component on each board and interfacing with PC

5.3.1 Data Acquisition, Constant Current and Signal Conditioning - Board 1

The basic principle for a chemoresistive sensor, used here, is that as an odour reacts with the gas sensitive element on top of the sensor electrode, it is going to trigger changes to the resistivity of the polymer composite film. Hence, the data acquisition system needs to be able to detect these changes and translate them to a signal or value that can be used in signal processing. It is important for the sensor to detect small changes in resistance to create a more sensitive sensor. In order to detect changes in resistance, a constant current source is used to supply constant current to an individual sensor. Changes in resistance will translate to changes in voltage (as the current is constant).

The sensitivity/selectivity and thus resistance change of each sensor varies from one sample odour to another and between polymers. Also, the actual measured baseline resistance can vary from its initial value (as deposited) due to factors, such as the age of the polymer film, environmental conditions (temperature, humidity, etc.) and poisoning. Thus, the data acquisition circuitry needs to be adaptable and robust enough to accommodate a large range of baseline resistances

as well as having gain control capable of detecting small resistance changes for each particular composite film in the sensor array. Consequently, in designing the electronics, some plug-in components and programmable components were used to increase the flexibility. Some flexibility to the board is the ability to change current source by changing a plug in resistor and four gain control set in a programmable gain amplifier.

Board 1 is basically a data acquisition system for 300 sensors with baseline, gain and constant current control. As shown in Figure 5.3, the sensor voltage is measured using National Instrument AT-MIO-16-XE-50 data acquisition card with the ability to read analogue channel at 16 bit resolution[6].
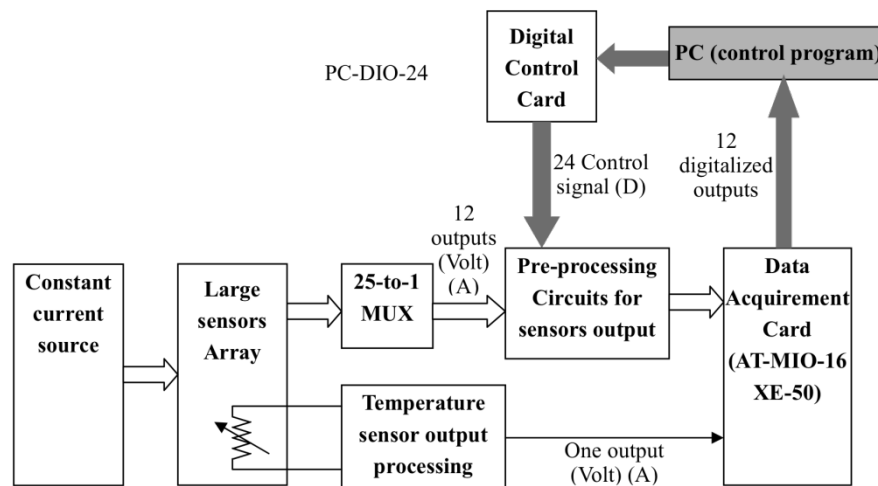
Figure 5.3: Functional Diagram of Data Acquisition System

As discussed in Chapter 3, the 300 sensors arrays were arranged in a 25 x 12 arrangement. This makes data acquisition easier with only 37 pads required instead of 600 (2 per sensor) if each sensor is measured individually. Here, 12 constant current sources were used to supply current to the sensor column pad. They provide the capability to measure 12 sensors at once. Instead of having to scan between sensors 300 times, having 12 identical constant current source, all 300 sensors can

be read with only 25 sequential scan. A 25 to 1 multiplexer was designed using three ADG608 (8 to 1) and one DG417 to switch between the 25 rows of sensor. Digital component on the board was controlled using Digital Control card (PC-DIO-24) via software written in Labview 7.1[7]. Twelve programmable gain amplifiers (PGA205, Burr-Brown) were used to control gain of 1, 2, 4 and 8 to the sensors. These amplifiers are controlled via software with the ability to control individual gain during data acquisition. Board 1 also contained circuitry to interface and measure the temperature from the on-chip temperature sensor. Figure 5.4 shows a photo of Board 1 with all the component sited.
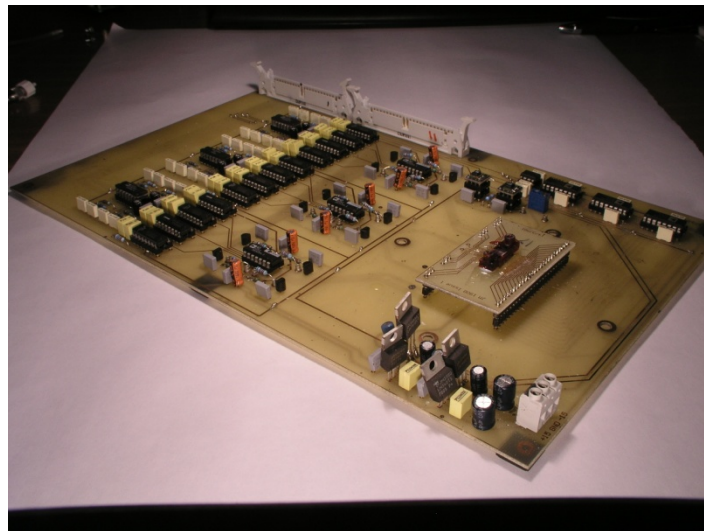
Figure 5.4: Board 1- Data Acquisition and Signal Conditioning Board

5.3.2 Sensor Array Multiplexer and Odour Delivery - Board 2

Board 2, as shown in figure 5.5, functions as a 4 to 1 sensor array multiplexer and odour delivery controller. It has been designed to accommodate four sensor arrays that translate to 1200 individual sensors. The board is controlled via a software interface (National Instruments Labview7.1) through a National Instrument M Series PCI-6229 Multifunctional card [8].
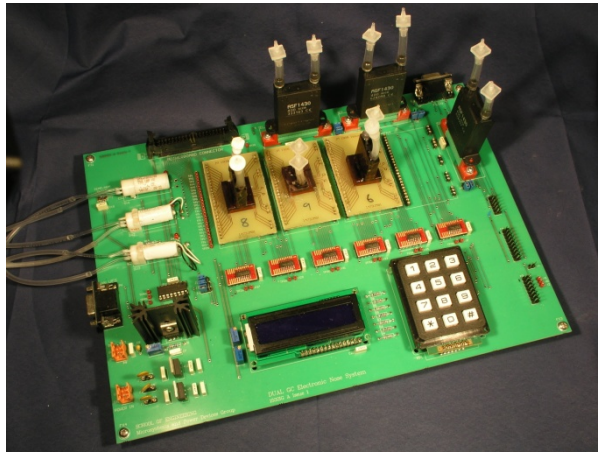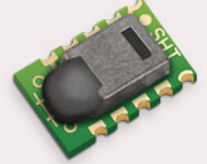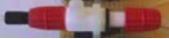
Figure 5.5: Board 2- Senor array multiplexer and Odour Delivery control

The four sensor arrays are multiplexed using 12 four to 1 multiplexer (MAX4052). Each sensor array column is connected to one of the four multiplexer connections and there are 12 connections corresponding to 12 columns. Only one array can be selected at one time and the other remains at high impedance (effectively unconnected). In order to read all 4 sensor array, the data acquisition software will be switched on and measure sequentially between the arrays.

The odour delivery system on Board 2 consists of a pump, three flow sensors, temperature and humidity sensors and three micro valves. The odour delivery system will be described further in the next section. Apart from the odour delivery component, Board 2 also contains a 20 x 2 Liquid Crystal Display (LCD) and a 4x3 keypad. These components are built together with the board as a prototype to evaluate the system before miniaturizing it. The LCD and the keypad provides the ability of the system to operate independently without PC software. Interconnection to microcontroller has been placed as shown in Figure 5.5. A microcontroller kit (PICDEM HPC Explorer) based on Microchip PIC18F8722 was used as an alternative to PC Software to control the system. These provide a way to evaluate the system to

ensure the portable device will work accordingly. Table 5.1 shows the individual component of the odour delivery system.

Table 5.1: Component function in odour delivery system

Part	Picture	Supplier	Usage
Flow Meter ASF1430		Sensirion	Flow rate measurement
Three Way Valve		Lee Co	Select between refrence gas and test odour
12V DC Pump		KNF	Transport odour and gas through the system
Temperature Humidity Sensor SHT15		Sensirion	Temperature /Humidity Measurement
Throttle Valve		Cole Parmer	Control Flow rate
Tubing		Cole Parmer	Interconnection between component

5.4 Odour Delivery System
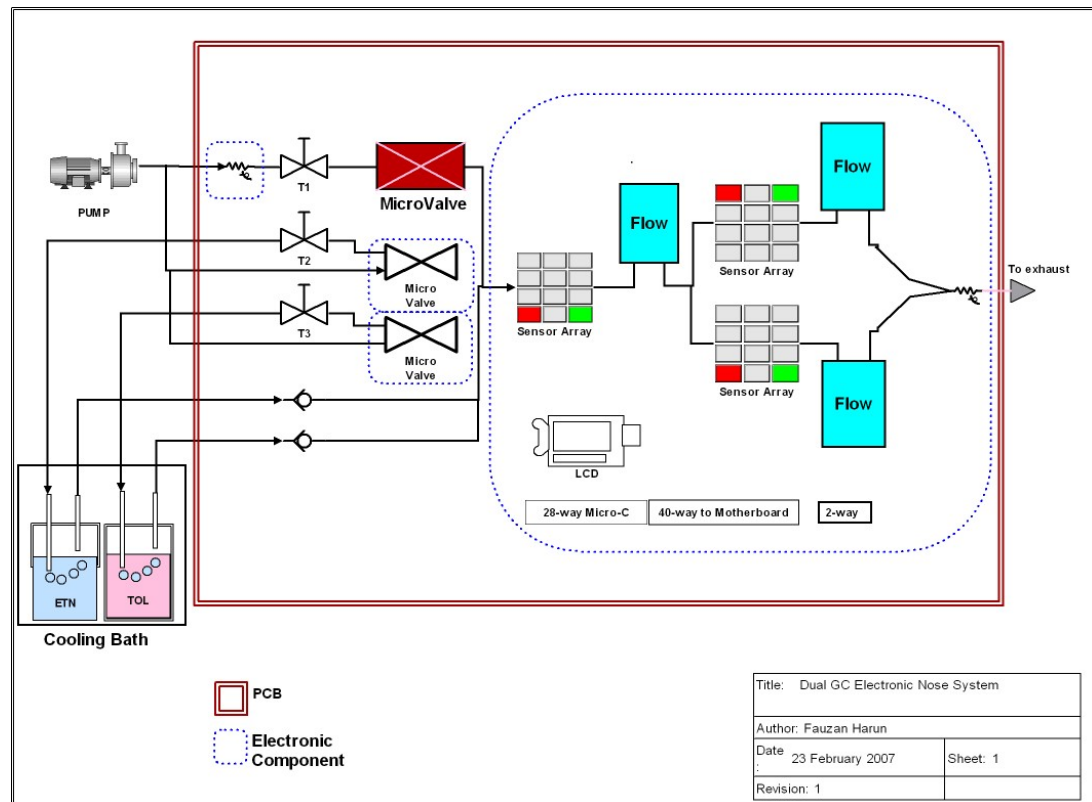
Figure 5.6: Integration- Odour delivery system and Data Acquisition Electronics Diagram

Figure 5.6 shows the odour delivery system connections to the electronic circuitry. The pump will push either the test samples or lab air into the sensor chamber. Throttle valve T1 controls the flow of reference air through a micro valve before going into Sensor Array 1. Throttle valve T2 and T3 control the flow rate from the two test analytes into Sensor Array 1. A non-return valve is placed at the outlet of each sample to prevent the reference air from going into the sample headspace. A temperature and humidity sensor is placed on the inlet of the reference gas to check the condition of air coming into the system. An automated long duration test without human intervention can be performed with both test samples using this arrangement.

The flow rates throughout the system were monitored using three flow sensors, each placed after one sensor array. This provides the ability to check for leakage on individual sensor array chambers. All connections were made using plastic tubing and each tube run was kept as short as possible to reduce the dead space within the system. A cooling bath as in Figure 5.7 was used to maintain the temperature of the test analytes to reduce error in the experiment. The cooling bath also provides a way to reduce the concentration of tested analytes.
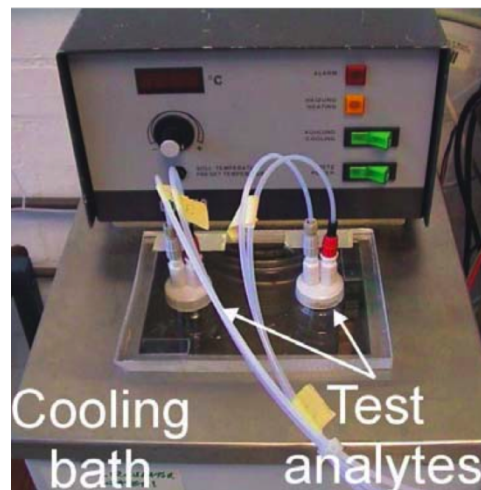
Figure 5.7: Cooling Bath for test analytes

5.5 Data Acquisition Software

The software used for data acquisition and odour delivery control were developed using National Instrument Labview 7.1, combined with various data acquisition cards (AT-MIO-16-XE-50, M6229 and PC DIO 24) connected to a custom electronic circuit. Figure 5.8 shows the data acquisition panel for one sensor array of Board 1. The software, connected to a data acquisition card AT-MIO-16-XE 50 measured up to 12 channels (corresponding to 12 columns) at a time. The measurement is repeated 25 times to get a total of 300 sensor voltages corresponding to the changes in

resistance on the chemosensor array. The measurement is saved in two files, one containing the sensor response voltages and the other containing the time data. As mentioned before, within the signal conditioning circuitry there are programmable gain amplifiers to boost the voltage signal from the sensors. There are 12 programmable gain amplifiers on the board, grouped into blocks of 4. Each amplifier has four different gain levels that can be set via software to amplify the sensors accordingly.
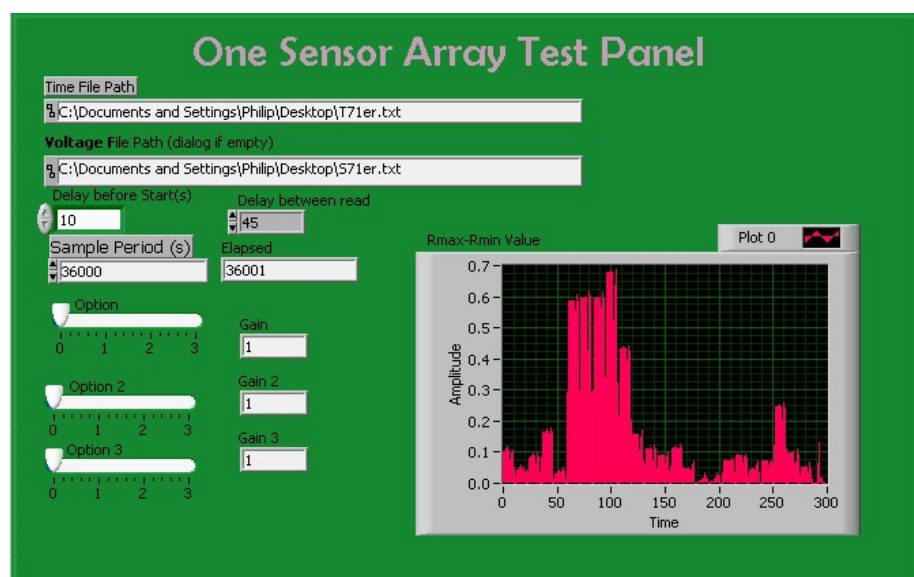
Figure 5.8: Test panel for Data Acquisition Board 1

Before running the software, the total test period is set according to the vapour delivery system end time. This is to synchronize the data acquisition and vapour delivery system. The vapour delivery system (shown in Figure 5.9) used to test the 300 sensor array was previously developed here at the University of Warwick and used a separate PC and software[9].
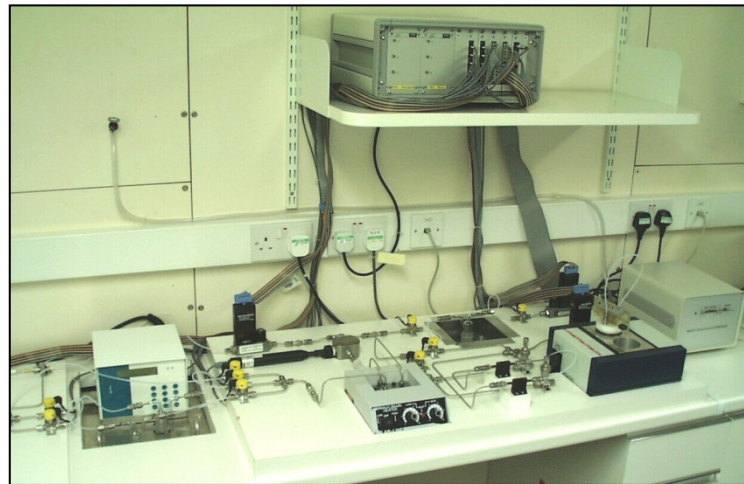
Figure 5.9: Vapour Delivery system developed at University of Warwick [9]

At the end of the measurement, the software will calculate R_{max}-R_{min} value from the response and plot a graph representing all 300 sensors in term of magnitude of response. This provides a quick look of the total sensor response pattern to certain test sample.
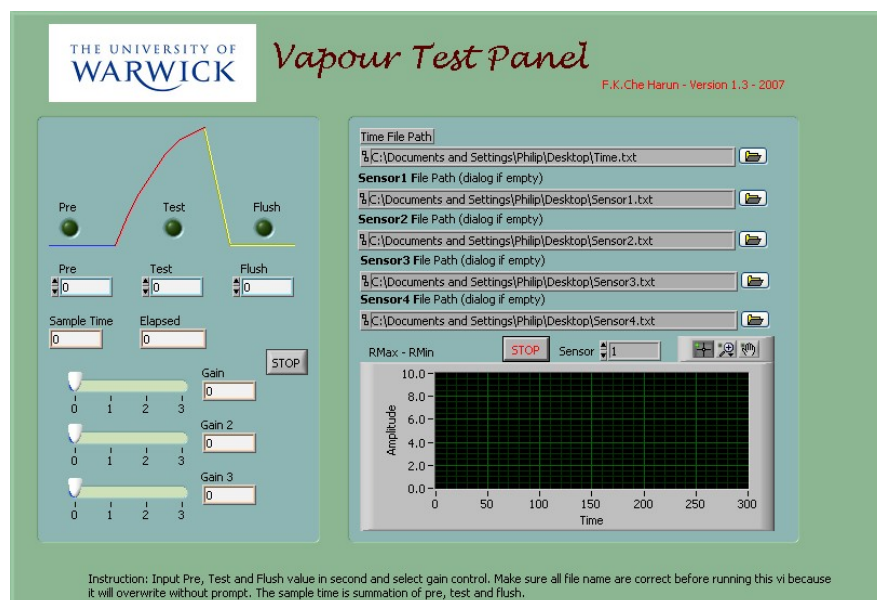
Figure 5.10: Vapour Test panel for 1200 sensor in 4 sensor arrays

Figure 5.10 shows the main panel of the vapour test rig, which is used to control the 4-sensor arrays. The software controls both Board 1 and Board 2 using multiple

National Instrument data acquisition cards. Similar to the test panel of 300 sensors, this panel also includes gain control and 300-sensor pattern display on graph. However, the difference here is the number of 'save files' available, where the sensor responses of the four-sensor arrays are saved in separate txt file for easy management during data processing. The Time data is saved only to one txt file.

The software also includes control code for the odour delivery system, allowing the period of test for each stage (Pre-Test, Test and Flush) to be adjusted. These timing periods control the exact time when the valve on the board should be opened or closed.

Separate software was developed to read, display and record the sensor responses. The reason why no 'live' viewing is implemented is to focus as much CPU cycle as possible on data acquisition, instead of data display. This is important in a system with a large sensor number. The sensors response viewer, as shown in Figure 5.11, is used to display up to 5-sensor responses for a quick view of the sensor reaction. The graph on the left displays a detail view of the first selected sensor while the second graph displays a total of up to 5-sensor responses.
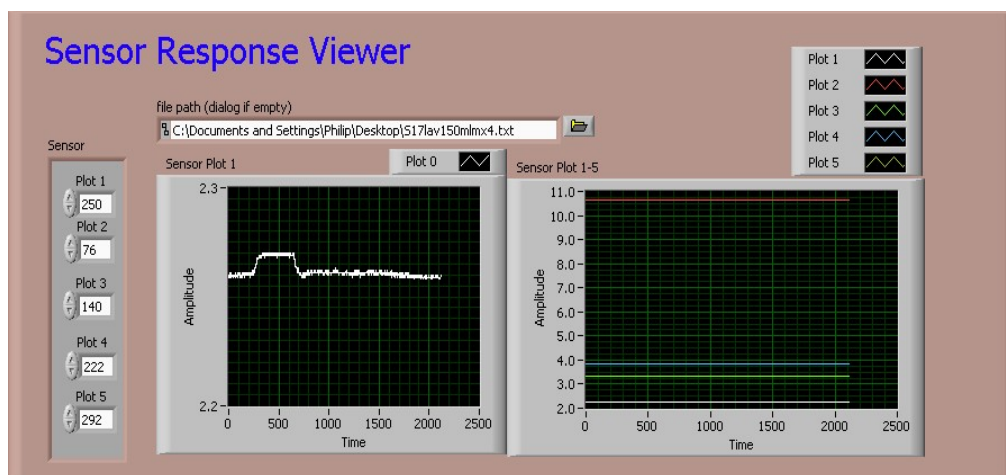
Figure 5.11: Sensor response viewer

5.6 Support Software

Several other software programs were developed to support the instrument. Here we explore the other software programs created to support the instrument including Live Deposition Viewer, Vapour Concentration Calculator and XML Nose II Converter. A brief explanation of the software used for data processing is also described here.

5.6.1 Live Deposition Viewer
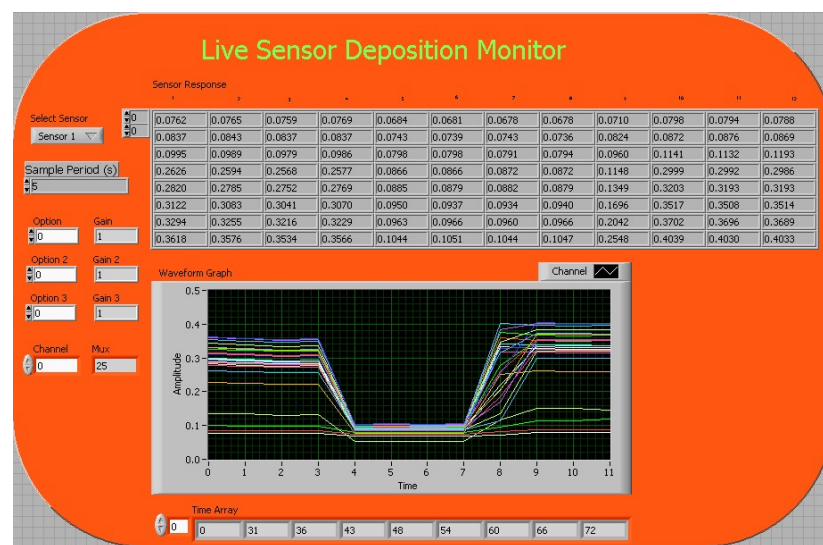
Figure 5.12: Live Sensor Deposition Monitor

As mentioned before, the resistance of each sensor is monitored during deposition to ensure repeatability and that the resistance is within a useable range. The live sensor deposition monitor as shown in Figure 5.12 was developed to perform this role. A graph was also plotted to quickly see the changes in resistance for easier deposition. An interface was created to mount and connect the sensor array to the 'Live Deposition Monitor', achieved through a custom made cable, as shown in Figure 5.13.

Figure 5.13: Interface cable from mask aligner to data acquisition board

5.6.2 Vapour Concentration Calculator

The vapour concentration is calculated using Antoine Vapour Pressure equation [10] for several test vapours. The Labview program, shown in Figure 5.14, was developed to calculate the sample flow from a specified vapour concentration. Other variables that are taken into consideration are the sample temperature and total flow rate, which is calibrated at 300 ml/m for the gas test rig. Constant for each analytes (ethanol, toluene, ethyl acetate, n-pentane, xylene and propanol) is extracted from Lange's Handbook of Chemistry[10].
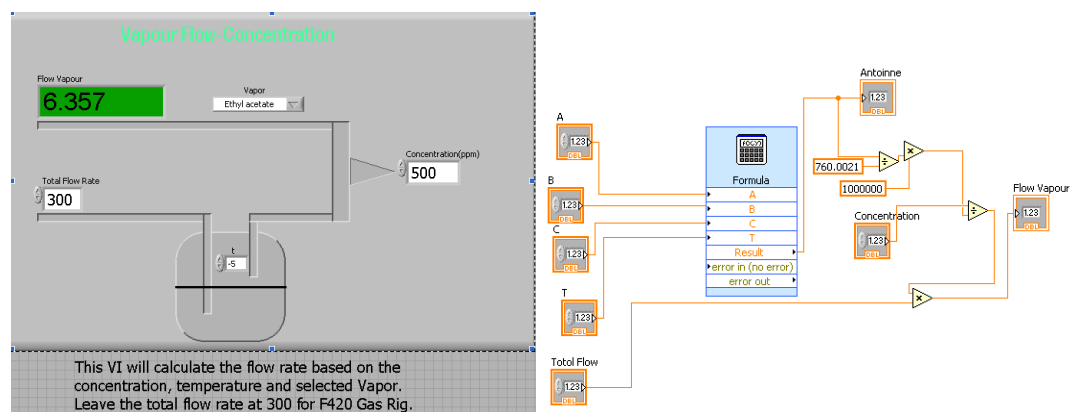
Figure 5.14: Main panel of Vapour Concentration Calculator with Functional Block Diagram

5.6.3 NOSE II XML Converter

The Nose II network has develop a standard official data format of e-nose data, lead by Jan Mitrovics of JLM Innovations [11]. The objective of the standard was to reduce time taken to convert data, thus making data exchange easier and strengthen inter-partner collaboration. A standard data format is also a prerequisite for the building of a database for electronic nose data. The general requirement that has been outlined by the Nose Network regarding the format is as follow[12]:

1. *The data format shall be platform (OS) independent.*
   Most users currently use Windows, but other platforms (e.g. Linux) become more and more important.
2. *The data format shall allow easy deployment over the Internet.*
3. *The data format shall facilitate the storage in a database.*
4. *The data format shall be easy to read and understand.*
5. *The data format shall be flexible and extensible, to be able to adapt the data format to various instruments / applications and to incorporate future developments.*

To meet the requirement, XML (extensible Mark-up Language) has been selected as the base of the format due to the advantages of meeting all of the listed criteria. The fact that it is easily read and understood makes it easier to create a converter. The simplified structure tree for a simple e-nose XML data is shown in Figure 5.15. The complete structure of a valid NOSE II file is defined in the data definition file enose.dtd, and is available from the official NOSE II website.
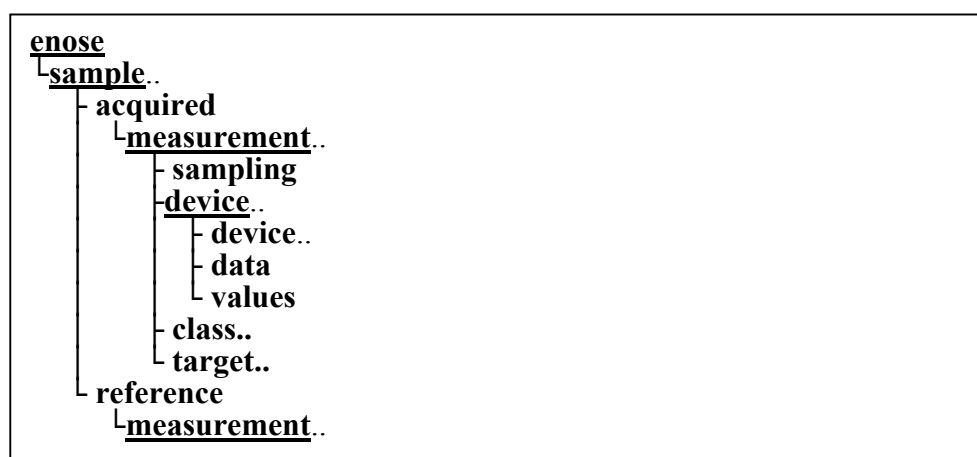
Figure 5.15: E-nose XML data structure[12]

For this project it was decided that response data would be recorded in the e-nose XML data format for easier distribution. Thus the sensor data would be available for distribution to other researchers to study different methods of data processing, especially the spatio-temporal response. Furthermore, this makes it possible to use several programs, already developed for this e-nose format, such as the XMLViewer and Multisens Analyzer (previously known as E-Nose Analyzer)[13] to explore the data.
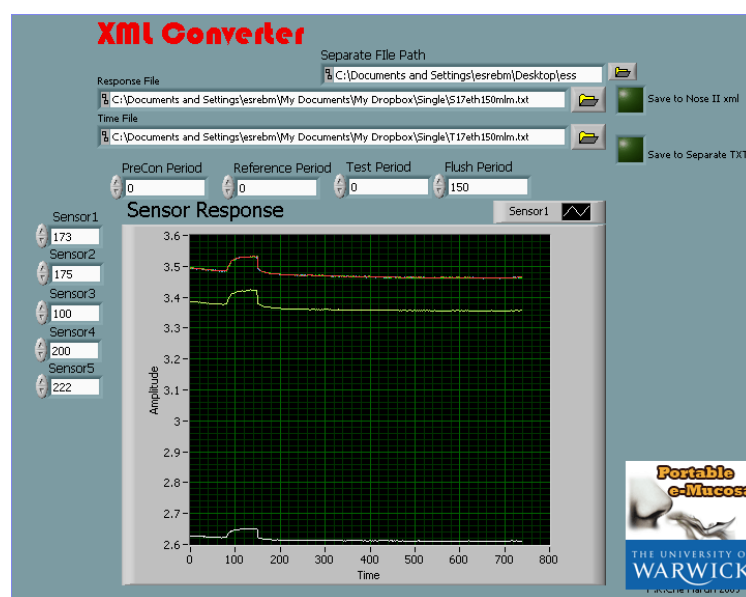
Figure 5.16: XML Converter for 1200 sensors

Figure 5.16 shows the main panel of the XML Converter software. On this panel, the response file and time file were loaded and saved file format was selected. Data can be saved in XML format or TXT for use in Matlab. Furthermore, a quick view of the sensor response was also available. At the core of the program, the response data and other parameter including test period are rearranged in a cluster and then flattened into XML using EasyXML vi from JKI Software[14]. A sample XML e-nose file is presented in Appendix A. The converted file can then be used in the XML viewer or Multisens Analyzer for further processing.

5.7 Data Proccessing Software

Data processing associated with this research (especially for the spatio-temporal data) is being done in detail in a separate study [15]. However, data representation and simple data processing such as Principal Component Analysis (PCA) have been performed using Matlab 2008 and Multisense Analyzer by JLM Innovation. Graph representation and Colour Plots from the large sensor arrays have been performed in Matlab, while most PCA or LDA processing was performed in Multisens Analyzer. One advantage of using the Multisens Analyzer program was the ability to view and select the best sensor without the need to review all 300 sensors. Figure 5.17 shows Multisens Analyzer software with two windows displaying 300 sensors response to Ethanol and Toluene vapour in air.
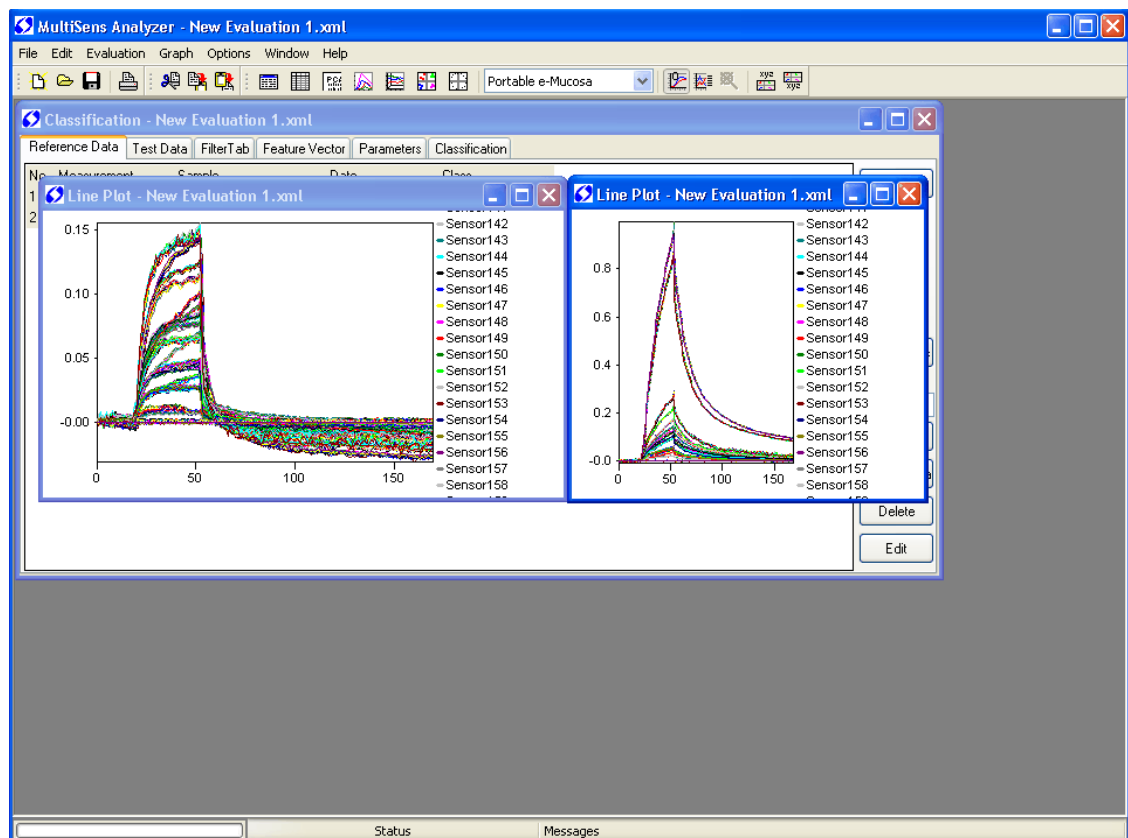
Figure 5.17: Multisens Analyzer displaying 300 sensors response to Toluene and Ethanol

5.8 Conclusions

In this chapter we have discussed the integration of the large sensor arrays and odour delivery fluidic system to create a complete the e-nose instrument. This discussion has covered the concept of the complete e-nose instrument, consisting of; a) three large sensor arrays, b) two micro retentive columns and c) the interface circuitry that binds the instrument together. The main instrument consists of two separate boards, Board 1 contains the data acquisition and signal conditioning circuitry for one (300 element) sensor array, whilst Board 2 contains the 4-sensor array multiplexer with odour delivery system control. Both boards are controlled with a PC containing various data acquisition cards (AT-MIO-16-XE-50, M6229 and PC DIO 24) via software developed with Labview 7.1. The data acquisition software has been explained with reference to the test rig configuration. Two test rigs (odour delivery systems) were used to test sensors, one previously was developed at the University of Warwick[9] and the other one was built onto Board 2. The interface board was configured so that the voltage gain from any one sensor, of the 300 sensor elements, can be set (in real-time) to one of four values (note we use a constant current source to drive the sensors and measure the resultant voltage drop). In this way we ensure that even with variations in sensor baseline (due to deposition, aging, poisoning etc.) we can still monitor the sensor response. The software has also an integrated viewer for quick evaluation of the overall system. Separate software was designed to display the sensor response after the data acquisition was completed. The reason separate software was developed is to focus CPU power towards data acquisition, thus improving the speed of the instrument.

Finally, subsidiary support software for the instrument was described including Live Deposition Viewer, Vapour Concentration Calculator and XML Nose II Converter. The Live Deposition viewer was important to maintain similar deposition properties of the gas sensitive polymer composite layers. The data acquired by the instrument was converted into XML Nose II format to conform to the European e-nose data standard. The main advantage of a standard format was the ability to exchange data easily between researchers strengthening inter-partner collaboration.

The next chapter will discuss the design, fabrication and software development of a portable device based on the electronic-mucosa-nose system discussed in this chapter.

5.9 References

1. F.K. Che Harun, J.E.Taylor., J.A. Covington, J.W. Gardner, *Dual-Channel Odor Separation Columns with Large Chemosensor Arrays for Advanced Odor Discrimination.* International Meeting of Chemical Sensor, 2008.
2. M.M. Mozell, M.J., *MECHANISMS UNDERLYING THE ANALYSIS OF ORDORANT QUALITY AT THE LEVEL OF THE OLFACTORY MUCOSA I. SPATIOTEMPORAL SORPTION PATTERNS*.* Annals of the New York Academy of Sciences, 1974. 237(Odors: Evaluation, Utilization, and Control): p. 76-90.
3. J.W.Scott, *Sniffing and Spatiotemporal Coding in Olfaction.* Chem. Senses, 2006. 31(2): p. 119-130.
4. S.M.Briglin , et al., *Exploitation of spatiotemporal information and geometric optimization of signal/noise performance using arrays of carbon black-polymer composite vapor detectors.* Sensors and Actuators B: Chemical, 2002. 82(1): p. 54-74.
5. S.L. Tan, *SMART CHEMICAL SENSING MICROSYSTEM: TOWARDS A NOSE-ON-A-CHIP.* PhD Thesis, 2005.
6. Instrument, N. *E Series Multifunction DAQ – 20 kS/s, 16-Bit, 16 Analog Inputs*.
7. Instrument, N. (1996) *PC-DIO-24 User Manual*.
8. Instrument, N. *NI PCI-6229 16-Bit, 250 kS/s, 32 Analog Inputs*.
9. J.A.Covington, *PhD Thesis.* University of Warwick, 2001.
10. N.Lange, and J. Dean, *Lange's handbook of chemistry*. 1973: McGraw-Hill New York.
11. J. Mitrovics, *Workgroup: Standard data format for electronic nose data*. Available from: http://www.nose-network.org/content/view/24/51/.
12. J.Mitrovics, *NOSE II data format version 0.4.* 2005, JLM Innovations.
13. J. Mitrovics, *MultiSens Analyzer*. 2008; Available from: http://www.jlm-innovation.de/products/multisens_analyzer.
14. *Easy XML Documentation*. 2008; Available from: http://jkisoft.com/easyxml/docs/.
15. J.W.Gardner, J.E.Taylor, *Novel Convolution Based Signal Processing Techniques for a Simplified Artificial Olfactory Mucosa.* Transducer, 2007: p. 2473-2476.

CHAPTER 6

Portable Electronic Mucosa System

6.1 Introduction

For many years researchers have been interested in developing portable e-nose instruments. Such systems would allow the operator to take a sample at source (for example, an environmental measurement) instead of either taking a sample or taking the headspace of the sample to the lab. These developments culminated in the Cyranose 320 by Cyrano Sciences[1]. Although the Cyranose is now owned by Smiths Detection, USA, other researchers and companies are coming up with their own version of portable and handheld e-nose device. The zNose 4500 by Electronic Sensor   Technology is a portable instrument utilizing GC/SAW(DB-1 column) detection method with part per billion (ppb) sensitivity [2] (achieved through the use of a pre-concentrator). TechnoBiochip also produces a portable device called LibraNose based on GC/QCM array detection method [3]. However, these two devices are both portable but not handheld and still require a laptop/PC to operate. PEN3 by Airsense Analytics is a handheld device that is capable of identifying up to 10 different compounds that has been previously trained [4].

In 2000, Hyung demonstrated a portable electronic nose instrument using an metal oxide gas sensor array with artificial neural network for signal processing[5]. A

year later, Perera demonstrated a portable device with 12 metal oxide sensor with built in signal processing technique[6]. In 2005, a portable e-nose based on 16 carbon black composite with interface to PDA or Laptop was demonstrated[7]. It can be seen here that the maximum number of sensor which has been used for portable device is still less than 32 (as with the Cyranonose). In almost all aspects the Cyrano is still at the pinnacle of portable e-nose instrumentation.

Some researchers have also shown the possibility of developing a portable gas chromatograph instrument. Terry et. al was a pioneer in this area when he demonstrated his Air Analyzer in 1979[8]. Recently, there are a few other attempts in the development of portable GC with different methods including a tandem GC column separation stage [9] and silicon/glass integrated micromachined flushed injector and doubled thermal conductivity detectors (TCD)[10].

Here in this chapter, the design and fabrication of the Portable Electronic Mucosa(PeM) is discussed. Based on the design principle described in previous chapters, a PEM is built. This instrument tries to mimic the way mammalian nose functions by using a large sensor array combined with two retentive columns focused on mimicking the olfactory mucosa. Also embedded in the PeM is a pre-concentrator that tries to improve the system by concentrating the odour being tested. This chapter outlines the design and specification of the portable e-mucosa. Then the components and modules used will be described. The choice of microcontroller, data acquisition and storage method is then explained. Finally, casing and software design for the portable device is discussed.

6.2 Design and Specification

Figure 6.1 illustrates the complete flow of vapour through the portable instrument. As seen here, the overall system is similar to previously described principles for generating spatio-temporal responses, but in this design we have added a preconcentrator. In this design, a sample first passes over a pre-concentrator employing a carbon black layer as the absorbent coating. In a measurement mode the sample is released through a thermal desorption process.
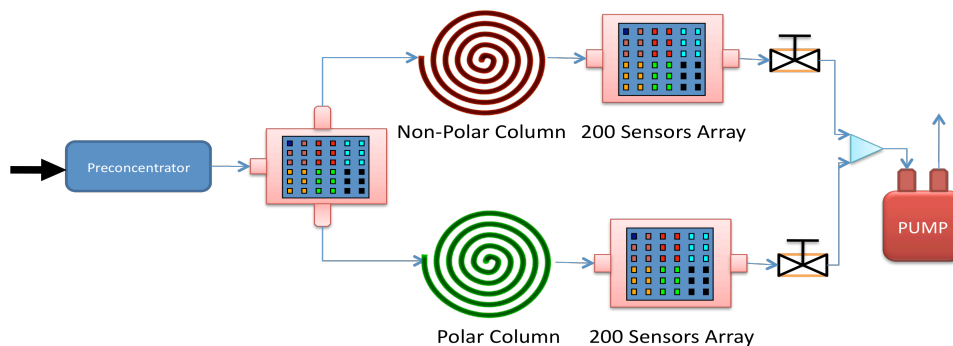
Figure 6.1: Portable e-Mucosa concept diagram with built in preconcentrator

This is connected to an initial sensor array of 200 chemoresistive sensors that gives a traditional e-nose output. The sample flow is then divided (controlled via two valves) and passed through two micro retentive channels coated with Carbowax 20M and OV-1 (polar and non-polar compounds) with channel dimensions of 0.25 mm $\times$ 0.38 mm $\times$ 1 m. As the odours are emitted from the channels they pass over additional sensor arrays, (also with 200 sensors), producing spatio-temporal data.
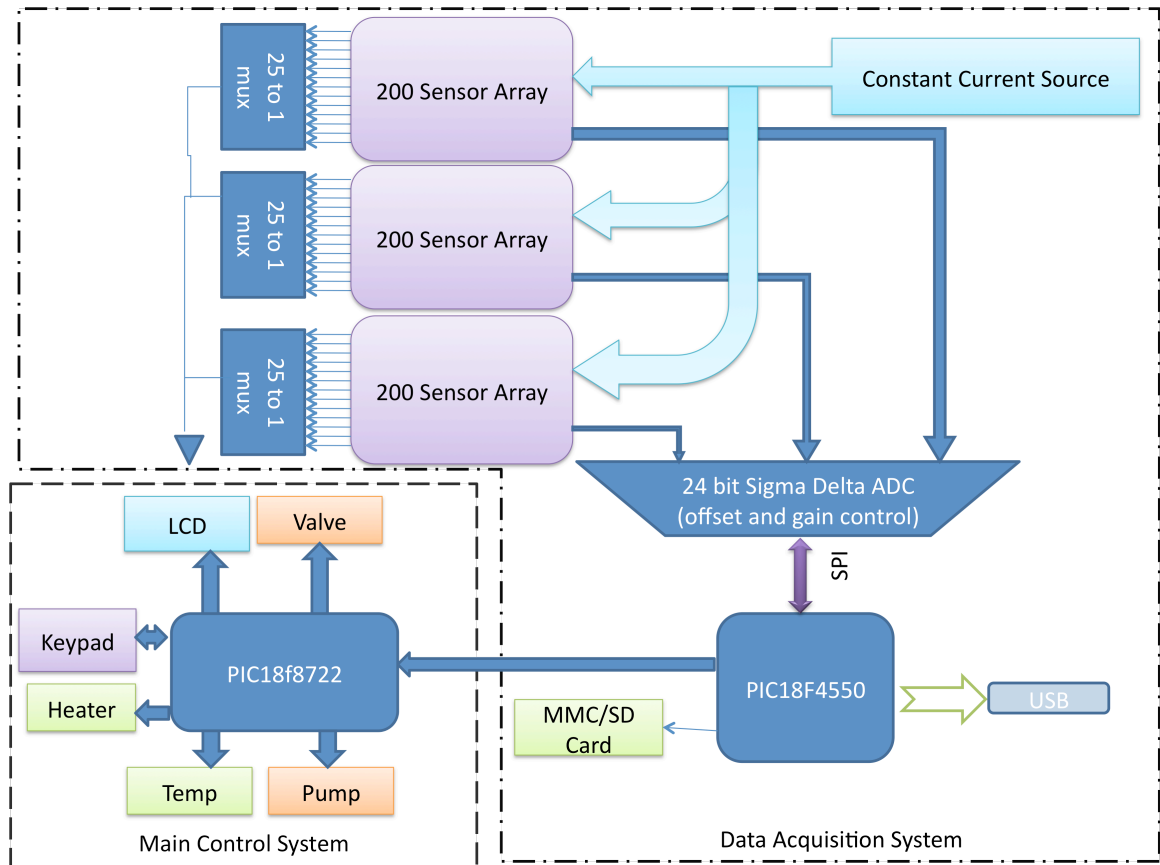
Figure 6.2: Block Diagram of complete portable e-Mucosa

The instrument is fully contained with integrated electronics and micro fluidic components. The system is divided into 2 sections, which are the control, and data acquisition, as illustrated in Figure 6.2. Two separate microcontrollers from Microchip Technology are used for each system.

The PIC18F8722 can control and measure the heater, valves, temperature, humidity, LCD, Keypad and timer control. While the PIC18f4550 will do the data acquisition, storage through MMC Card with FAT16 files system and USB.

The reason two microcontrollers are used is because data acquisition and storage needs to be as fast as possible in order to record usable data from the 600 sensors in the array. Furthermore, separate control and acquisition systems provide the option of simple re-configuration. This provides the ability to upgrade the instrument, either improving the data acquisition system to make it faster or by

improving odour delivery system by adding more complex modules. These can be done without affecting the other separated sub-systems. The list below shows the specification and/or the summary of the PeM.

6.2.1 Specifications

Weight	700g
Dimensions	11 x 20 x 11 cm
Sensor Array Module	600 polymer carbon black 24 Different Tunings
Retentive Column Module	2 x Retentive Column (2m x 0.25 mm x 0.38 mm)
	- Coated with 0.01 mm OV-1
	- Coated with 0.01 mm Carbowax 20M
Preconcentrator Module	(0 – 150°C)
Temperature Sensor	SHT15, TC77 and PT100
Data Acquisition Module	24 bit Sigma Delta ADC
Current Source Module	4 Programmable Current Source
Battery Type	6 x AA battery pack
Processor	PIC18F8722 (32Mhz) and PIC18F4550(96Mhz)
Universal Power Adapter	110-240 V 12V 5A external power adapter
	5V USB Port – with reduced functionality
Display	128 x 128 Nokia Color Graphic LCD
Inlet Probe	One 2" needle interchangeable: Luer Lock Compatible
Keypad	4x3 Character Keypad, RUN and ESC
Warm up time	(at room temperature) < 1 minutes
Data Storage	MMC/SD Card Up to 4GB
Communication	USB
Sampling Pump	200 ml/minute
Operating Temperature	0 to 40°C (32 to 104°F)

6.3 System Modules

6.3.1 Large Sensor Array

Color	Code	Color	Code
	P1		P13
	P2		P14
	P3		P15
	P4		P16
	P5		P17
	P6		P18
	P7		P19
	P8		P20
	P9		P21
	P10		P22
	P11		P23
	P12		P24
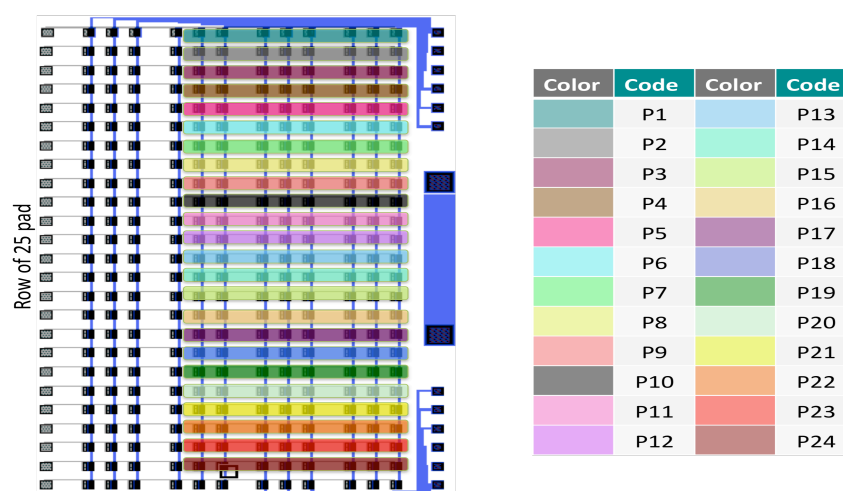
Figure 6.3: Coating Arrangement based on Table 3.2

Chapter 3 describes the design and fabrication of a 300 sensors array. Here, we are utilizing the same sensor array, however only 200 sensors out of 300 were used (coated/connected). The portable e-mucosa utilizes three 200 chemosensors arrays providing a total of 600 sensors. These sensors were deposited with 24 different carbon black polymer composite films, similar to Table 3.2. Figure 6.3 shows the coating arrangement of the sensor array with a 24 rows × 8 columns of sensors coated with gas sensitive film as in Table 3.2.
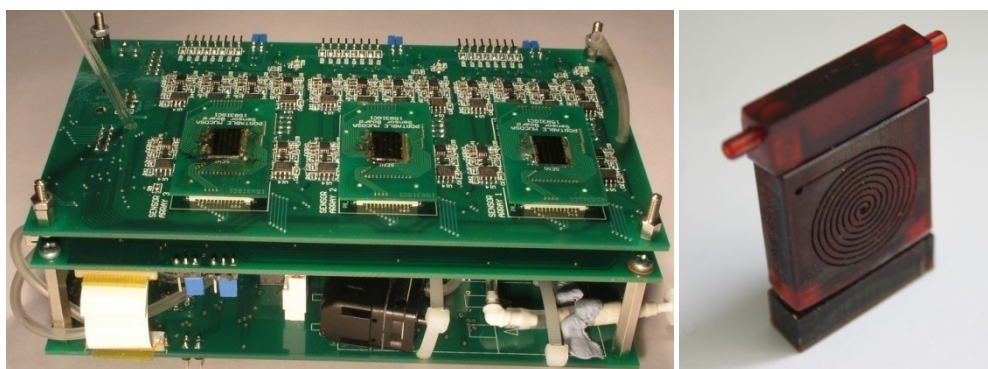
Figure 6.4: a) Bottom view of the peM with three 200 sensors array b) Retentive column with connection adapter

Figure 6.4a shows the bottom view of the PeM with a total 600 sensors. A similar micro sensor chamber was used to that described in Chapter 4. However, in this arrangement, to be able to keep the size down, the chamber was not attached directly to the column. Instead a converter was developed as in Figure 6.4b to decrease the size of the connector to match the standard tubing size used in the instrument.

6.3.2 Retentive Column
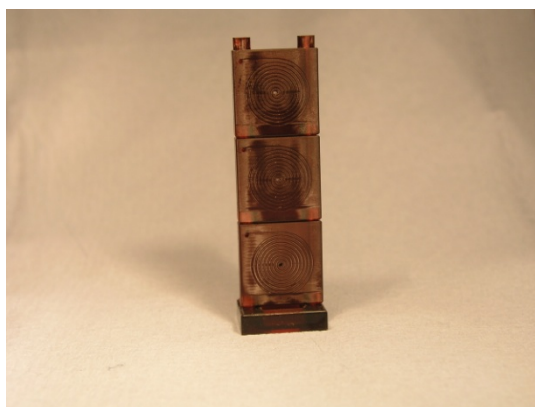
Figure 6.5: Retentive column and sensor chamber formed of three sections

Two retentive columns (coated with different polarity materials (OV-1 and Carbowax 20M) were used to create the 'nasal chromatograph' effect. Each channel was built (using an Envisiontec Perfactory Mini machine) with dimensions 0.25 mm × 0.38 mm × 512 mm each column. The column was built so that it can be stacked together, to create a longer column, as described in detail in Chapter 4. For the purpose of the Portable E-Mucosa, we are utilizing only one column to optimize the flow rate through out the instrument. Although the temporal delay produced with only one column is less compared to more columns, it is enough to generate spatio-temporal information that is usable.

6.3.3 Preconcentrator
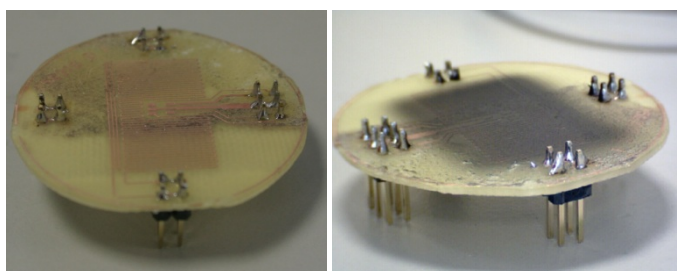
Figure 6.6: Preconcentrator Uncoated and coated with Carbon Black

Figure 6.6 shows the preconcentrator PCB board with absorbent layer (carbon black) coated on top of a heater. The preconcentrator used here, is essentially a PCB heater with an absorbent material coated on top. The preconcentrator works by absorbing the vapour molecules at lower temperature in a sampling period. The vapour is then released and channelled to the chemical sensors, through a rapid thermal desorption process. At a temperature of 150 ^{o}C, the absorbent material will release the concentrated odour in a short pulse to the sensor. The absorbent material used for this device was carbon black (a similar material to that used is a large number of pre-concentrators). The chamber to house the preconcentrator was built using the same Envisiontec Perfactory Mini Machine.

6.4 PeM Electronics

The complete instrument consists of three boards: a) Main Control System (Board A), b) Data Acquisition System (Board B) and c) Power Supply Board (Board E). As mentioned before, two microcontrollers are used as the core-processing unit in this device located on Board A and Board B. The main advantage is the ability to separate the instrument into two-sub system, namely control system and data acquisition system. In the odour delivery subsystem, the microcontroller controls the timer, pump, valve and micro heater. The data acquisition system's function is to read 600 sensors and record it to a MMC card continuously. Here we describe both systems with all electronic modules within each system.

6.4.1 Main Control System : Board A
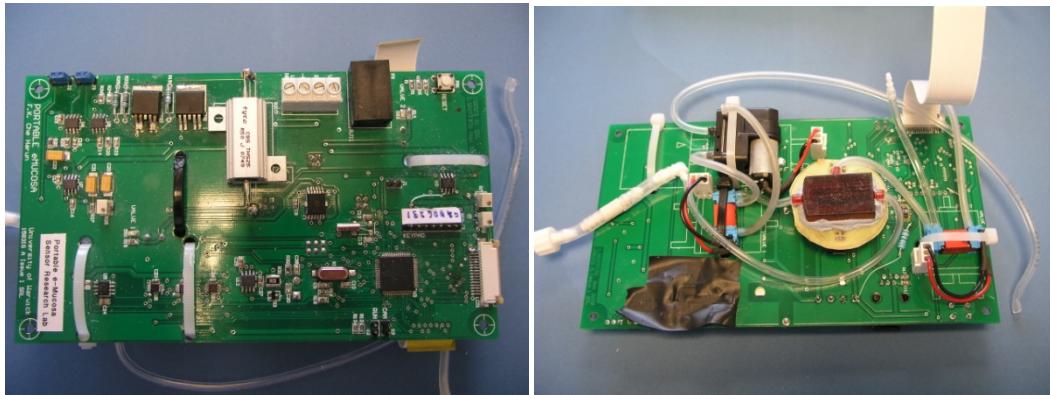
Figure 6.7: View of Font and back of Board A

The main microcontroller controlling Board A, as in Figure 6.7,is a Microchip PIC18F8722 8-bit processor with 128kB of program memory and 3936 bytes of RAM. This is the main processor that controls timing period, temperature sensor, heater, pump and valve. It also triggers the data acquisition microcontroller to start or stop acquiring data.

6.4.1.1 Timer Control

On-board real time clock (RTC) is used to control the timing period during test to ensure proper timing. There are four timing periods used in the system; pre-concentrating period, reference period, testing period and flushing period. These periods can be set under Settings menu. The RTC interrupt is called every second and valve position is switched on every time the counter reaches each a timing period.

6.4.1.2 Temperature Sensor

There are five temperature sensors in total in this device:

1. One on the pre-concentrator,
2. One on the temperature/humidity sensor on the input to the instrument
3. One of each sensor board

A Microchip TC77 is used to measure the temperature on the pre-concentrator as it ramps from 30 to 150 $^{\circ}$C. The TC77 was placed in the middle of the heater to measure the temperature. As for the input odour, a SHT15 (Sensirion) will measure the temperature and humidity simultaneously. A small chamber housing for the SHT15 was built to ensure that the inlet temperature/humidity measurement was valid. A PT100 temperature sensor was used for the sensor array to monitor the sensor temperature. The running temperature can be selected in the Settings menu with a maximum of 50 C. A high operating temperature is not required as the magnitude of the response of a composite polymer sensor falls exponentially with temperature.

6.4.1.3 Pump Control

The pump is controlled using a digital to analogue converter using SPI communication. The user is able to select three pump voltage levels, from the settings menu, to control the flow rate of the system. The user can also check the pump power by going to the Diagnostics menu.

6.4.1.4 Valve Control

The valve used in the PeM instrument is the x-series miniature three-way valve from Sensor Technics. The valve is controlled using a standard MOSFET switch. The valve control is an ON/OFF function to select which inlet is connected to the outlet. The

user can diagnose the valve function from the Diagnostic Menu in the instrument.

Two LED indicators were placed on the PCB for indication of the valve status.

6.4.1.5 Heater Control

There is a total of 4 heaters on this instrument. One of the pre-concentrator and one for each of the three sensors arrays. The pre-concentrator requires a temperature range of 0-150°C to function, while the sensor heater needs to be maintained at a running temperature lower than 30°C. The heater for the pre-concentrator is controlled via a feedback mirrored current source while the sensor heater is controlled via software through a buck converter.

6.4.1.6 User Interface Unit

The display unit consists of a 128 × 128 colour graphic LCD control via SPI. User Input is realized using 2 buttons (RUN and ESC) and a 4 × 3 keypad.

6.4.2 Data Acquisition System – Board B
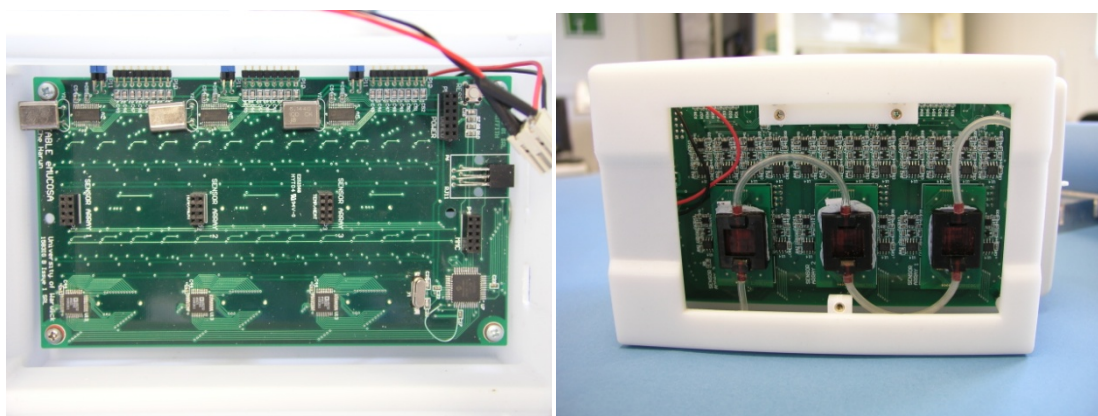
Figure 6.8: View of Front and Back of Board B

The data acquisition processor (Microchip PIC18f4550) controls Board B as in Figure 6.8. This controls the ADC sigma delta converter; current sources and MMC card storage. Data acquisition is achieved using a 24-bit sigma delta converter AD7738. The converter has 8 analogue input channels, corresponding to the 8 columns of sensor array. Each column is sampled 25 times to make a total of 200 sensors (note, the ground of each sensor (thus row) is multiplexed, so that the channel current source is only connected to one sensor at a time). The microcontroller for the data acquisition system waits for the trigger from the main control system before starts acquiring data. Data is ranged from 0-2.5V and is converted to a digital value (of the voltage) before saving it in RAM. Once the RAM reaches the limit (360 bytes), all the values will be transferred onto the memory card.

6.4.2.1 Current Sources

There are a total of 24 current sources on board this device, 8 for each column. In order to acquire data faster, we opted for using 8 current sources instead of one and performing further multiplexing. This eliminates the need to wait for the current source to stabilise before taking measurements.

Each current source can supply four different current values. These are selected by the user (by multiplexing four resistors within the current source circuit), with values ranging from 10 μA to 500μA. The current can be selected by the user via the settings menu. Information regarding the current source selection is saved in the XML file for reference.

6.4.2.2 Data Storage

Data is stored in the MMC/SD Card using SPI communication. The main advantage of using an MMC card for storage is that it allows for a truly portable system without the need of a PC, Laptop or PDA during data acquisition. FAT16 format was implemented to enable the file created with this instrument is compatible with a Windows or Mac environment. The file created can be read directly using a card reader, with a MAC or PC, for further data post processing. The system is capable of using an MMC Card with up to 4GB of storage. Data is stored using standard, comma separated, values .txt format and can be converted into Nose II XML data format for further processing using Matlab 2008 or Multisens Analyzer. Currently, the electronics circuitry for the board includes a USB port, which enables the possibility of measuring and viewing real time data using a PC or Laptop. However, this function has not been implemented yet since the MMC card is already able to collect the response for processing.

6.5 Odour Delivery System
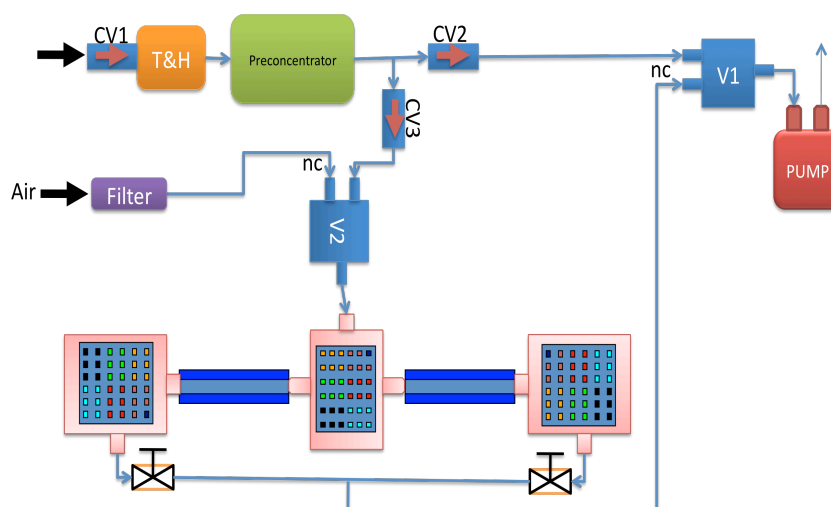
Figure 6.9: Block diagram of odour flow in the system

Figure 6.9 shows the block diagram of the odour delivery system for the portable instrument. The odour delivery system is different from the concept showed in previous chapter as this device uses the pump vacuum to pull the odour from the inlet instead of pushing the odour, as used before. Since a vacuum is used, the whole delivery system is changed to fit the device functionality.

The odour delivery is divided into 4 steps, similar to the timing period; pre-concentrator period, reference period, test period and flush period. Before the instrument starts taking measurements, the sensor heater and temperature sensor will maintain the temperature at the selected value to eliminate the effect of temperature change to the sensor response. The user can select the temperature value up to 50 $^{\circ}$C in the Settings menu.

After the temperature of the sensor is stabilised, the vapour will be passed through the preconcentrator and out the exhaust. This is to trap the odour inside the preconcentrator. During this period, the micro heater underneath the preconcentrator is turned off to ensure maximum absorption of odour by the carbon black layer. To further ensure the odour remains in the pre-concentrator, a check valve is placed on the inlet before the temperature and humidity sensor.

After the pre-concentration period is finished, a reference baseline of air is pulled through V2 into the sensor array. An air filter is placed on the inlet of the reference air to filter big particles from going into the instrument. Ten seconds before the reference period end, the pre-concentrator heater is turned on to start heating the carbon black layer releasing the odour attached to it. Although this is done during the reference air period, the odour released will just accumulate inside the pre-concentrator chamber waiting to be released to the sensor. The reason this

step is done, during reference period, is because it will take around 10 seconds for the pre-concentrator heater to heat up to the maximum temperature to ensure full desorption of the odour.

Then during test period, V2 will be switched on to pull the concentrated odour from the pre-concentrator. During this time, the pre-concentrator heater remains high. Finally, the sensor array is flushed with air to recover the response back to the reference baseline. The sensors temperature is maintained at the selected temperature during the whole test. Table 6.1 shows the valves condition and heater condition during each period.

Table 6.1: Valves and heater condition at certain period

	Valve1	Valve2	Pre-concentration Temp
Precon Period	NO	NC	OFF
Reference Period	NC	NC	ON 10s before period end
Test Period	NC	NO	ON
Flush Period	NC	NC	OFF

NC=normally closed; NO=normally open

6.6 Casing Design and Fabrication
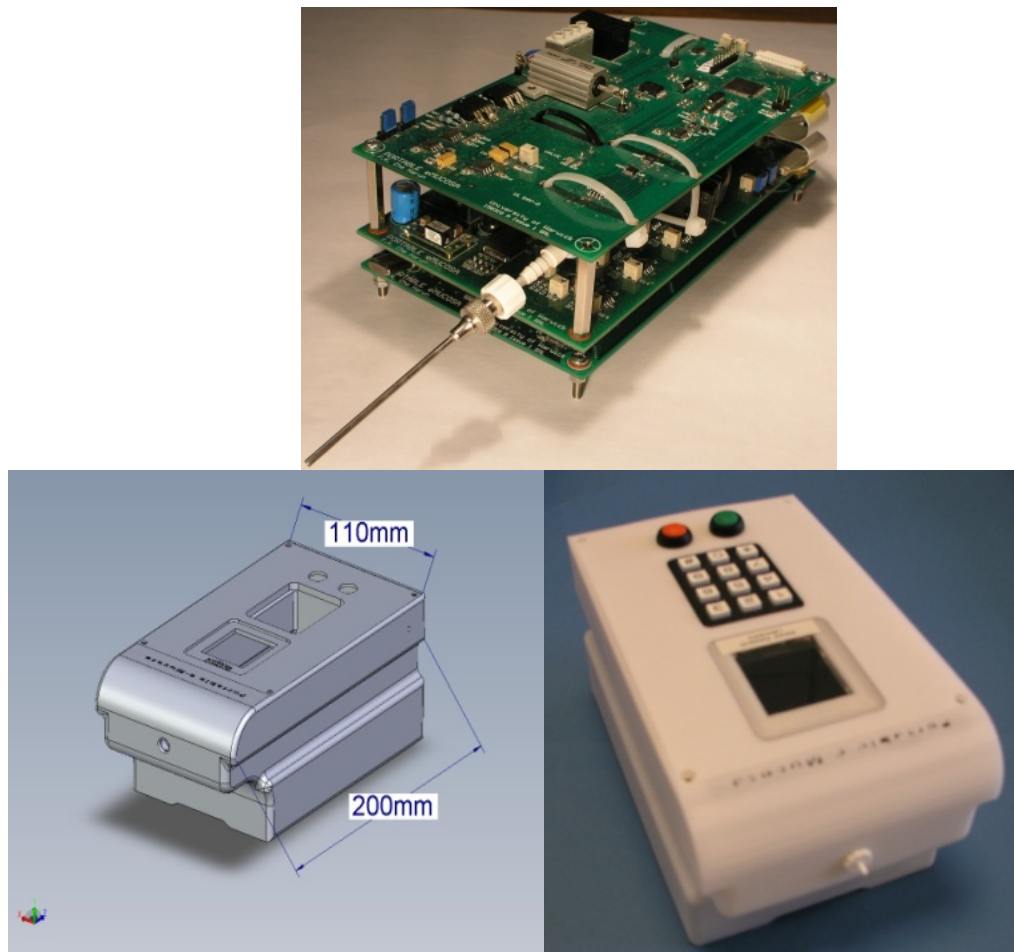
Figure 6.10: a) Three layer PCB of Portable e-Mucosa b) CAD Design of PeM casing c) Casing for PeM created with deposition

A custom casing for the PeM was designed and fabricated here, at the University of Warwick. A CAD design of the casing is shown in Figure 6.10b. This was produced in Solidworks 2009 and the casing itself was fabricated using a fused deposition modeller (FDM) technique, using Dimension from Stratasys.

Figure 6.10a shows the PeM PCB boards connected together, forming an instrument with dimensions of 96 mm x 180 mm x 86 mm. The casing itself was designed to be slightly bigger at 110 mm x 200 mm x 100 mm so that the board can

fit in properly. The casing was designed in 3 pieces; main body, top cover and bottom cover.

The three boards are screwed onto the main body with all the pipefittings. The odour inlet, air inlet and exhaust are placed on different sides of the instrument to avoid contamination between the inlet and the exhaust. A luer lock connector is fitted on the inlet to allow different sample collection methods to be deployed. The LCD, keypad and buttons are fitted onto the top cover. The bottom cover, as in Figure 6.6d, is accessible separately to allow the sensor arrays or columns to be easily changed without the need to disassemble the whole casing.

6.7 Software Development

For the microcontrollers, several languages are available including assembly, c, basic and pascal. There are various factors that should be taken into consideration when choosing a language to write the firmware code. Assembly language is usually used when speed and efficiency of firmware is important. However, development time using assembly language is slower compared to c since the code written is low level machine code that requires manual management of memory. Development using the C language is preferable since it is more widely used and shared libraries are available, making code development much easier and faster.

Here we have chosen C as the main language for the PeM. However, assembly language is used for certain routines to improve the efficiency. The code is compiled with MikroElektronika MicroC for PIC compiler and is then burnt onto the microcontroller through the In Circuit Serial Programming (ICSP), using Microchip ICD2 Debugger.

6.7.1 Board A Firmware

The firmware on Board A controls components on the main control system, including temperature control (heater and temperature measurement), LCD display, Keypad, Buttons, Timer control, valve and pump.

Heater power to the sensor is controlled using a digital potentiometer (AD8400) that sets the output voltage of the dc-to-dc converter connected to the sensor heater. A digital potentiometer is also used to control the pre-concentrator power. The 10-bit potentiometer value is defined using a Software Serial Peripheral Interface (SPI). SPI is also used to control the pump voltage through a 12-bit digital to analogue converter (DAC). The display used was a 128 x 128 pixel, 4096 colour graphic LCD communicating using SPI. The temperature module for pre-concentrator and sensor arrays also utilizes an ADC with SPI communication. Each module that uses SPI has its own chip select pin to ensure correct data is sent to the correct chip.

The temperature and humidity sensor used to measure the inlet environmental conditions, is the SHT15 from Sensirion. Communication with the sensor is done with two lines, using Sensirion propriety communication protocol[11].

Real Time Clock (RTC) on board the micro controller was used to implement the period counter to control timing when the valves and heater should be turned on or off as shown in Table 6.1. Finally, the valve was controlled digitally with a MOSFET ON/OFF switch.

Three pins were used to communicate with the data acquisition system microcontroller from the main controller board. These pins are used to send the constant current source selection and to trigger the data acquisition to start acquiring and saving the sensor response to the MMC card.

Figure 6.11: Sample Menu Item in the Portable e-Mucosa

Figure 6.11 shows several of the menu items from the PeM display. A complete flow of the software system is shown in the flow chart in Appendix B.

6.7.2 Board B Firmware

The board B firmware controls modules on the data acquisition system including the Sigma Delta Analogue Digital Converter (ADC), MMC Card, USB Connection and constant current source. Both the MMC card and sigma delta converter use the SPI protocol to communicate with the microcontroller. In order to optimize the measurement of the large sensor array, the SPI protocol is implemented in assembly language instead of C.

Each of the three sensor arrays have their own 25 to 1 multiplexer, 8 channel Sigma Delta ADC chip and 8 constant current sources. This is to improve speed and efficiency of the measurement. The constant current source is selected by changing

the resistor value connected to the circuit. The selection resistor is multiplexed using a 4 to 1 multiplexer.

The system works by first setting the constant current source multiplexed resistor depending on the data sent by the main controller, via pin Bac1 and Bac2 (see Appendix C for schematics). Then, after receiving a trigger on pin StartAq from the main microcontroller, the system selects the first row of sensors by switching the 25 to 1 multiplexer. The microcontroller then starts reading the voltages of the sensors on each channel (8 channels – one column) one after another. The digital voltage value is then converted to analogue representation before saving it to the microcontroller RAM. Then, the system continues by reading the next 8 channels of the following row. The system transfers the data from RAM to the MMC card after reading 5 rows of sensor voltages. This is repeated five times to acquire all the voltages from the 200 sensor in the array. This process is then repeated for the two other arrays. The data acquisition system keeps acquiring data until the main microcontroller sends a stop signal through the StartAq pin.

6.8 Data Viewer and XML Converter.

As mentioned before, at this point in time there is no on board pattern recognition implemented in the PeM. Similar to the previously described software in Chapter 5, a data viewer and XML converter have been created for the portable device. File saved as XML will be processed further using the Multisens Analyzer software. Matlab is also used for processing data. Figure 6.12 shows the response viewer and file format converter software interface.
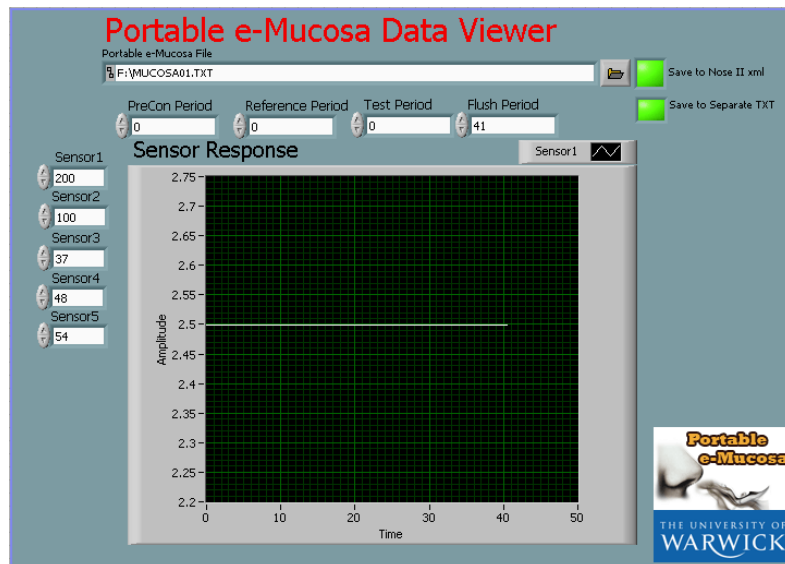
Figure 6.12: Response Viewer and Format Converter

6.9 Conclusions

Here we have described the design and fabrication of the Portable e-Mucosa instrument. The design was based on previously described concepts, except for the addition of a preconcentrator and a heater for each sensor array. Another change to the previous design was that the number of sensors was reduced from 300 to 200 to decrease the complexity and increase the speed of the instrument.

A pre-concentrator was added to so that a higher concentration of sample vapour could be passed over the sensor array in a test cycle. The pre-concentrator operates by having sample air passed over it for an extended period of time (minutes) to trap odour molecules on, what is effectively, a sticky pad – formed of carbon. These odour molecules are rapidly desorbed by a step change in the pre-concentrator temperature. The temperature of the sensor arrays are controlled by a heater beneath the array. This is used to stabilise/maintain the sensor array temperature to improve the repeatability of the sensors.

The odour delivery system was also compressed, from the system described in chapter 4, to fit into the portable instrument. Instead of using pressure to push two samples into the system, the instrument uses a vacuum to pull only one sample through the inlet. Only two valves are needed to implement this method.

The casing was designed and fabricated with a Dimension (Strassys) to fit the three PCB board inside. An opening was made at the bottom of the boards where the sensor and column is located. This is to allow easy access to the sensor array for modification and changes.

Figure 6.13 shows the comparison shot with Cyranose 320. The PeM is slightly shorter than the Cyranose but significantly thicker. It is important to recognise that this thickness is required to fit the 600 sensors and the two micro retentive columns, instead of the 32 sensors used in the Cyranose. Both are handheld but the Cyranose have a built in pattern recognition system (though it will be possible to integrate this function into the instrument in the future).

The instrument is fully contained with integrated electronics and micro fluidic components. The instrument has been designed with separate control and acquisition systems offering simple re-configuration. Upgrading the system would be easier with this separate microcontroller configuration.

Figure 6.13: Comparion shot between PeM and Cyranose 320

Firmware for both boards was written in C and compiled using Mikroelektronika MicroC for PIC. Some of the codes were written in assembly to optimize the system for speed especially the data acquisition system board. Results and characterisation of the PeM instrument and those described in chapter 5 is given in the following chapter.

6.10 References

1.   *Cyranose 320 Portable Handheld Electronic Nose*. Available from:
        http://www.smithsdetection.com/eng/Cyranose_320.php.
2.   ES Technology, *Mobile Ultra-Fast GC Analyzer Model 4500*, Electronic Sensor Technology.
3.   TechnoBiochip (2006) *Libranose Brochure*.
4.   Analytics, A. *Portable Electronic Nose Intelligent chemical Sensor* Available from:
        http://www.airsense.com/english/index20.html.
5.   H.K. Hong, et al., *Portable electronic nose system with gas sensor array and artificial neural network.* Sensors and Actuators B: Chemical, 2000. **66**(1-3): p. 49-52.
6.   A.Perera, S. Marco, *IPNOSE: A Portable Electronic Nose Based on Embedded Technology for Intecnsive Computation and Time Dependent Signal Processign.* Proceedings of the 8th Intl. Symp. On Olfaction and Electronic Nose, 2001.
7.   Y.S.Kim, , et al., *Portable electronic nose system based on the carbon black-polymer composite sensor array.* Sensors and Actuators B: Chemical, 2005. **108**(1-2): p. 285-291.
8.   S.Terry, J. Jerman, and J. Angell, *A gas chromatographic air analyzer fabricated on a silicon wafer.* IEEE Transactions on Electron Devices, 1979. **26**(12): p. 1880-1886.
9.   C.J.Lu, , et al., *Portable Gas Chromatograph with Tunable Retention and Sensor Array Detection for Determination of Complex Vapor Mixtures.* Analytical Chemistry, 2003. **75**(6): p. 1400-1409.
10.   J.A.Dziuban, , et al., *Portable gas chromatograph with integrated components.* Sensors and Actuators A: Physical, 2004. **115**(2-3): p. 318-330.
11.   Sensirion *Datasheet SHT1x (SHT10, SHT11, SHT15) Humidity and Temperature Sensor*

CHAPTER 7

Microsystems characterisation and experimental results

7.1 Introduction

A major objective of this research is to obtain multi-dimensional spatio-temporal data, in order to improve the discrimination and classification ability over traditional electronic noses. Several other researches have already suggested the use of spatio temporal data to improve e-nose instruments [1, 2]. These researches suggested that spatio temporal data does improve the overall recognition. However, these researches only focused on one-dimensional temporal information, instead of the two dimensions proposed here. Research by the Sandia Laboratory, developing a full GC analysis instrument has shown the possibilities of using two dimensional GC combined with SAW sensors in a portable instrument [3]. Our concept is similar but we are focusing on using dual dimensional retentive column to improve conventional e-noses.

As discussed in previous design chapters, here three large sensor arrays have been combined with two micro-retentive columns. Furthermore, a portable instrument has been designed and fabricated to make the instrument easier to use. In this chapter, we will discuss the experimental results obtained throughout this

study, including the portable instrument, followed by some discussion of pattern

recognition techniques proposed for this instrument.

7.2 Large Sensor Array Characterisation

The large sensor array system was characterized both in terms of electrical

characteristics of the measurement circuit/sensor (in a static environment) and to

different test sample conditions – be in sample concentration, environmental

changes or flow rate. This evaluation is described within this section.

7.2.1 Stability test

Before performing further chemical characterisation, sensor drift and noise needs to

be identified to ensure the response acquired from the sensors are valid. This

experiment was performed by keeping the sensor running for 5 hours under

constant laboratory air, temperature (21 C) and humidity (30 % r.h.). Here we can

see that the maximum noise generated by the circuit is around 5 mV and drifted by 8

mV in 5 hours.
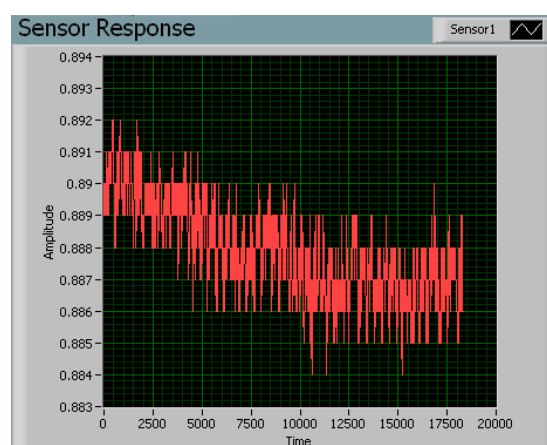
Figure 7.1: Drift and Noise for sensor expose to laboratory air

There are many factors that can contribute to a noisy system such as circuitry noise, sensing film noise, ADC noise and contamination noise. However in this test, we have shown that the signal to noise ratio is significantly high compared to the accumulated noise generated by the system.

7.2.2 Large Sensor Array Representation

Firstly, we will look at how the large sensor array will be presented in this thesis. Since there are 300 sensor on one sensor array as described in Chapter 3, is it difficult to present all 300 sensor at once in the same graph. For easier explanation, some of the large sensor array responses are represented in a colour map form as in Figure 7.2.
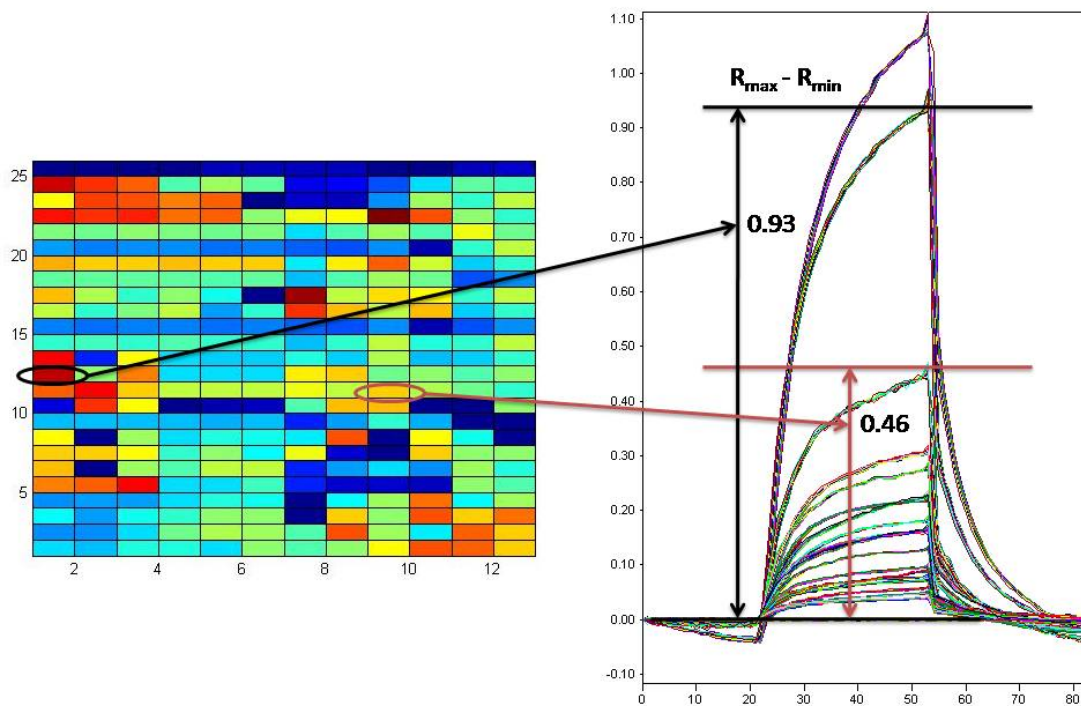
Figure 7.2: Large Sensor Array Representation

Several large sensor array colour plots will be presented throughout this chapter. This colour map is generated by Matlab 2006a by finding the normalised signal maximum magnitude and subtracting it with the minimum magnitude of response (R_{max}-R_{min}) as shown in Figure 7.2. These values are then converted to colour, based on a colour standard in Matlab 2006a. This is performed using 'pcolor' instruction.

7.2.3 Wide Sensor Diversity and Redundant Sensor Tunings

The large sensor array provides a wide, diverse and significant level of information. First, the 24 different tunings are providing 24 different responses to the same test analyte. Furthermore, the first sensor array in the system is going to provide a larger magnitude of response compared to the end array. This in itself is valuable information that can be used during data processing to enhance system performance (for identification). Figure 7.3 shows the diversity of the sensor array with 9 different tunings within the system.
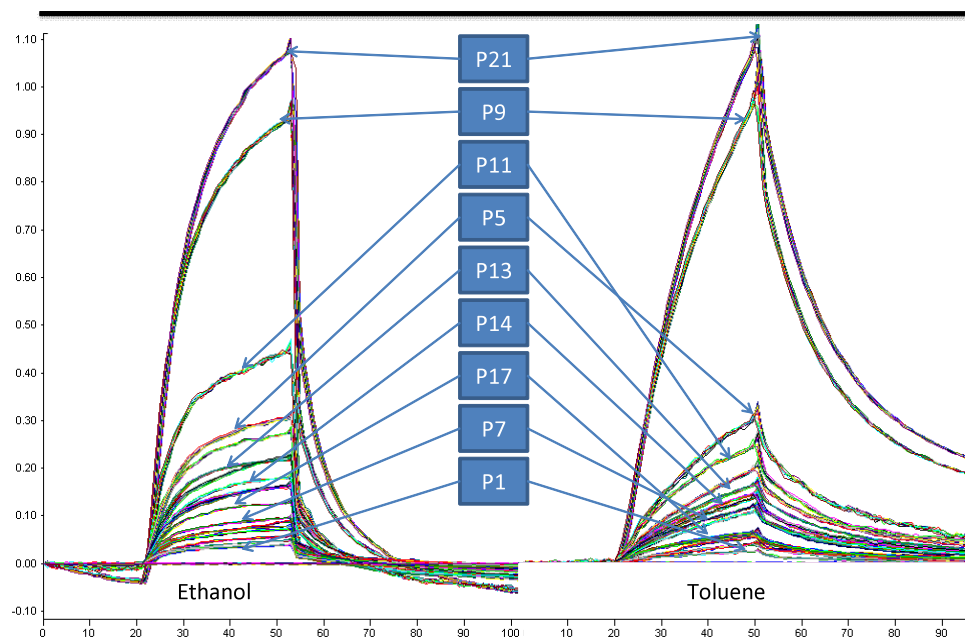
Figure 7.3: Sensor Response to Ethanol and Toluene with 9 polymer coating shown

As mentioned before, 12 sensors in the array are going to be coated with the same material. Although it is desirable to have 300 different tunings, it is difficult to practically achieve. Figure 7.4 shows the 24 different tunings in a colour plot. This shows group of 12 sensors each, with 24 different tunings. However, there are some sensors that show a larger response magnitude over others in the repeated group of 12 sensors. This is due to the fact that the sensors are deposited/sprayed in batches and that there is some variation in sensing film thickness. Furthermore, due to the small gap of 200 μm between the sensors, some of the polymer sensing materials may overlap with each other causing the sensor to respond differently. This is one of the reasons why sensor redundancy is required, where such outliers can be removed before the data is used for identification.

As illustrated in Figure 7.4, a group of sensors can have a very similar magnitude of response. However, there are sensors that produce very different magnitudes. This is due to the fact that the coatings are done in batches and some of the sensors are not coated properly or coating is not uniformed. It is also worth noting that there are a few faulty sensors within the array shown in dark blue. This colour plot makes it easy to select the best sensor and reject faulty sensor during data processing.
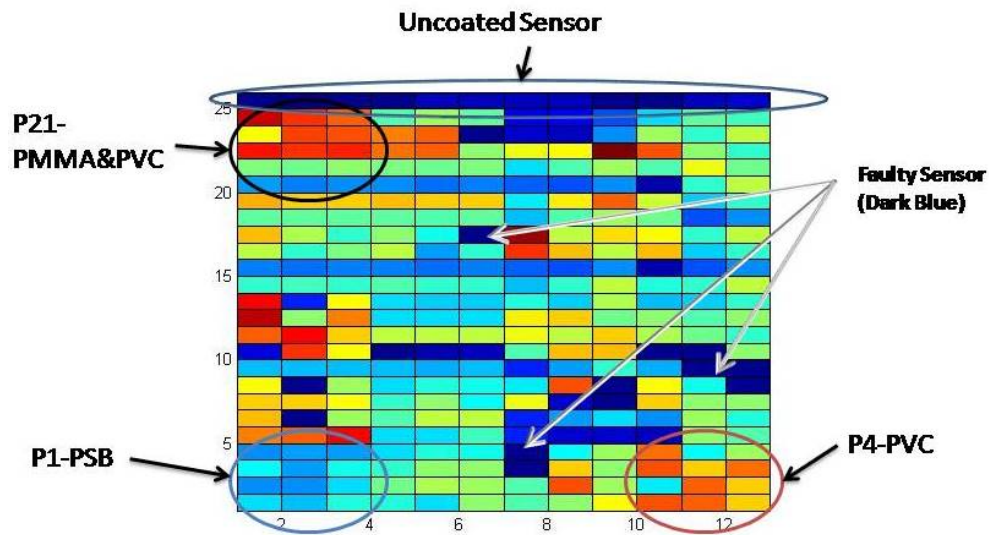
Figure 7.4: Group of redundant sensor with uncoated and faulty sensor

7.2.4 Temperature effects

The temperature dependence of the sensor array was characterised between 26°C to 35°C using the portable e-Mucosa. These measurements help select the optimum temperature to operate the sensor array.
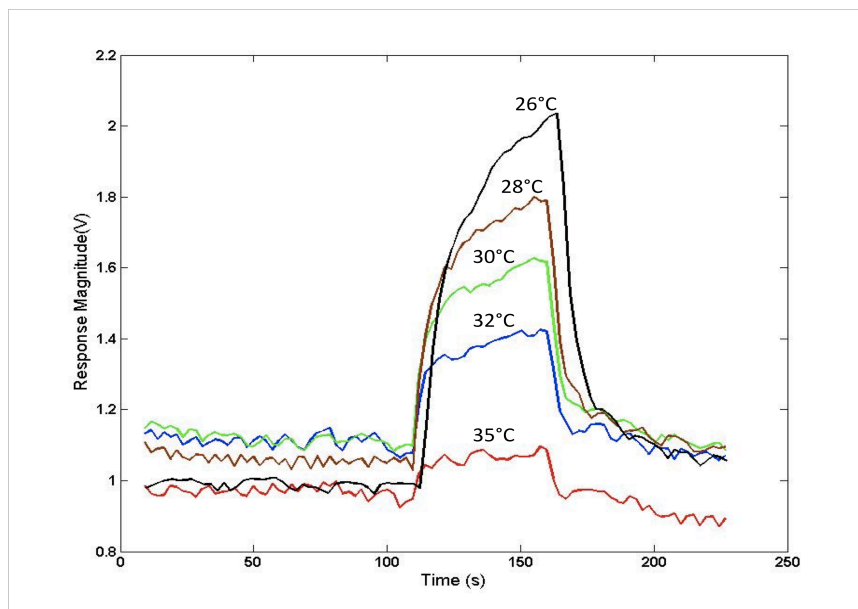
Figure 7.5: Sensor response to ethanol vapour in air at different temperatures

It can be seen from Figure 7.5b, that as the temperature increases (26-35°C) the magnitude of the response reduces. At 35°C, there is hardly any response from the sensor. This experiment is similar to other research [4], confirming that carbon black composite sensor give larger responses at lower temperatures. Thus the optimum temperature will be just above room temperature, as this will reduce effects in ambient variations.

7.2.5 Flow velocity effects

The flow rate across the sensor has a significant effect on the response of that sensor. As discussed before in Chapter 3, the sensor chamber was intentionally designed to generate higher flow velocity above the sensor to optimize sensor response. Here we demonstrate the effect of flow velocity towards response time and magnitude. In this experiment, the flow velocity was varied by changing the flow rates while other variable such as temperature and humidity remained constant. Figure 7.6a shows the sensor response magnitude versus flow velocity and figure 7.6b shows the sensor response time versus flow velocity.
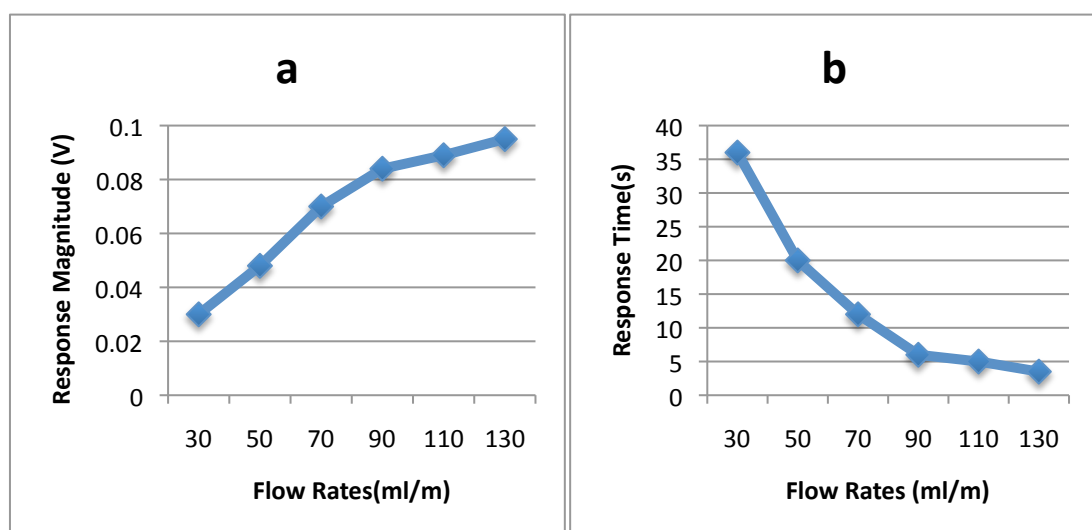
Figure 7.6: a) Response Magnitude vs Flow Rates b) Response Time vs Flow Rates

As shown in the graph, higher flow velocity contributes to faster response times and large response magnitudes. However, in the proposed portable system, the flow rates can only be maintained at around 50 ml/m due to complex odour flow across the system.

At 50ml/m, the lower response magnitude and slower response time is expected. However, this problem is compensated for by using a preconcentrator that will be discussed later. Preconcentrators increase the odour components in a sample to be analysed, before the sample goes to the sensors. The preconcentrator will significantly improve the response time and magnitude and thus will provide more informative spatio temporal data for processing.

The significance of this 'flow velocity' in this research is that it emulates the stereo olfaction feature of a biological olfactory system. In stereo olfaction, each nostril sniffed at different flow rates at a certain time and these different rates rotate between the two nostrils at certain interval. Higher flow rates clearly will give higher response and vice versa. In this research, we can mimic this feature by having two retentive columns with an array at each end to simulate the two biological nostrils. The flow rates through these two end arrays can be varied by changing the length of the retentive column or by using a bleed valve to alter the balance of flow rate between the two sensor chambers.

7.2.6 Large sensor array Classification

To demonstrate the large sensor array classification power, we have run experiments with simple odours and complex odours. Simple odours consist of one molecule. Those used here were ethanol, toluene and ethyl acetate vapour. For

more complex odours, four different essential oils were used to demonstrate the ability of the large sensor array to discriminate between odours. Figure 7.7 shows a PCA plot separating these simple odours (room temperature of 22 C, flow rate 60 ml/m , 20 s test time and three measurement each).
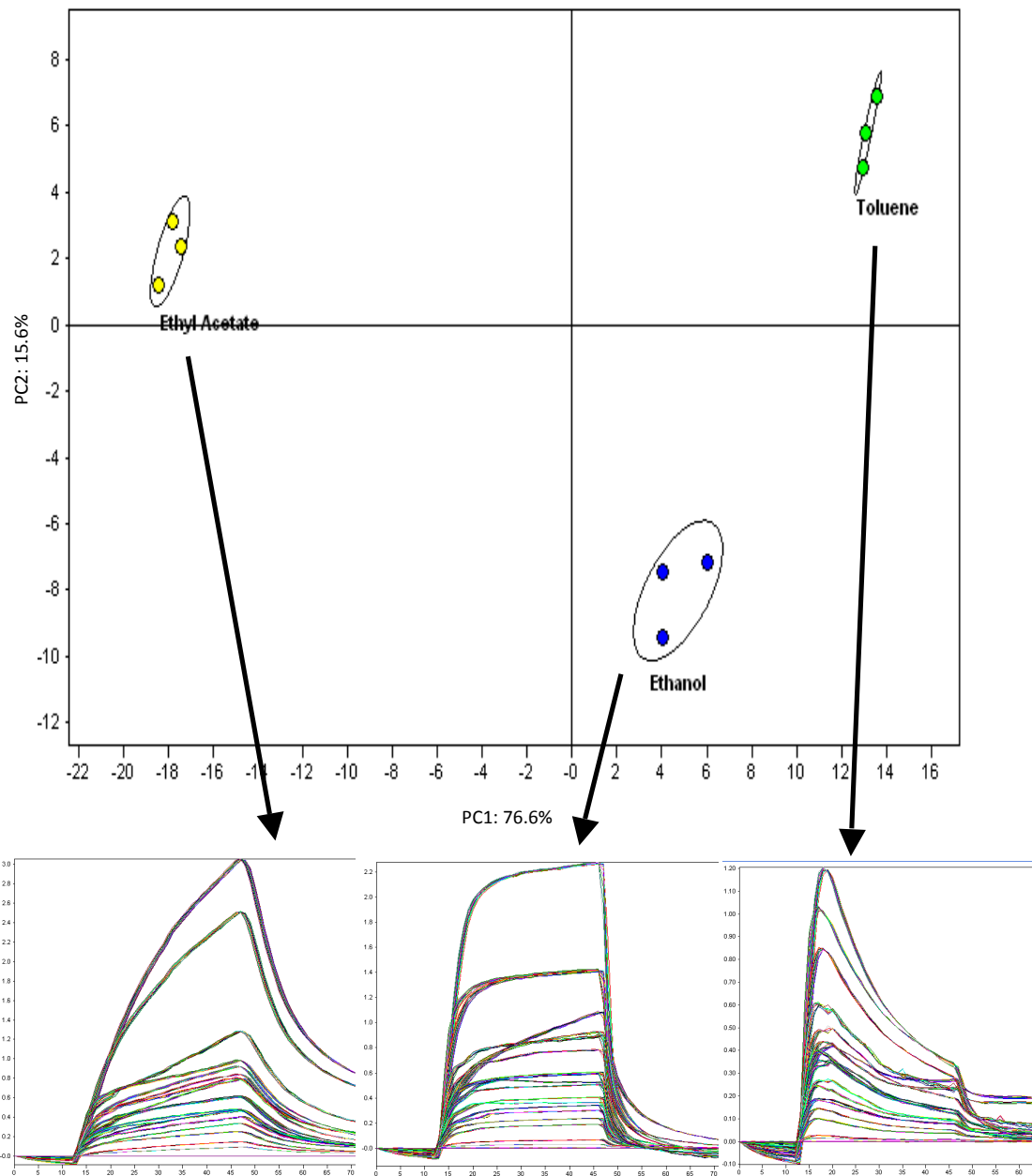
Figure 7.7: Simple PCA with three simple odour with sensor response

This experiment shows that simple odours can easily be classified using the large sensor array. Principal component 1 (PC1) in the PCA plot suggests that the PC1 axis

"extracted" 76.6% of the variation in the entire data set, and the second axis (PC2)

explained another 15.6%. Further data processing identified that actually only one

sensor was required to discriminate between these three simple chemical. However,

for more complex odours with multiple molecules, several sensors would be needed

to achieve significant discrimination. Figure 7.8 shows the PCA plot of four essential

oil; lavender, lemon oil, cinnamon and ylang ylang.
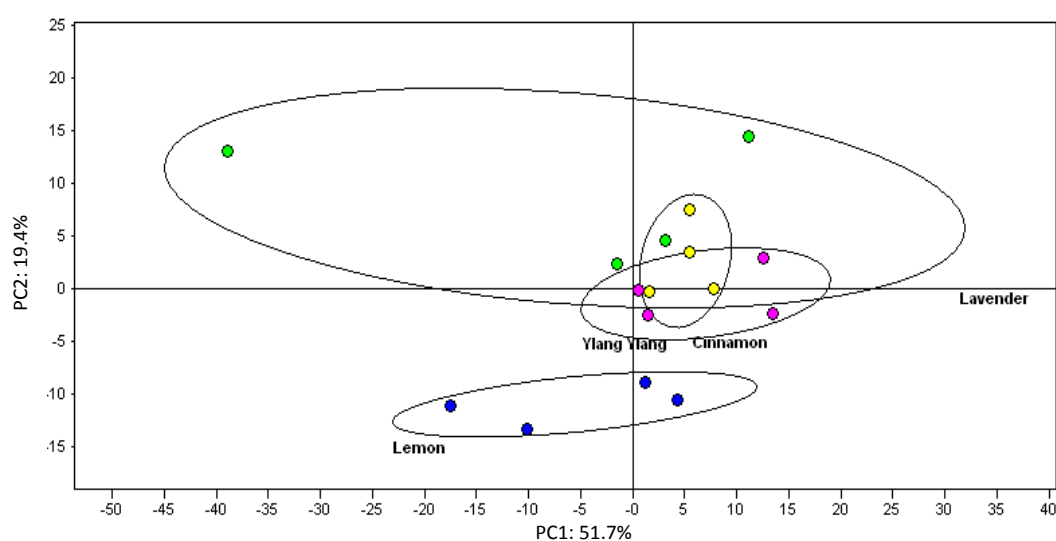
Figure 7.8: Simple PCA of Four Essential oil data

These experiment shows that large sensor array have the diversity to classify many

different simple analytes but on complex analytes, it struggle to classify them,

especially with a not perfectly uniformed film sensor array (though it maybe due to

the base chemicals/solvent of these oils being common). Only 51.7% of the data

variation is explained by axis PC1 and 19.4% with PC2. Although with some post

processing it is possible to separate the four essential oil, here in this research, we

are focusing on using spatio-temporal information for classification. So to

complement the large sensor array, temporal information will be generated by using

the micro retentive column in order to improve the overall performance of the

system.

7.3 Micro retentive Column characterisation

Here the micro retentive column characterization is presented. Diversity information from a one-dimensional retentive column is compared to a two-dimensional system. Next, the effect of column dimension and the polarity of the coating are evaluated in terms of its ability to discriminate complex odours. A comparison of the complete instrument to a conventional e-nose is performed to demonstrate the improvements that a dual-dimensional spatio-temporal instrument gives.

7.3.1 Temporal Information

The measurement of the temporal delay (thus temporal information) at first glance would seem a simple process, but there are in fact a number of ways of processing this. Here, temporal information is taken by the retention time between the first sensor array response and the second or third sensor array response (taken at 50% response of the total magnitude). Figure 7.9 shows a sample of temporal data determination.
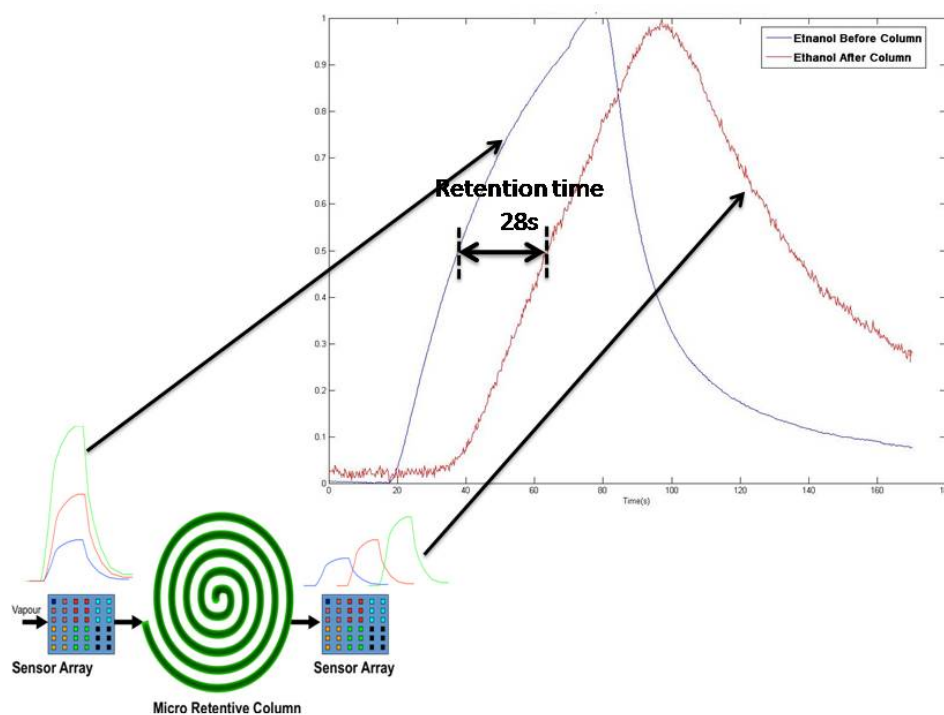
Figure 7.9: Temporal Information determination

As shown in figure 7.9, the temporal information is taken at 50% of the total response. Before processing the sensors response in normalized, removing the spatial information to focus on the temporal information. Here the retention time of ethanol after a 1.5m OV-1 column is 28 s and is measured between sensor S100 in the first sensor array and end array.
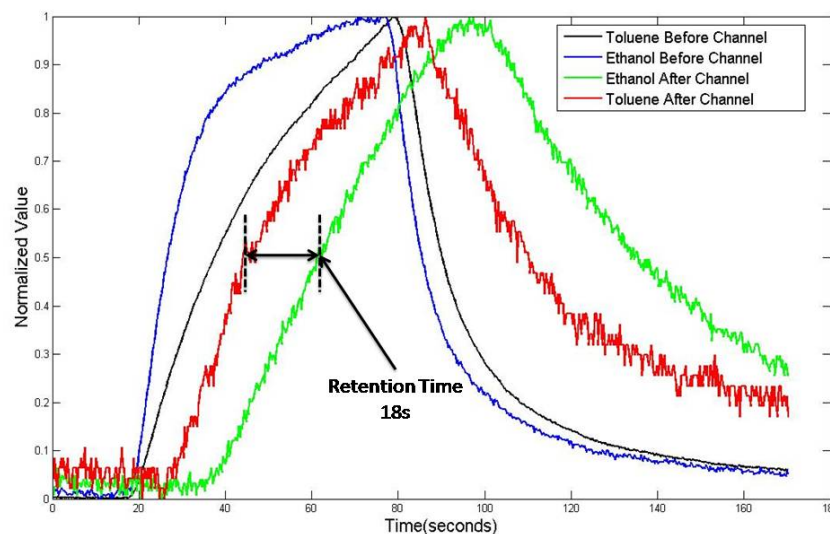
Figure 7.10: Temporal information for dual dimensional column setup

Another way to determine the temporal information is to compare the response of two different analytes before and after the retentive column, as shown in Figure 7.10. Here, ethanol and toluene vapour (in air) is pushed through a one dimensional setup with two sensor arrays and one micro channel coated with Carbowax 20M. The retention time here is taken by comparing the end sensor array output between the two readings. Here it is clear that the same column produced different delays that are dependent on the analyte. Ethanol is delayed more than toluene by 18s. Matlab 2008a was used to measure and calculate the retention time for further processing.

7.3.2 Comparison between uncoated and coated microchannel

In order to confirm the validity of the spatio temporal data, a comparison of coated and uncoated columns was performed. This will demonstrate that the delay caused by the column was generated by the polar/non-polar stationary phase coated inside

the column. The experiment was done using two columns with similar dimensions (0.025 x 0.038 x 0.5 m), one left uncoated and the other one coated with non-polar OV-1. The test was done at room temperature with flow rates 30 ml/m. Two simple analytes (toluene and ethanol vapour) was used in this experiment.
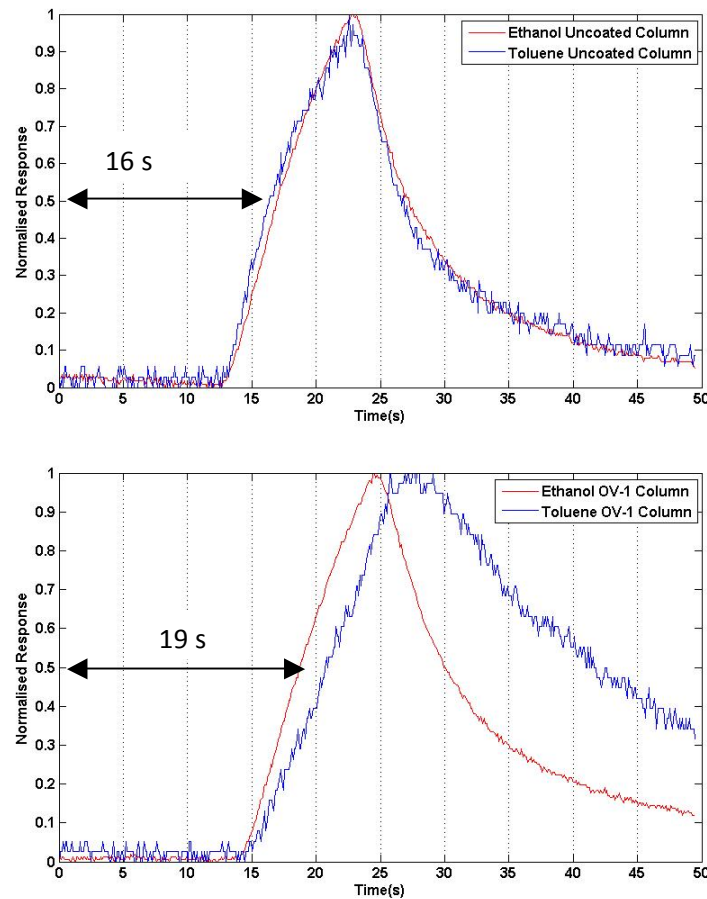
Figure 7.11: a) Response after uncoated channel b) Response after carbowax coated channel

Figure 7.11(a) shows the sensor response to both analytes before the column and the Figure 7.11(b) shows the sensor response after the column. The response has been normalized to focus only on temporal information. As the analytes pulse travel along the column, it became obvious that with the coated column, the toluene and ethanol pulse is separated by 3 seconds (in a 10 second test pulse), while with the uncoated column; both analyte pulses arrived at the sensor at approximately the

same time. This clearly shows the retentive nature of the column that can be use to generate the spatio temporal information needed in the system. Here, toluene is delayed more than ethanol due to the fact that the column used was a non-polar column, which reacts with non-polar molecules more than polar molecules.

7.3.3 Effect of various dimension micro retentive column

As mentioned in the design chapter, the micro retentive column was designed with several different dimensions to test their performance and thus select the best one for the instrument. Here, different columns were tested under similar test conditions to evaluate the performance of each column. In the test, similar length columns was used to determine the performance of the column height and width. These different columns were assessed under two criteria, a) response magnitude and b) retentive delay. Three tests were done using different column dimensions with similar length of 0.5 m (one block of spiral column) at 20 C and 20 ml/m flow. Figure 7.12 shows the sensor response using the three different columns. Column with size 0.50 x 0.25 mm seems to provide a greater response magnitude with no significant difference in retention time. Hence, for the final portable instrument, column dimensions of 0.50 x 0.25 was used. Furthermore, better flow rate is achievable with 0.5 x 0.25 mm column compared to other column.
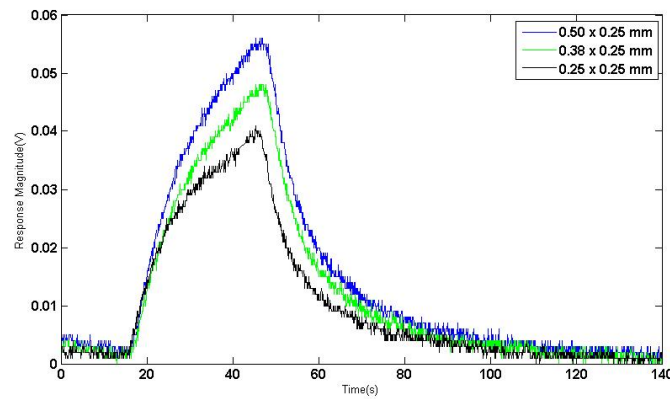
Figure 7.12: Sensor response with three different size columns

Further tests were performed to determine the effect of column length towards column performance. Here, a column with the same cross-section (0.25 x 0.38 mm) was used with various lengths, as showed in Figure 7.13. The sensor response shows that a column with a longer length provides more retention time but significantly reduces the magnitude of the response. Here we can see that increase of length from 0.5m to 3m, the sensor response decreases from 0.18V to 0.06V while the retention time increases by 20s.
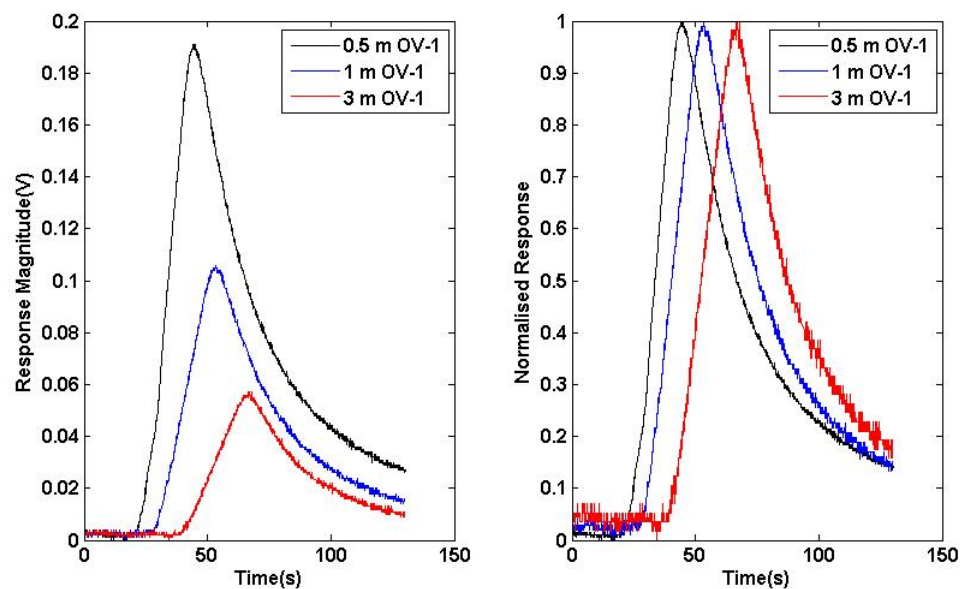
Figure 7.13: Effect of column length

7.3.4 Effect of Flow Rates

In the human olfactory system, the flow rate in each nostril is slightly different – due to natural variations. This results in 'stereo olfaction' as discussed earlier, which provides additional information to indentify aromas. Here, we demonstrate the stereo olfaction effect by varying the flow rates through the micro columns. Tests were performed with similar conditions (20 C, MSL 105 with 3m length) and with various flow rates, controlled using a needle valve. Figure 7.14 shows the sensor response after the column at several flow rates. This experiment shows that as the flow rate is reduced, the longer the retention time produced by the column, but it also decreases the magnitude of response of the sensor.
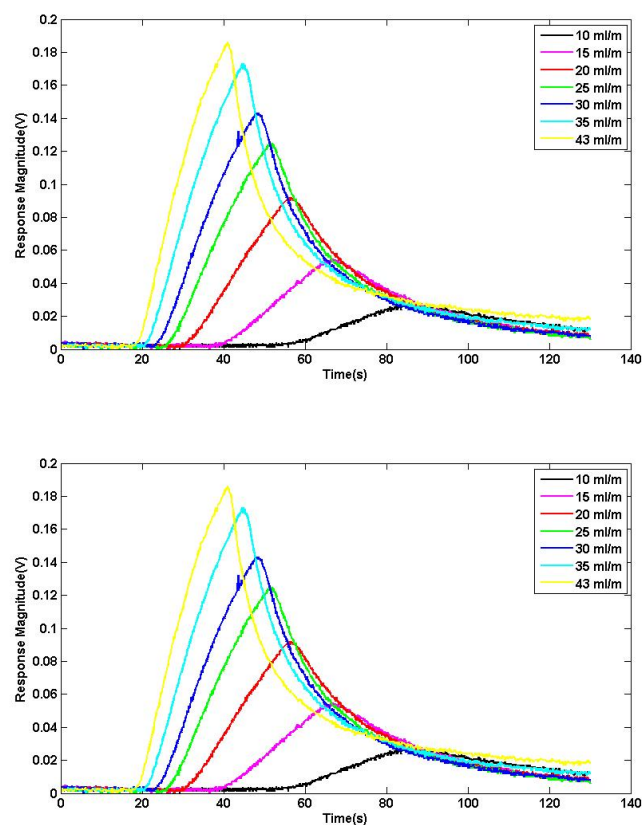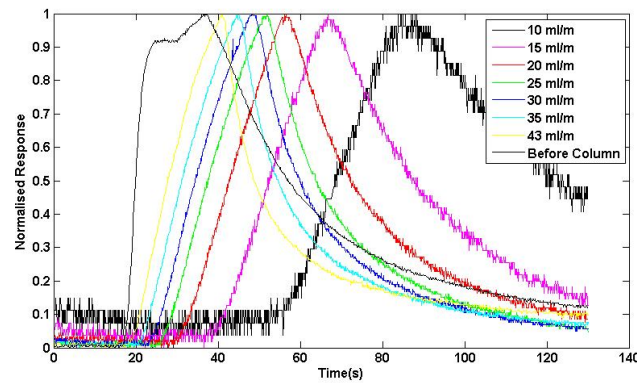
Figure 7.14: Sensor responses to ethyl acetate at different flow rate with OV1 column

As the flow rate is increased from 10ml/m to 43 ml/m, the sensor response decreases from 0.18V to 0.02V but the retention time increases from 10s to 45s. Note that the maximum flow rate tested is only 43 ml/m because that is the maximum flow achievable with a 3m long column. This result confirms that we are able to mimicked the 'stereo olfaction' features of a biological nose, by varying the flow rates between the two columns either by controlling the flow rate or choosing a different length for the column.

7.4 One Dimensional Column Performance
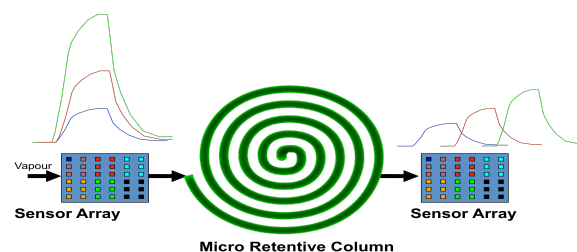
Figure 7.15: One dimensional setup for generating spatio temporal response

There are several ways to use the micro retentive column, to generate a spatio temporal signal. In a one dimensional setup, as in Figure 7.15, one micro retentive

column is used to delay the odour going from the first sensor array, producing a delayed response on the output.
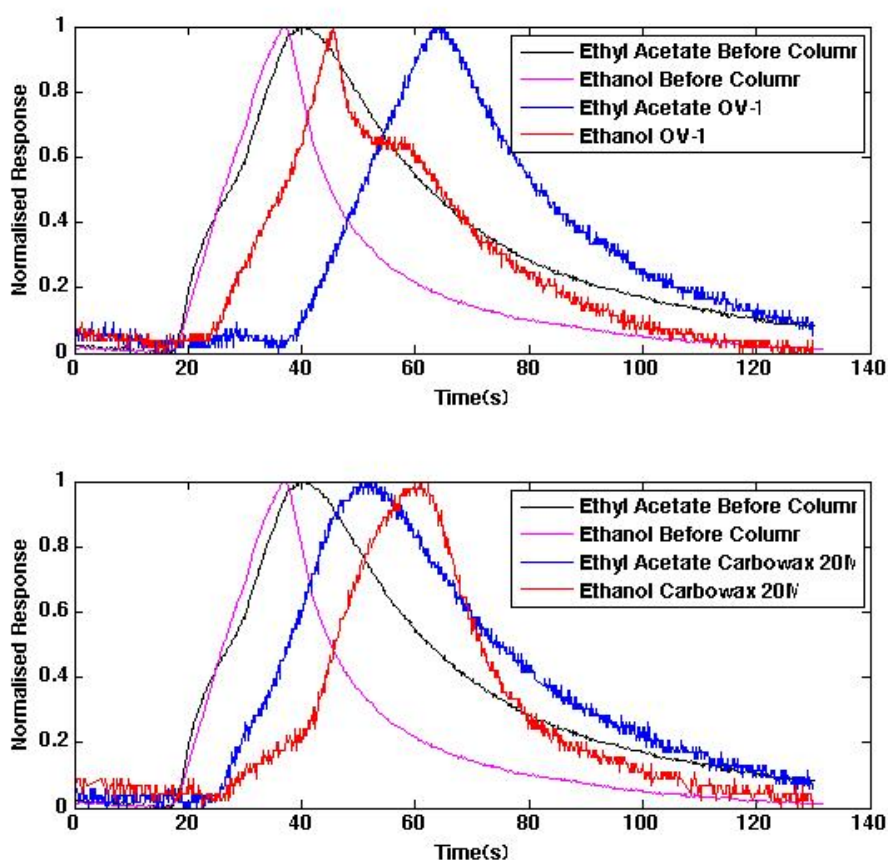
Figure 7.16: Ethyl acetate and Ethanol responses in one dimensional setup

Figure 7.16 shows two experiments performed using a one dimensional setup using two different micro retentive columns; one coated with OV-1 and the other with Carbowax 20M. The purpose of this experiment is to demonstrate the difference between the separation power of polar (Carbowax 20M) and non-polar (OV-1) stationary phase coating. In general, it is expected that ethanol vapour, being more polar than ethyl acetate, to be delayed more through a polar column (Carbowax 20M) and vice versa. In figure 7.16, it shows that ethanol is delayed further than

ethyl acetate on the Carbowax20M, while ethyl acetate is delayed more after the OV-1 column – as expected.

Furthermore, we can roughly estimate the retention caused by the stationary phase by calculating the partition coefficient between the mobile and stationary phase compounds. This can be done using the Linear Solvation Energy Relationship (LSER) equation.

Using constant and variables obtained in another research [5], the partition coefficient for ethyl acetate, acetone and ethanol towards SE-30 and Carbowax 20M can be calculated and plotted, as is Figure 7.17. Here, SE-30 was used because the constant values are available and it has the same content as OV-1 which is 100% PDMS.
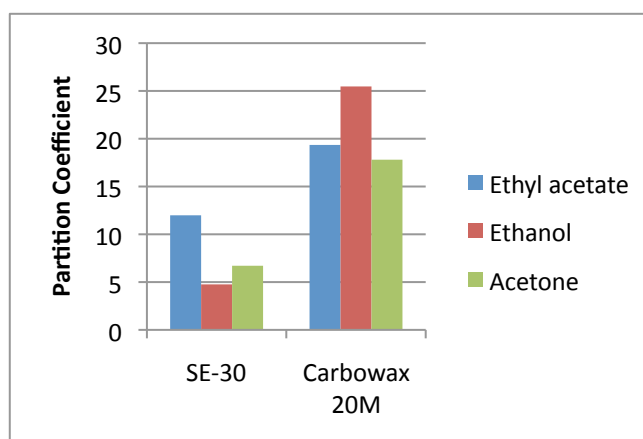
Figure 7.17: Partition Coefficient for three different chemicals with two stationary phase

This plot clearly shows that Ethyl acetate and Ethanol vapours have contradictory reactions towards SE-30 and Carbowax 20M. This supports the results we gained from our experiment, shown in Figure 7.18, where we can see that ethanol vapour is delayed more with a Carbowax 20M coated column and ethyl acetate vapour is delayed more with an OV-1 column.
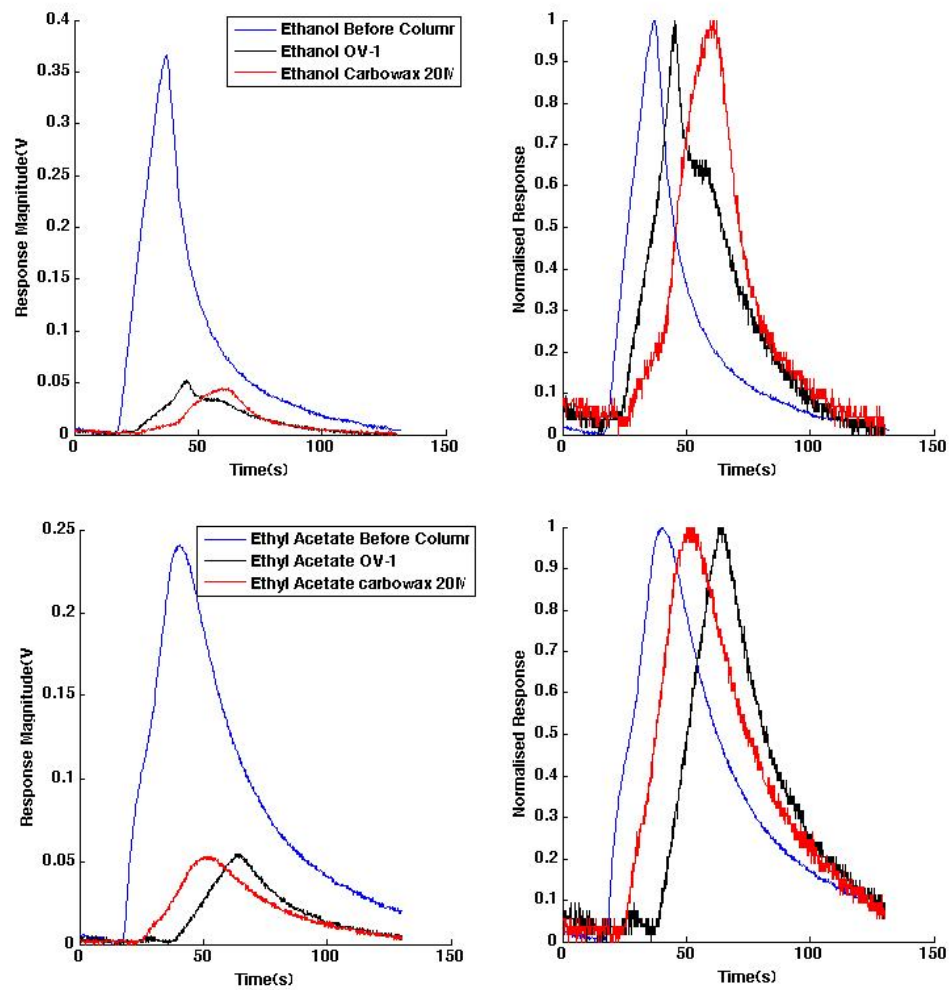
Figure 7.18: Sensor response towards ethanol and ethyl acetate vapour before and after the retentive column

It is worth noting that the first sensor array provides a larger sensor response compared to the end sensor, even though the flow rate through the system is the same. One reason for this is that there is a band broadening effect when the pulse travels through the column at low flow rates. These graphs prove the concept of spatio temporal data generation using the micro retentive column. Furthermore, we

have also demonstrated that each polar and non-polar stationary phase produce a different delay towards a similar odour.

One downside of this setup is that, since only one retentive column was used, if it was coated with polar stationary phase, it's going to react and delay polar molecules more than non polar. Similarly, a non-polar stationary phase will delay non-polar molecules more. These issues resulted in an evolution of our design where we employ two columns with different phase materials.

7.5 Dual Dimensional Column Performance
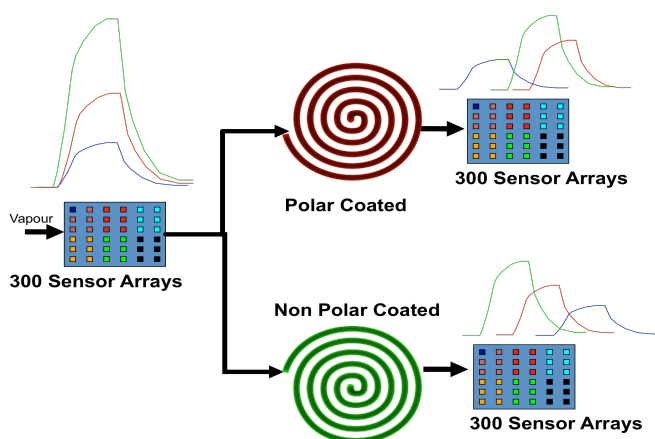
Figure 7.19: Dual Dimensioanal e-Mucosa setup

To further improve the spatio temporal information, a dual dimensional setup was designed, as in figure 7.19, consisting of two columns with different stationary phase coatings and column dimensions.

First thing to note is that the flow rate between the first sensor array and the end sensor arrays are different (divided by 2). This will cause a significant difference in the magnitude of response and response time of the sensors. A larger sensor

magnitude improves the spatial information, while faster response times increase the temporal information of the system.

With this arrangement, a stereo olfaction effect can be produced by using two columns with different length, creating different flow profile between the two retentive column. Another way to mimic the stereo olfaction effect is to use a micro valve to control the flow rate through each column while using two similar columns.

Apart from simulating the stereo olfaction feature, this dual dimensional setup is superior to the one dimensional setup, mainly because it produces much more data that can be used for identification. The two differently coated columns in itself will produce two different sets of temporal information. The large number of sensors and sensors tunings will also contribute to the wide diversity of data available from the instrument. Furthermore, only one cycle of test is required to gain all this information compared to several repeat tests with the one-dimensional setup.
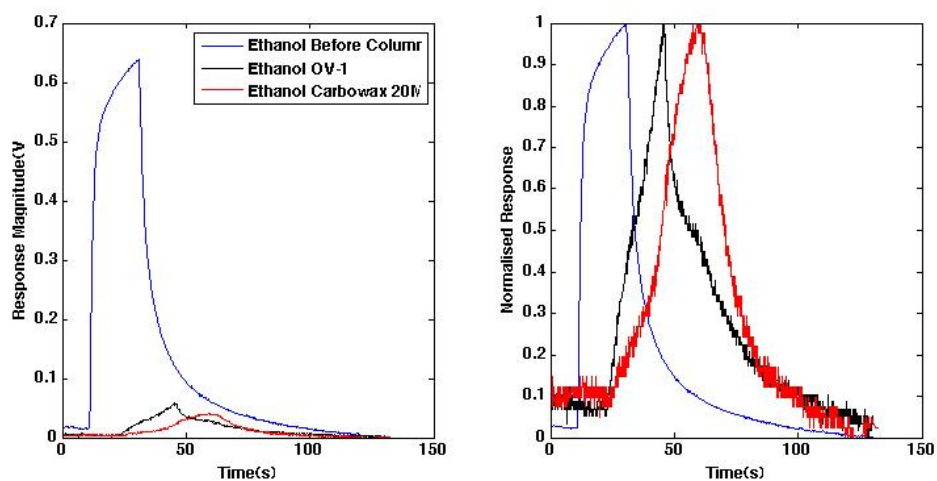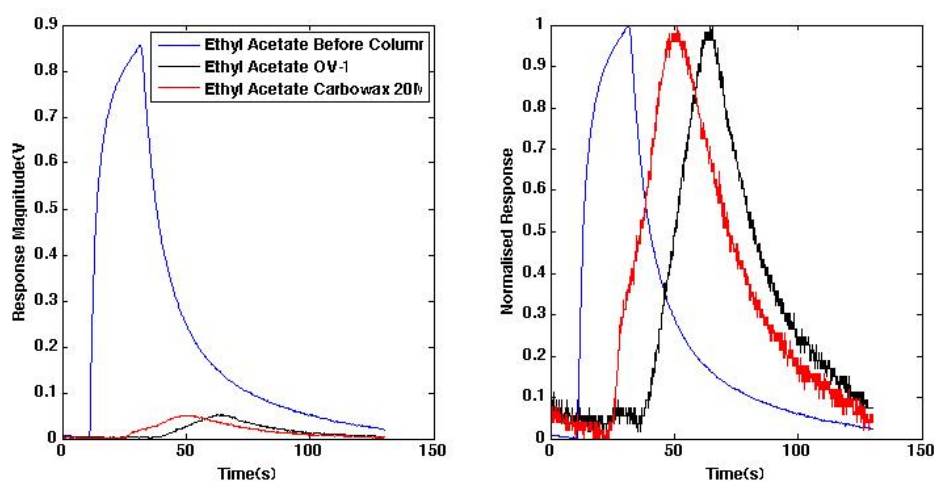
Figure 7.20: Temporal information with dual dimensional setup

In case of dual dimensional retentive column setup, another way to generate spatio temporal information is by measuring the time difference between the responses after the polar column and non-polar column. Figure 7.20 demonstrates this information comparing response from Sensor Array 2 and Sensor Array 3. Note that with one dimensional setup, two runs would be needed to produce this data.

This delay is a good indication of separation created by the differently coated columns (polar and non-polar). Here a retention time of 17 s was achieved comparing similar sensor from second and third sensor array between the two columns.

Comparing this graph with the similarly plotted graph in Figure 7.18, there are two main differences. Since the flow rate of the first sensor array is now doubled the flow in the two end arrays, response magnitude of the first sensor is significantly larger and faster compared to one dimensional setup. Here, we can see the maximum magnitude of response is 0.6 V compared to 0.25 V in the one dimensional setup.

Another major advantage of this setup is the faster sensor responses (effect of flow velocity) contribute to a higher retention time (comparing between the first array to the second or third array) produced by the system. Here, a retention time of 40 s is achieved with ethyl acetate through OV-1 column, while with the one dimensional setup in Figure 7.18, only 25 s is achieved.

7.6 Simple Spatio-Temporal Classification

Using data from the previous experiment, a simple PCA classification has been performed to show the resolving power of the temporal information. Figure 7.21 shows a PCA plot of acetone, ethanol and ethyl acetate using spatial information and temporal information.
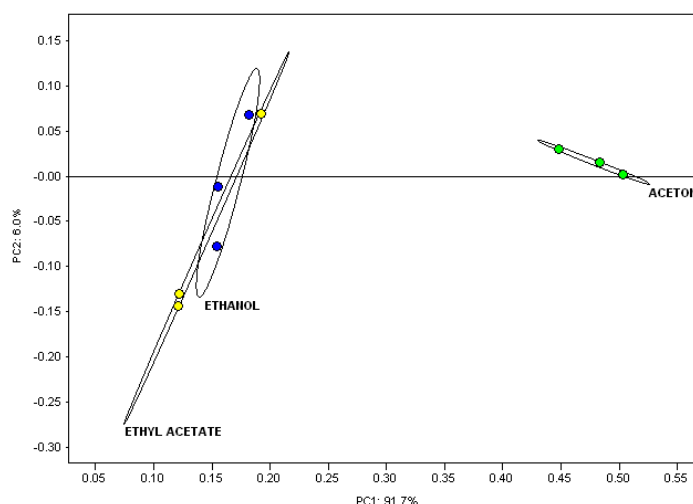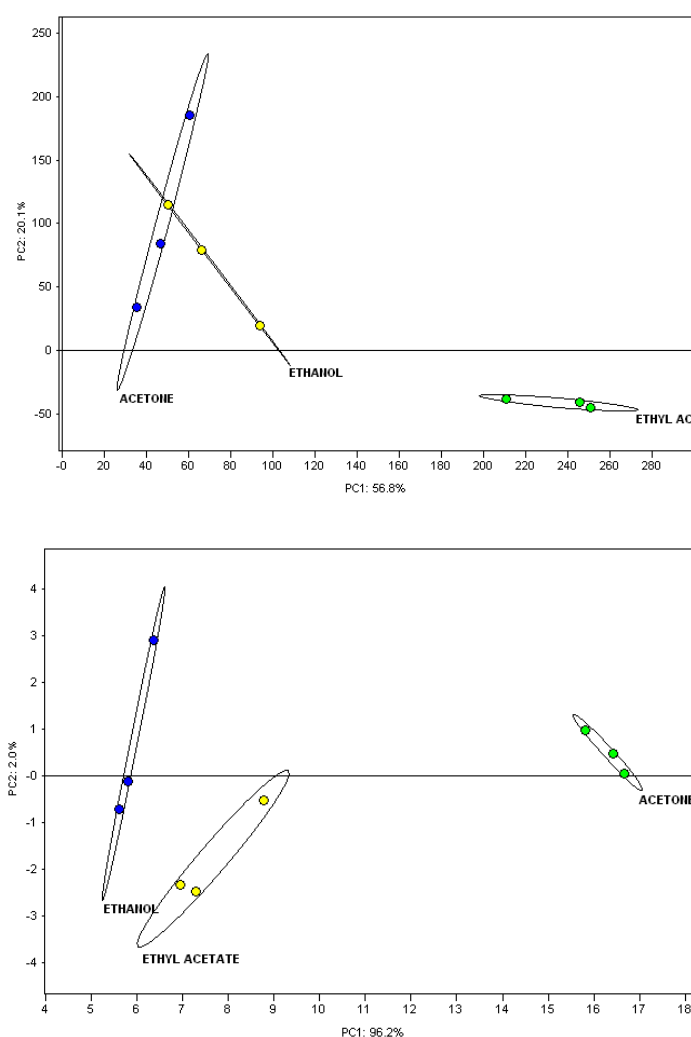
Figure 7.21: PCA Plot for three chemical using a) Spatial information only b) Temporal information only c) Combined Spatio-Temporal information

The experiment was performed with the one dimensional setup using 2 m OV-1 column under room temperature (20°C) with three randomize repeats. This experiment is done at lower concentration compare to the one in Figure 7.7 to show the ability of spatio-temporal information. This experiment is done at concentrations of 100 ppm for ethanol, 200 ppm for ethyl acetate and 500 ppm for acetone. We can see from the plot that temporal information does contain significant information to separate the chemicals. Figure7.8 (a) shows that spatial information separates acetone vapour far better than for ethanol and ethyl acetate vapour. On the other hand, with temporal information (Figure 7.8(b)), ethyl acetate is separated easier

than ethanol and acetone vapours. Combining these two sets of information, by multiplying the spatial information directly with the temporal counterpart, another PCA is plotted as in Figure 7.8(c) showing better separation of all three components. Thus, it is clear that temporal information can be combined with spatial information to improve the classification of the system. A more advanced technique is used to process both spatio-temporal information and will be discussed later in this chapter.

7.7 Portable e-Mucosa System Optimization

The portable e-mucosa instrument is composed of parts described and tested in this chapter, and thus further descriptions are not required. However, there are some changes made to the portable e-mucosa to enable the device to remain as small as possible, but still retain the wide diversity of data. As mentioned before, 200 sensors were used instead of 300 contained in the sensor array. This is to reduce the complexity of the interface circuitry and improve the overall speed of the system. Furthermore, the number of different sensing layers remains the same at 24 tunings. Since the portable e-Mucosa is designed to work in a normal ambient environment, a pre-concentrator is designed to help improve the overall system sensitivity by concentrating the odour being tested before it is pushed over the sensors.
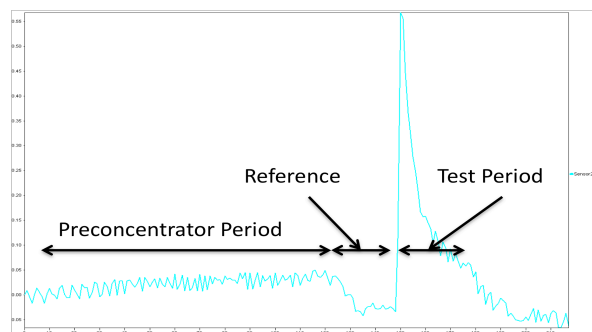
Figure 7.22: Sensor response with preconcentrator to ethyl acetate

Figure 7.22 shows Sensor 225 response to ethyl acetate odour that has been concentrated in the preconcentrator chamber for 2 minutes before thermally releasing it through to the sensor at 100°C. Here, no continuous flow of ethyl acetate is given to the sensor, only the preconcentrated odour from the preconcentrator chamber. We can see from the graph, a very fast sensor response, which quickly recovers to the baseline even during the test period (due to no continuous flow of ethyl acetate – thus the pre-concentrator has been 'emptied' of test sample). This is to show that the pre-concentrator itself does collect a significant amount of odour to be useful.

Figure 7.23 shows the sensor response to ethyl acetate with and without pre-concentrator in a continuous odour flow of 20s during test with 150s pre-concentration time. This clearly shows that the pre-concentrator improves the initial response of the sensor.
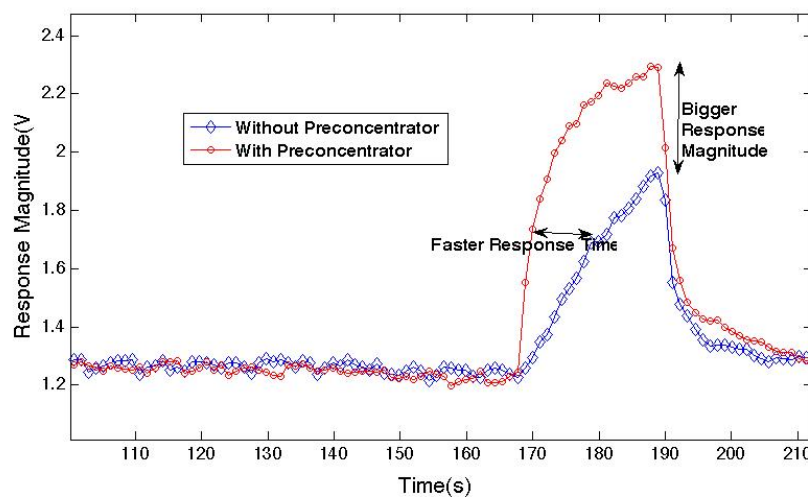
Figure 7.23: Sensor 225 response to ethyl acetate with and without preconcentrator

In addition, the magnitude of response increased by almost 40% with the pre-concentrator. Furthermore, the sensor response is about 10 s faster with the pre-

concentrator. This feature significantly improves the instrument, as it enhances both the spatial and temporal information.

7.8 Advanced Spatio-Temporal Odour Classification

In order to evaluate the artificial olfactory mucosa spatio-temporal response, a more advance technique has been utilized. Here, the odour headspace from essentials oils was pumped through the first chamber containing the first sensor array, then into the two differently coated micro-fluidic retentive channels that are connected to the second and third sensor arrays. During this time, a software control program takes readings from all three arrays continuously. The flow rate was controlled using a mass flow controller, set to 300 ml/min, in order to maintain the concentration of the odour throughout the test. The carrier gas used for all the experiments was laboratory air. It is important to remember that the biological system functions without needing specialised carrier gases or humidity control. Here we are developing an instrument to mimic the biological system, thus we have used real life conditions. The laboratory air was passed through a filter to remove any large particles that might affect the system (similar to the function of the hairs in the nostrils). Although humidity was not controlled, it is monitored on the inlet as well as the temperature using temperature/humidity sensor SHT15 from Sensirion (Switzerland). The system was tested with 300 s pulses of essential oil vapour at temperature 22°C (± 1°C). The essential oils used in these experiments were lemon grass, ylang ylang, cinnamon and lavender. Such oils are formed out of several chemical components, and so again relate more closely to real-world applications. For example, 'lemon grass' is formed from myrcene, citronellal, geranyl acetate,

nerol, geraniol, neral and traces of limonene and citral. Thus calculating the exact headspace concentrations for each oil and its components is difficult. It is important to remember the biological system is poor at providing odour concentration information, but is very good at identifying odour class. These odours were introduced for 60 s with 100 s pre-test air as a reference. Five repetition of each odour was done.

The spatio-temporal data, produced by the instrument, was processed using the convolution method reported in [6]. The three chemoresistor arrays make available several options when processing the two signals to be convolved; the front-end array can be combined with either the polar or non-polar arrays, or the polar and non-polar arrays can be combined with each other. Also, the large numbers of sensors provide a level of redundancy not encountered before, and needed to be considered during the processing phase.
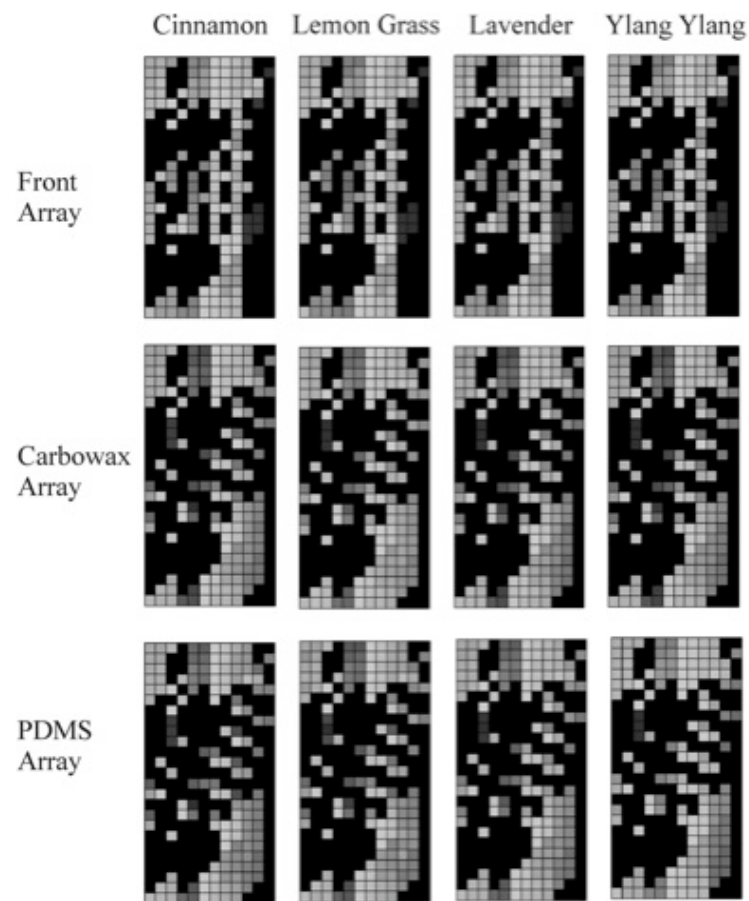
Figure 7.24: Spatial information representation of three sensor array with four essential oil[7]

First, valid sensors within each array were identified and selected, illustrated in Figure 7.24. It can be seen that there is much correlation between the sensor arrays at this stage. These sensors were then normalized and a convolution performed between corresponding sensor pairs in each array to produce a new characteristic time-series signal. The area of the convolution integral signal was then computed, and the resulting feature set is illustrated in Figure 7.25. The convolution process produces a set of data with much more pronounced differences.
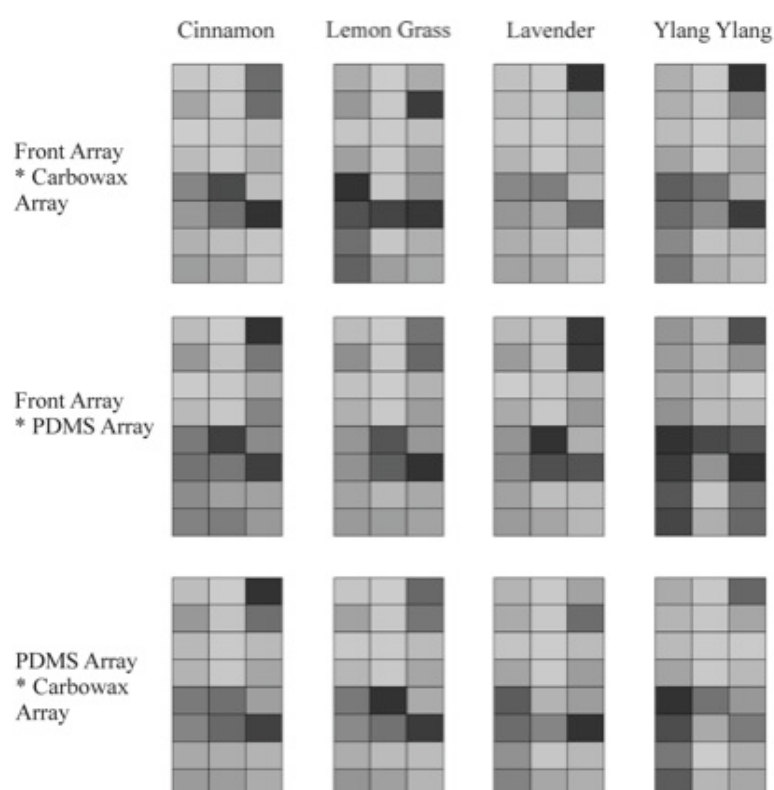
Figure 7.25: Convolution results of four essential oil [7]

The feature sets produced were then classified using a probabilistic neural network (PNN) classifier. Table 7.1 shows the accuracy of the classification on this optimum sensor subset.

Table 7.1: Accuracy matrix for PNN classifier utilizing an optimum sensor subset [7]

Array Pair	Omit 1st Group	Omit 2nd Group	Omit 3rd Group	Omit 4th Group	Omit 5th Group	Overall Accuracy
Front Array * Carbowax Array	100%	100%	100%	75%	50%	85%
Front Array * PDMS Array	50%	75%	75%	75%	100%	75%
PDMS Array * Carbowax Array	75%	75%	75%	75%	25%	65%

The best accuracy is achieved by a convolution of sensors in the front array and the corresponding sensors following the Carbowax 20M channel. We believe that this was because the chemical nature of the oils was more diverse in terms of their polar interactions than differences in their boiling points. Other array combinations produced poorer results, but still produced an improvement in accuracy. This shows

that the flexibility within the layout and redundancy of the system allows selection of

a problem appropriate processing scheme.

7.9 Conclusions

In this chapter, we have discussed the characterization of both the large sensor array

and micro retentive column with several experiments. It is very clear that there is a

substantial diversity, in terms of sensors, columns and configurations, which can be

used to aid odour recognition during classification. However, a more complex

pattern recognition technique is needed to process this huge diversity of data. Here

we have only presented simple processing techniques, such as PCA, to process each

spatial and temporal data individually. This is to prove the concept of dual dimension

spatio temporal information. Comparing this with conventional spatial response

data, we can conclude that the temporal information can be used to aid odour

classification during data processing. We also proposed another processing

technique that utilize all this information in other research [6].

7.10 References

1.   S.M. Briglin, et al., *Exploitation of spatiotemporal information and geometric optimization of signal/noise performance using arrays of carbon black-polymer composite vapor detectors.* Sensors and Actuators B: Chemical, 2002. 82(1): p. 54-74.

2.   S.L Tan, *SMART CHEMICAL SENSING MICROSYSTEM: TOWARDS A NOSE-ON-A-CHIP.* PhD Thesis, 2005.

3.   S. A. Casalnuovo, J. Kottenstette, Edwin J. Heller, Carolyn M. Matzke, Patrick R. Lewis, Ronald P. Manginell, Albert G. Baca, Vincent M. Hietala, and Joel R. Wendt, *Gas Phase Chemical Detection with and Integrated Chemical Analysis System.* Sandia National Laboratories, 2000.

4.   Y.S.Kim, , *Microheater-integrated single gas sensor array chip fabricated on flexible polyimide substrate.* Sensors and Actuators B: Chemical, 2005. In Press, Corrected Proof.

5.   M.H.Abraham, , C.F. Poole, and S.K. Poole, *Classification of stationary phases and other materials by gas chromatography.* Journal of Chromatography A, 1999. 842(1-2): p. 79-114.

6.   J.W.Gardner, J.E.T., *Novel Convolution Based Signal Processing Techniques for a Simplified Artificial Olfactory Mucosa.* Transducer, 2007: p. 2473-2476.

7.   F.K. Che Harun, J.E.Taylor, J.A. Covington, J.W. Gardner, *An electronic nose employing dual-channel odour separation columns with large chemosensor arrays for advanced odour discrimination.* Sensors and Actuators B: Chemical, 2009, 141, p. 134-140.

CHAPTER 8

Conclusions and further work

8.1 Overview

Although electronic nose technology has been an active area of research for over 25 years, it is still far behind compared to the biological olfactory system in term of selectivity and sensitivity. However, it is still being used in wide range of applications in several industries such as environmental, food industry and medical field. The main reason is the ability of an electronic nose to solve specific problem at a lower cost within a short period of time.

E-nose system provides an alternative to the use of organoleptics panels and is better in several areas. Using humans to evaluate the smell of products such as perfumes, foods and beverages is a costly process, because trained panels of experts are required and they can only work for relatively short periods of time. Furthermore, in areas such as explosive detection and several medical applications, it is impossible to use human organoleptics panels to classify toxic and dangerous odorants.

However, most existing commercial e-nose instruments are bulky desktop units, requiring a PC to operate, and is expensive. In addition, these systems usually require a trained operator to gather and analyse the data. Furthermore, most of these systems need a controlled environment to work properly compared to

biological olfactory systems that are mobile and capable of adapting to environmental changes.

Motivated to improve the performance, size and cost of e-nose instruments, this research is aimed at mimicking the biological olfactory system in order to improve current state of electronic nose technology. In an attempt to extract the features that contribute to the superiority of the biological olfactory system, this study has focused on several key features such as large olfactory receptor count, the nasal chromatograph effect, stereo olfaction, sniff rate and odour conditioning. Based on these features, a portable, cost effective instrument called Portable e-Mucosa (PeM) have been designed, fabricated and tested. The term 'e-mucosa' or 'electronic mucosa' refers to the ability of the instrument to generate spatio-temporal response similar to the function of human mucus that creates the 'nasal chromatograph' effects.

8.2 Project objectives

Objectives, discussed in chapter 1, have been mainly realized in this study, is summarized as follows:

$\Rightarrow$ Extracting biological olfactory system functionality and implementing it in an e-nose to improve overall odour discrimination.

$\Rightarrow$ Large Micro chemo sensor arrays have been designed, fabricated and tested in order to mimic the large number of olfactory receptors in the olfactory epithelium

$\Rightarrow$ 3 Dimensional micro retentive columns have been designed and fabricated using an Envisiontec Perfactory Mini MSL machine and coated with a range of

retentive materials. The channel has been characterized and used to mimic the 'nasal chromatograph' effect of the biological olfactory system.

$\Rightarrow$ Other biological olfactory operations, such as temperature control by the nasal cavity and stereo olfaction (different flow rates in two nostrils) have been investigated.

$\Rightarrow$ Finally, a bio-inspired portable Instrument called Portable e-Mucosa mimicking these principles has been designed, fabricated and tested.

8.3 Development of an artificial bio inspired olfactory systems

The main focus of this research was to extract key biological features from the human olfactory system and develop a bio inspired artificial nose instrument based on these extracted features. Although many features are being imitated, the main features that will enhanced current e-nose instrumentation is the 'nasal chromatograph' effect combined with large number of sensors in the system[2]. Utilizing dual GC column in a gas sensing system has already been develop and proven by Sandia Lab when they produce µChem Lab consisting of two micro GC column coated with two different stationary phase [3]. However, in their system, the function of the GC is to separate the tested vapours completely before detecting the peaks of each vapour molecule using a SAW sensor. Our approach in the portable e-mucosa is different. In our instrument we have used three large sensor arrays to provide a huge, diverse dataset on a tested odour. Furthermore, the retentive column used here does not produce perfect separation, instead just enough relative difference between the two columns to produce spatio-temporal information at the end sensor arrays.

Other features that have been developed in this research, is the ideas of stereo olfaction, odour conditioning and sniffing rate. These extracted were tested and optimised before miniaturizing the system producing a portable e-mucosa instrument containing 600 sensors in total with two micro retentive columns.

The large sensor array was designed to have fewer electrode pads for connection compared to normal (if 2 pads where given over to each sensor then 600 pads would be required to connect to 300 sensors). The 'pad stack' design reduces the number of sensor pads from 600 to only 37 thus simplifying the interface circuitry to the sensors. This is an important feature in order to create a small, cost effective, and portable instrument. The large sensor number is mimicking the large number of olfactory receptor in human olfactory system. Unfortunately, having a large sensor count creates several problems during deposition.

Firstly, depositing the 300 sensors individually would be time consuming, especially in an instrument with a total of 1200 sensors. Furthermore, although having 300 sensors coated with 300 different polymer composite films is desirable, it is not practical and would consume too much time in chemical preparation. Here we deployed a spray coating method (for ease) to produce multiple sensors, of the same type, at one time. In our instrument, 24 different polymers composite coatings were used to make sensor development faster. The sensor array is coated in batches of 12 each, to create redundancy that will be useful during data processing. Another challenge, faced during deposition, is to maintain the deposition features such as thickness, baseline resistivity and uniformity of the film. This was solved by closely monitoring the baseline resistivity during deposition. Although all precautions were taken to reduce the dissimilarity between the coated films, there will clearly be some

variations across a batch (due to uneven deposition). The three sensor arrays used in the instrument were coated with similar polymer composite films to compare the response before and after the retentive column.

The retentive column is used to create a temporal delay from an incoming sample, mimicking the 'nasal chromatograph' effect. This was achieved by designing a simple GC like column. Although in gas chromatography, complete separation of the test sample is desirable, in this study, we only aim to gain a relative temporal difference between the two differently coated columns. This temporal difference can be used as complementary information to the spatial response to aid sample identification.

The complete instrument was created by combining the three sensor arrays and two retentive columns, where the first array provides spatial information (due to the significant response magnitude). The two end sensor arrays respond slower due to lower flow rates, and are affected by sample band broadening (so contain poor spatial information), but provide temporal information through the interaction between the sample and the column coating.

8.4 Portable e-Mucosa

Based on the study on key biological features of biological olfactory system, a portable instrument is developed. This instrument tries to mimic many of the features extracted from the biological olfactory system. Table 8.1 lists the comparison of features in the artificial olfactory system compared to biological olfactory system.

Table 8.1: List of Components with comparable function to biological olfactory system

Biological Olfactory	Artificial Olfactory	Comments
Nose Hair	Air Filter	To Filter dust and big particles from entering the system
Olfactory Receptor	Large Sensor Array	Total of 600 sensors array with 24 different tunings.
Nasal Cavity	Preconcentrator	Temperature Control
Nasal Mucous	Stationary phase on Retentive Column	Generate Spatio Temporal response from the 'nasal chromatograph' effect.
Stereo Olfaction and Sniff Rate	Two Micro Retentive column with different flow rates	Different flow rates on two nostril.

The aim of this study was to obtain a significant level of information, from a test sample, in order to increase the possibility of identification. The main information generated by this instrument is the multi dimensional spatio-temporal information.

8.5 Characterisation and performance of the e-mucosa system

Various experiments have been performed to characterise the e-mucosa instrument. The effect of changes in temperature, flow velocity and sample analyte on the large sensor array has been tested and analysed. For the carbon black sensors

used in this study, we see similar characteristics that have been reported before, i.e. room temperature operation and than an increase in temperature decreases the magnitude of response [4, 5]. However, an increase in flow velocity, did increase the response time and the response magnitude, as suggested by Tan [6]. PCA analysis on simple analytes, (toluene and ethanol vapour), show that carbon black sensors can easily separate these analytes. However, on more complex odours, such as essential oil, it is more difficult to divide.

A comparison between a coated and an uncoated column proved that the stationary phase coating did delay a sample as it travelled through it. Comparing polar and non-polar columns indicated that the polar column delay polar compounds (in this case ethanol) more than non polar compound (ethyl acetate) and vice versa. A simple PCA using temporal information alone, showed the ability of the temporal information to separate simple chemicals. Furthermore, using the final system, we are able to separate essential oil data, which is difficult to do using only spatial information.

8.6 Further Works

There are a few areas in this research that are still open to exploration. Many features that have been mimicked are in the 'front-end' of the biological system. However, there are still features that can be researched to further improve instruments. Features, such as flow direction (including turbulence) and receptor location in the nasal cavity, have still to be explored.

Pattern recognition techniques that utilize all this information still need to be developed, especially how the human olfactory system processes the large quantity

of information. One possibility is using neural networks based on integrate and fire neurons, as in the biological system.

There is also room for improvement in the portable e-mucosa design. Currently the instrument is able to store data on MMD/SD card for further processing on a PC. However, a direct connection through USB will enable user to view the response in real time while recording it. The system has been designed with a USB module including the required circuitry and the USB connection has been tested to be working properly. However, software needs to be developed to interact with the instrument in order to read the response from the sensors.

The portable instrument still lacks built-in pattern recognition methods. A nice addition to the instrument would be a built in pattern recognition method that mimicked the human olfactory processing technique, which is the 'integrate and fire' neuronal model. During this research, we have also studied the possibility of using a hardware 'integrate and fire' model that could be integrated into the instrument. The aVLSI neuromorphic olfactory chip was designed and developed by ourselves, the University of Leicester and the University of Edinburgh. Here, we have designed the circuitry for this chips and run initial tests to check its functionality.
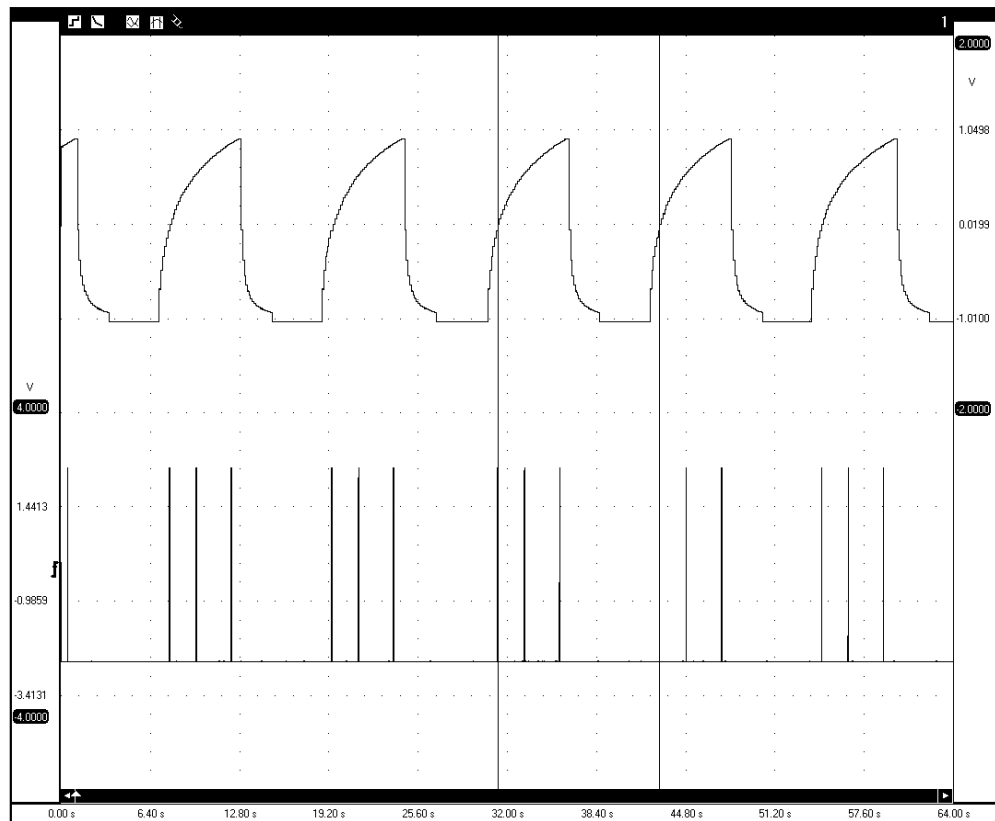
Figure 8.1: Neuromorphic Olfactory chip responding to e-nose sensor response

Figure 8.1 shows the ability of this chip to integrate and fire at a certain set threshold. Here we can see that the spike only occurs when the sensor response reach a certain threshold. Further work on this system would include miniaturizing and integrating this into the instrument to produce a truly portable bio-inspired e-nose instrument.

8.7 References

1.   K. Persaud, *Analysis of discrimination mechanisms in the mammalian olfactory system using a model nose.* Nature, 1982.
2.   F.K. Che Harun, J.E.Taylor, J.A. Covington, J.W. Gardner, *Dual-Channel Odor Separation Columns with Large Chemosensor Arrays for Advanced Odor Discrimination.* International Meeting of Chemical Sensor, 2008.
3.   S. A. Casalnuovo, J. Kottenstette, E. J. Heller, Carolyn M. Matzke, Patrick R. Lewis, Ronald P. Manginell, Albert G. Baca, Vincent M. Hietala, and Joel R. Wendt, *Gas Phase Chemical Detection with and Integrated Chemical Analysis System.* Sandia National Laboratories, 2000.

4.   M. Homer, J.R. Manatt, K. Kisor, A. Lara, L. Jewell, A.D. Shevade, A. Yen, S.P.S. Zhou, H. Ryan, *Using temperature effects on polymer-composite sensor arrays to identify analytes.* Sensors, 2003. **1**: p. 144-147.

5.   Y.S.Kim,*Microheater-integrated single gas sensor array chip fabricated on flexible polyimide substrate.* Sensors and Actuators B: Chemical, 2006, 114, p. 410-417.

6.   S.L. Tan, *SMART CHEMICAL SENSING MICROSYSTEM: TOWARDS A NOSE-ON-A-CHIP.* PhD Thesis, 2005.

Appendix A : Sample XML e-nose file

```xml
<?xml version="1.0" encoding="UTF-8" ?>
<!DOCTYPE enose SYSTEM "enose.dtd">
<enose distribute="CONFIDENTIAL" shortform="no">
  <owner name="Fauzan Khairi Che Harun" email="apauaie@gmail.com"/>
  <sample name="Portable E-Mucosa Data">
    <acquired>
      <measurement name="Data01" date="20090609T103631">
        <device name="Portable e-Mucosa" Manufacturer="University of Warwick"
serial="PeM001">
          <parameter value="YES" name="TimeControl" format="BOOL"/>
          <parameter_2 value="27" name="Temperature" format="INT" unit="dC"/>
          <parameter_3 value="2.4E+0" name="TimeInterval" format="INT" unit="spS"/>
          <parameter_4 value="CB" name="PreCon Coating" format="STRING"/>
          <parameter_5 value="10" name="Precon Period" format="INT" unit="s"/>
          <parameter_6 value="5" name="Reference Period" format="INT" unit="s"/>
          <parameter_7 value="5" name="Test Period" format="INT" unit="s"/>
          <parameter_8 value="30" name="Flush Period" format="INT" unit="s"/>
          <parameter_9 value="1" name="PumpPower" format="INT"/>
          <parameter_10 value="3" name="Constant Current" format="INT"/>
          <device name="Sensor1">

<values>2.499000;2.499000;2.499000;2.499000;2.499000;2.499000;2.499000;2.499000;2.4990
00;2.499000;2.499000;2.499000;2.499000;2.499000;2.499000;2.499000;2.499000;2.
499000;2.499000;2.499000;2.499000;2.499000;2.499000;2.499000;2.499000;2.499000;2.49900
0;2.499000;2.499000;2.499000;2.499000;2.499000;2.499000;2.499000;2.499000;2.4
99000;2.499000;2.499000;2.499000;2.499000;2.499000;2.499000;2.499000;2.499000;2.499000
;2.499000;2.499000;2.499000;2.499000;2.499000;2.499000;2.499000;2.499000;2.49
9000;2.499000;2.499000;2.499000;2.499000;2.499000;2.499000;2.499000;2.499000;
2.499000;2.499000;2.499000;2.499000;2.499000;2.499000;2.499000;2.499000;2.499
000;2.499000;2.499000;2.499000;2.499000;2.499000;2.499000;2.499000;2.499000;2
.499000;2.499000;2.499000;2.499000;2.499000
</values>
          </device>
          <device name="Sensor2">

<values>2.499000;2.499000;2.499000;2.499000;2.499000;2.499000;2.499000;2.499000;2.4990
00;2.499000;2.499000;2.499000;2.499000;2.499000;2.499000;2.499000;2.499000;2.
499000;2.499000;2.499000;2.499000;2.499000;2.499000;2.499000;2.499000;2.49900
0;2.499000;2.499000;2.499000;2.499000;2.499000;2.499000;2.499000;2.499000;2.4
99000;2.499000;2.499000;2.499000;2.499000;2.499000;2.499000;2.499000;2.499000
;2.499000;2.499000;2.499000;2.499000;2.499000;2.499000;2.499000;2.499000;2.49
9000;2.499000;2.499000;2.499000;2.499000;2.499000;2.499000;2.499000;2.499000;
2.499000;2.499000;2.499000;2.499000;2.499000;2.499000;2.499000;2.499000;2.499
000;2.499000;2.499000;2.499000;2.499000;2.499000;2.499000;2.499000;2.499000;2
.499000;2.499000;2.499000;2.499000;2.499000
</values>
          </device>
          <device name="Sensor3">

<values>2.499000;2.499000;2.499000;2.499000;2.499000;2.499000;2.499000;2.499000;2.4990
00;2.499000;2.499000;2.499000;2.499000;2.499000;2.499000;2.499000;2.499000;2.
499000;2.499000;2.499000;2.499000;2.499000;2.499000;2.499000;2.499000;2.49900
0;2.499000;2.499000;2.499000;2.499000;2.499000;2.499000;2.499000;2.499000;2.4
99000;2.499000;2.499000;2.499000;2.499000;2.499000;2.499000;2.499000;2.499000
;2.499000;2.499000;2.499000;2.499000;2.499000;2.499000;2.499000;2.499000;2.49
9000;2.499000;2.499000;2.499000;2.499000;2.499000;2.499000;2.499000;2.499000;
2.499000;2.499000;2.499000;2.499000;2.499000;2.499000;2.499000;2.499000;2.499
000;2.499000;2.499000;2.499000;2.499000;2.499000;2.499000;2.499000;2.499000;2
.499000;2.499000;2.499000;2.499000;2.499000
</values>
          </device>
```

```
            <device name="Sensor4">

<values>2.499000;2.499000;2.499000;2.499000;2.499000;2.499000;2.499000;2.499000;2.4990
00;2.499000;2.499000;2.499000;2.499000;2.499000;2.499000;2.499000;2.499000;2.499000;2.
499000;2.499000;2.499000;2.499000;2.499000;2.499000;2.499000;2.499000;2.499000;2.49900
0;2.499000;2.499000;2.499000;2.499000;2.499000;2.499000;2.499000;2.499000;2.499000;2.4
99000;2.499000;2.499000;2.499000;2.499000;2.499000;2.499000;2.499000;2.499000;2.499000
;2.499000;2.499000;2.499000;2.499000;2.499000;2.499000;2.499000;2.499000;2.499000;2.49
9000;2.499000;2.499000;2.499000;2.499000;2.499000;2.499000;2.499000;2.499000;2.499000;
2.499000;2.499000;2.499000;2.499000;2.499000;2.499000;2.499000;2.499000;2.499000;2.499
000;2.499000;2.499000;2.499000;2.499000;2.499000;2.499000;2.499000;2.499000;2.499000;2
.499000;2.499000;2.499000;2.499000;2.499000
</values>
            </device>
            <device name="Sensor5">

<values>2.499000;2.499000;2.499000;2.499000;2.499000;2.499000;2.499000;2.499000;2.4990
00;2.499000;2.499000;2.499000;2.499000;2.499000;2.499000;2.499000;2.499000;2.499000;2.
499000;2.499000;2.499000;2.499000;2.499000;2.499000;2.499000;2.499000;2.499000;2.49900
0;2.499000;2.499000;2.499000;2.499000;2.499000;2.499000;2.499000;2.499000;2.499000;2.4
99000;2.499000;2.499000;2.499000;2.499000;2.499000;2.499000;2.499000;2.499000;2.499000
;2.499000;2.499000;2.499000;2.499000;2.499000;2.499000;2.499000;2.499000;2.499000;2.49
9000;2.499000;2.499000;2.499000;2.499000;2.499000;2.499000;2.499000;2.499000;2.499000;
2.499000;2.499000;2.499000;2.499000;2.499000;2.499000;2.499000;2.499000;2.499000;2.499
000;2.499000;2.499000;2.499000;2.499000;2.499000;2.499000;2.499000;2.499000;2.499000;2
.499000;2.499000;2.499000;2.499000;2.499000
</values>
            </device>
            <device name="Sensor6">

<values>0.000000;0.000000;0.000000;0.000000;0.000000;0.000000;0.000000;0.000111;0.0000
00;0.000000;0.000008;0.000000;0.000000;0.000000;0.000000;0.000000;0.000000;0.000000;0.
000000;0.000000;0.000049;0.000000;0.000000;0.000176;0.000341;0.000253;0.000243;0.00001
3;0.000000;0.000000;0.000000;0.000000;0.000000;0.000000;0.000267;0.000000;0.000000;0.0
00000;0.000000;0.000000;0.000000;0.000080;0.000229;0.000321;0.000000;0.000000;0.000000
;0.000000;0.000000;0.000000;0.000347;0.000000;0.000000;0.000000;0.000000;0.000000;0.00
0000;0.000000;0.000336;0.000156;0.000030;0.000000;0.000000;0.000000;0.000000;0.000000;
0.000000;0.000000;0.000339;0.000000;0.000000;0.000000;0.000000;0.000120;0.000232;0.000
000;0.000000;0.000000;0.000000;0.000188;0.000028;0.000000;0.000000;0.000000;0.000000;0
.000059;0.000000;0.000000;0.000000;0.000288
</values>
            </device>
            <device name="Sensor7">

<values>2.499000;2.499000;2.499000;2.499000;2.499000;2.499000;2.499000;2.499000;2.4990
00;2.499000;2.499000;2.499000;2.499000;2.499000;2.499000;2.499000;2.499000;2.499000;2.
499000;2.499000;2.499000;2.499000;2.499000;2.499000;2.499000;2.499000;2.499000;2.49900
0;2.499000;2.499000;2.499000;2.499000;2.499000;2.499000;2.499000;2.499000;2.499000;2.4
99000;2.499000;2.499000;2.499000;2.499000;2.499000;2.499000;2.499000;2.499000;2.499000
;2.499000;2.499000;2.499000;2.499000;2.499000;2.499000;2.499000;2.499000;2.499000;2.49
9000;2.499000;2.499000;2.499000;2.499000;2.499000;2.499000;2.499000;2.499000;2.499000;
2.499000;2.499000;2.499000;2.499000;2.499000;2.499000;2.499000;2.499000;2.499000;2.499
000;2.499000;2.499000;2.499000;2.499000;2.499000;2.499000;2.499000;2.499000;2.499000;2
.499000;2.499000;2.499000;2.499000;2.499000
</values>
            </device>
            <device name="Sensor8">

<values>0.146000;0.136500;0.137700;0.129100;0.132400;0.132100;0.135300;0.145000;0.1325
00;0.139100;0.156600;0.156400;0.151500;0.146400;0.129900;0.139800;0.128700;0.134100;0.
134200;0.133900;0.143900;0.138700;0.141600;0.157000;0.151800;0.154100;0.154900;0.15790
0;0.152400;0.144900;0.129300;0.133900;0.135700;0.133600;0.148200;0.156100;0.148300;0.1
29100;0.131000;0.132700;0.130700;0.142900;0.146100;0.152300;0.155400;0.131200;0.129700
;0.132400;0.140000;0.141300;0.151100;0.150500;0.148000;0.139900;0.127900;0.134600;0.13
7500;0.139500;0.150000;0.155600;0.158200;0.139300;0.130000;0.133800;0.132800;0.129300;
0.131800;0.132600;0.152100;0.146600;0.132200;0.128500;0.136700;0.145000;0.156600;0.139
```

700;0.130100;0.127200;0.136300;0.155500;0.158500;0.147800;0.127800;0.132200;0.137400;0.157200;0.134900;0.127900;0.130700;0.148000
</values>
			</device>
			<device name="Sensor9">

<values>2.499000;2.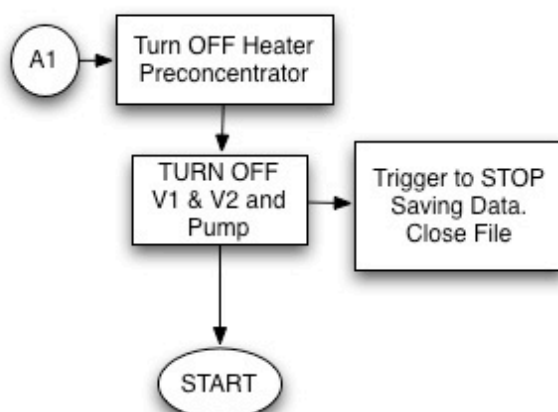499000;2.499000;2.499000;2.499000;2.499000;2.499000;2.499000;2.499000;2.499000;2.499000;2.499000;2.499000;2.499000;2.499000
</values>
			</device>
			<device name="Sensor10">

<values>2.499000;2.499000
</values>

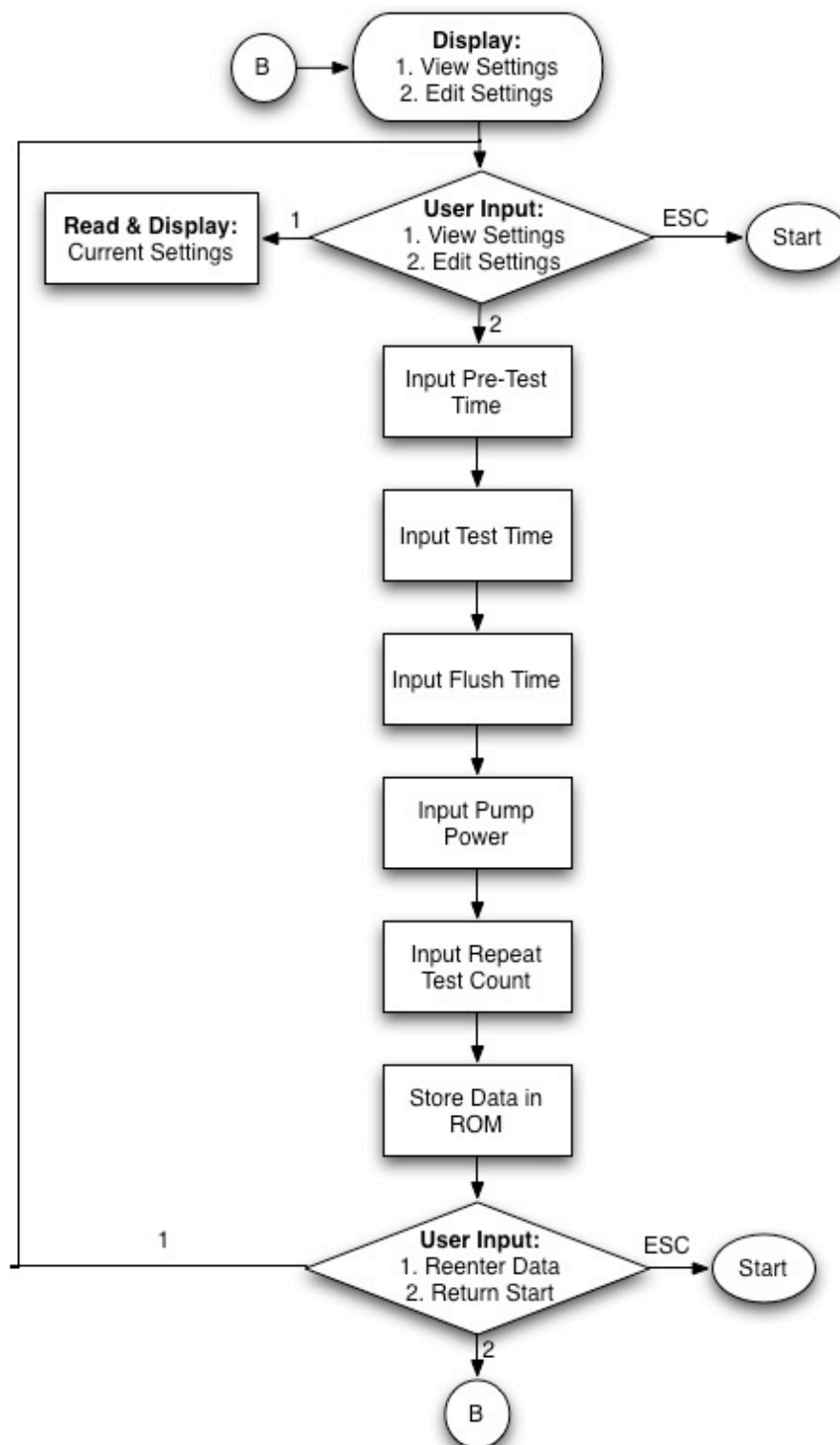</device>
			</measurement>
		</acquired>
	</sample>
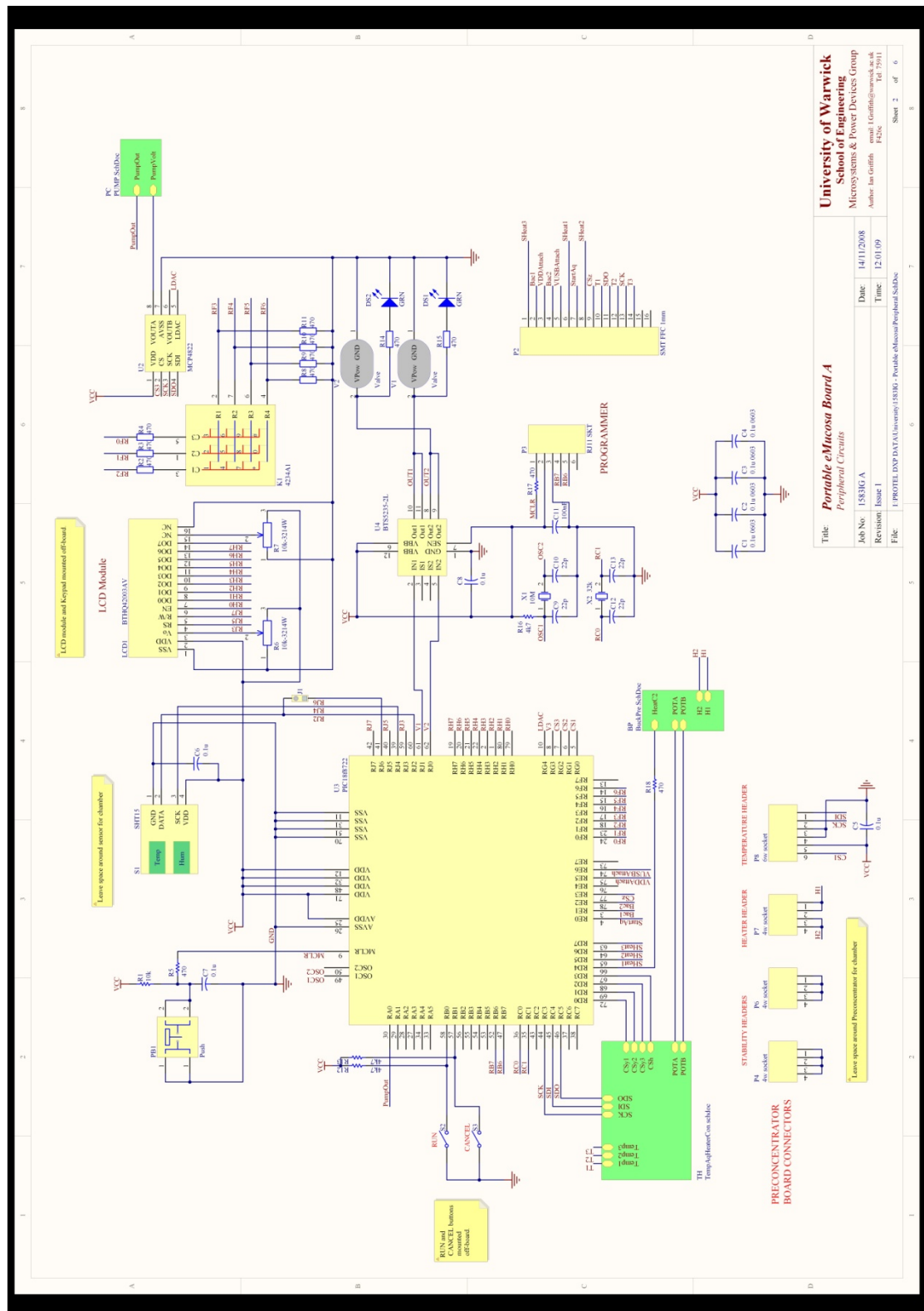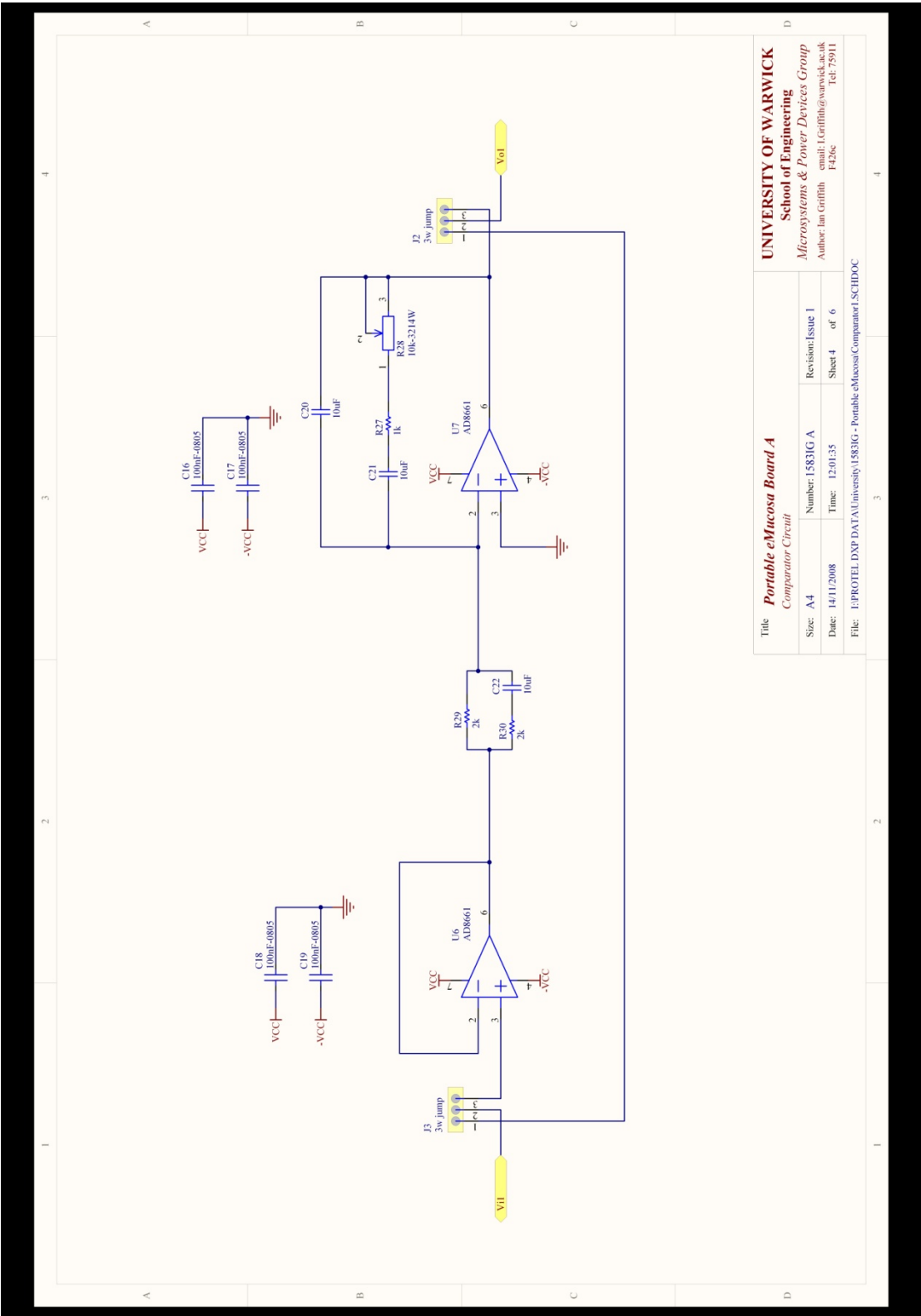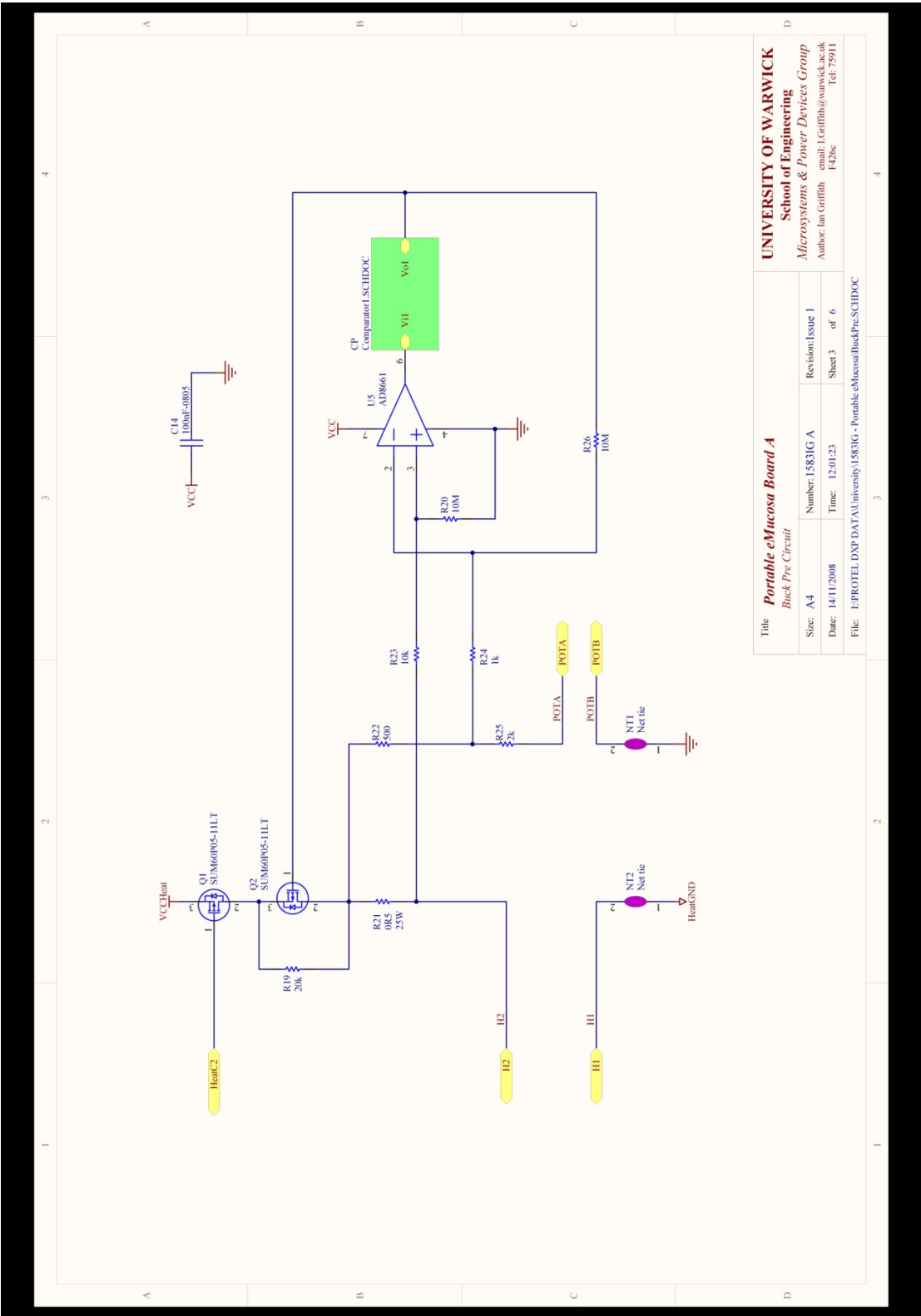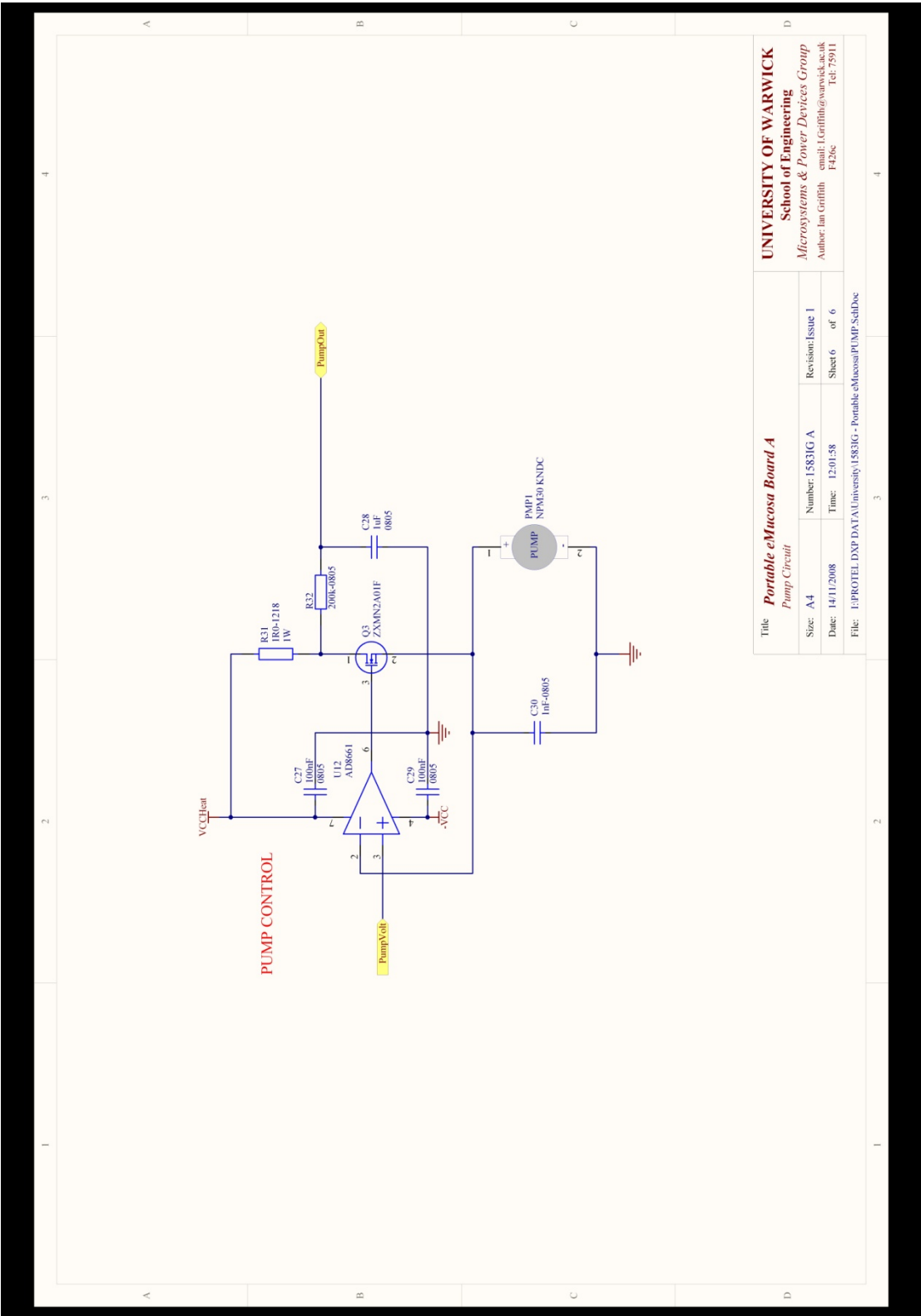</enose>

Appendix B : Firmware Flow Chart

Appendix C : Portable e-Mucosa Schematics

PUMP CONTROL

PumpVolt

PumpOut

VCCHeat

R31
1R0-1218
1W

R32
200R-0805

C28
1uF
0805

Q3
ZXMN2A01F

C27
100nF
0805

U12
AD8661

C29
100nF
0805

-VCC

C30
1nF-0805

PMP1
NPM30 KNDC

PUMP

Title *Portable eMucosa Board A*
Pump Circuit

Size: A4   Number: 1583IG A   Revision: Issue 1

Date: 14/11/2008   Time: 12:01:58   Sheet 6   of 6

File: I:\PROTEL DXP DATA\University\1583IG - Portable eMucosa\PUMP.SchDoc

UNIVERSITY OF WARWICK
School of Engineering
Microsystems & Power Devices Group
Author: Ian Griffith   email: I.Griffith@warwick.ac.uk
F426c   Tel: 75911

Portable eMucosa Board B
Sensor Array Schematic

University of Warwick
School of Engineering
Microsystems & Power Devices Group

Title **Portable eMucosa Board B**
Current Source Schematic

UNIVERSITY OF WARWICK
School of Engineering
Microsystems & Power Devices Group
Author: Ian Griffith   email: I.Griffith@warwick.ac.uk
F426c   Tel: 75911

Size: A4	Number: 1583IG B	Revision: Issue 1
Date: 14/11/2008	Time: 12:07:40	Sheet 3 of 3
File:	E:\PROTEL DXP DATA\University\1583IG - Portable eMucosa\Current Source.SchDoc	

STABILITY HEADER

P1
4w terminal

STABILITY HEADER

P2
4w terminal

HEATER COIL

TEMPERATURE HEADER

P4
6w terminal

VCC
CS1
SCK
SDI

U1

SCL VDD
GND
SDA CS

TC77-5.0

H2
H2
H1
H1

P3
4w terminal

HEATER HEADER

Title: **Portable eMucosa Board D**
Preconcentrator

Size:	A4	Number: 1583IG D		Revision: Issue 1
Date:	14/11/2008	Time: 12:31:47		Sheet 1 of 1
File:	I:\PROTEL DXP DATA\University\1583IG - Portable eMucosa\Preconcentrator.SchDoc			

UNIVERSITY OF WARWICK
School of Engineering
Microsystems & Power Devices Group
Author: Ian Griffith   email: I.Griffith@warwick.ac.uk
F426c   Tel: 75911